A Gessel–Viennot–Type Method for Cycle Systems with Applications to Aztec Pillows

Christopher R. H. Hanusa

A dissertation submitted in partial fulfillment
of the requirements for the degree of

Doctor of Philosophy

University of Washington

2005

Program Authorized to Offer Degree: Mathematics

TABLE OF CONTENTS

LIST OF FIGURES

Figure Number Page

LIST OF TABLES

Chapter 1

INTRODUCTION

The subject area of this dissertation is the study of enumeration of tilings of certain regions, or equivalently matchings of certain bipartite graphs. In Chapter 1 of this paper, we present a brief history of the subject. In Chapter 2, we specify the concept of Aztec pillows and discuss constructions related to their study. In Chapter 3, we present purely combinatorial and matrix-theoretical results on Aztec pillows. In Chapter 4, we present a new method of cycle counting and show how it applies to the enumeration of domino tilings of Aztec diamonds and Aztec pillows. Lastly, in Chapter 5, we generalize a conjecture on Aztec pillows, present additional conjectures extrapolated from experimental calculations, and expose open questions in the vein of the research.

1.1 Tilings and Matchings

Throughout this paper, we will be enumerating the number of complete tilings of regions with dominoes. In general, consider any tiling of the plane with polygons. We consider a diform to be the union of two adjacent polygons. In the particular case when the polygons are all squares, these diforms are called dominoes. As an example, consider a chessboard. A domino will be the union of two adjacent squares.

A tiling of the region will consist of an arrangement of non-overlapping diforms which cover all polygons on the board. In our example, this implies that we use 32 non-overlapping dominoes to cover the chessboard.

Another way to think of a complete tiling of the region is to consider a perfect matching of the dual graph of the region (excluding the outer face). In our chessboard example, we have 64 vertices which represent the squares of the chessboard, and 112 edges representing the adjacencies of the squares. We wish to count the number of ways that 32 of these edges form a perfect matching. In terms of this research, we shall never create a partial matching, so hereafter any reference to a "matching" is a reference to a "perfect matching".

In this paper, to abbreviate "the number of tilings of" in formulas, we will use # notation, as in $\#AD_n$. This notation appears in [32] by Pachter.

1.2 History of the Enumeration of Matchings

The problem in its current form originated in physics and chemistry in the 1930's [28, 35]. Physicists were looking for a model of the liquid and gaseous states, by considering diatomic molecules (dimers) as edges in the square lattice. For this reason, the model is sometimes called the dimer model. Chemists were interested in aromatic hydrocarbons; hydrocarbons

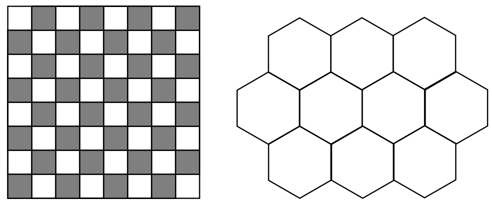

Figure 1.1: Rectangular board and honeycomb graph

form a honeycomb grid, and double bonds need to be placed in this lattice such that each vertex has exactly one double bond attached to it. (See Figure 1.1 for examples of these graphs.)

Progress was made with the infinite square grid in the 1960's, as Kasteleyn was able to count the number of tilings of a rectangular region as well as the associated torus. Given an $n \times m$ board, with both n and m even, there are

$$\prod_{j=1}^{n/2} \prod_{k=1}^{m/2} \left(4\cos^2 \frac{\pi j}{n+1} + 4\cos^2 \frac{\pi k}{m+1} \right) \tag{1.1}$$

domino tilings of the board [21]. This result involves products of cosines and is not obviously an integer. If we consider only the one-parameter family of graphs that is an $2n \times 2n$ subgraph S_n of the infinite square lattice, computation shows that its formula has even more structure, being either a perfect square or two times a perfect square.

Using Galois Theory, we can prove that the formula in Equation 1.1 is an integer [5], but this is less than appealing. The region seems "nice", so there should be a simple proof of this result. In 1996 Pachter [32], based on work by Ciucu [7], found a nice way to decompose the square region S_n into two congruent regions H_n and prove combinatorially that $\#S_n = 2^n(\#H_n)^2$. This result is much more satisfactory, because it explains the formula much more clearly than just "a perfect square or two times a perfect square". As for the general rectangle case, the formula becomes no simpler, but thanks to Percus [33] it can be proved using determinants by exploiting the bipartite nature of the graph instead of with the Pfaffian method that Kasteleyn used initially.

As for the honeycomb grid, it has been studied in depth as well. For a combinatorialist, the most interesting aspect about the matchings on a honeycomb grid or lozenge tilings of a hexagon is their many combinatorial interpretations. They relate to plane partitions and thus to solid Young diagrams [8, 12]. Lozenge tilings of an equiangular hexagon with side lengths (a, b, c) are in one to one correspondence with a solid Young diagram on $[0, a] \times [0, b] \times [0, c]$. This correspondence can be understood visually by thinking of unit cubes fitting inside a box of size $a \times b \times c$, and looking at the box from a point far away, gives the appearance of a hexagon with rhombi tiling it. For an example of this visualization, see Figure 1.2.

At MIT in the 1990's, Jim Propp organized the Undergraduate Research Project in Random Tilings. (Archived website: http://www.math.wisc.edu/~propp/tiling/www/.) Over

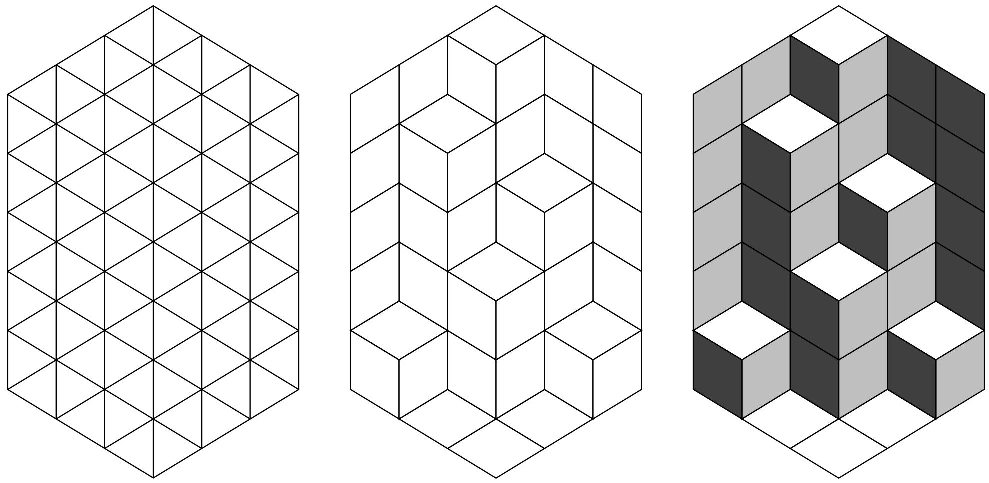

Figure 1.2: A lozenge tiling on a triangular grid and the associated plane partition

its five years this program had over 50 participants. The goal of the program was to understand more fully random tilings of Aztec diamonds (see the next section) and other regions. After moving to the University of Wisconsin, Jim Propp wrote a survey paper [35] on diform tilings in 1999. This survey included a summary of research in this field and thirty-two problems to answer and is a good starting point for additional information about diform tilings and the lines of research considered. In addition, Jim Propp maintains a mailing list focusing on domino tilings. With all this organization, the domino tiling community is well established.

1.3 Aztec Diamonds and Height Functions

When rectangular regions were first considered, they were chosen for study because they seemed to be the most natural regions — the regions that would minimize edge effects on tilings. However, another region proved to yield simpler results. In the 1980's, physicists Grensing, Carlsen, and Zapp [16] presented a regularly bounded region that had a nice formula for its number of tilings, but gave no proof of the formula. Later, mathematicians Elkies, Kuperberg, Larsen, and Propp [10] rediscovered this region and gave four proofs of the formula

$$\#AD_n = 2^{n(n+1)/2}. \tag{1.2}$$

This region was called the Aztec diamond (see Figure 1.3a for an example), denoted by AD_n, where n is the number of steps along any diagonal. With respect to discussing Aztec diamonds and later Aztec pillows, we start from the center of the left plateau and consider a "step" to be a movement along the boundary of the region tracing upward along one square, followed by tracing right for at least one square until the next square begins. In particular, the Aztec diamond in Figure 1.3a has four steps.

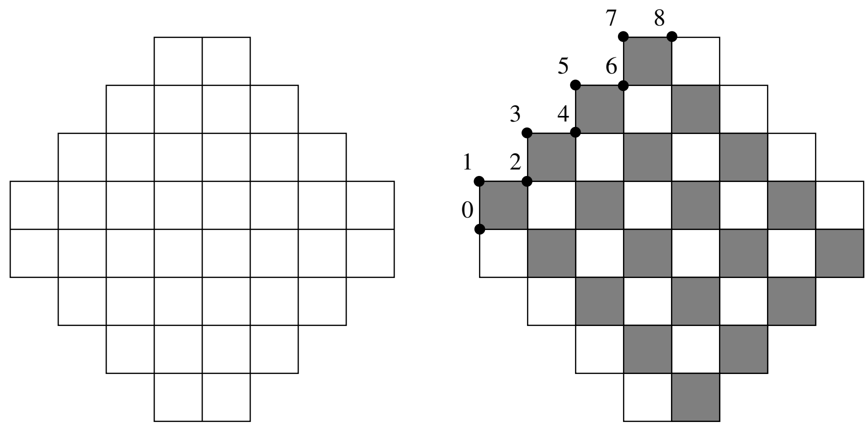

Figure 1.3: The Aztec diamond AD_4 and its associated boundary height function

One reason why the enumeration of tilings of Aztec diamonds is believed to have such a nice formula is because of the restrictions the edge effects have on the structure of tilings that appear in this region. To describe these edge effects, we define the concept of a height function along the boundary of the region. We will define the value of this height function at the points on the boundary on the integer lattice.

After coloring the Aztec diamond like a chessboard so that the left-most plateau is a black square above a white square, we define the height function for the central point of the plateau to be zero. Increase the height incrementally when following edges of a black square clockwise or those of a white square counterclockwise (and decrease if you change directions). In an Aztec diamond, these values steadily increase as you go up the top left diagonal (see Figure 1.3b), so that between the left or right sides and the top or bottom sides of the Aztec diamond there is a very large difference in height.

For any tiling of the region, we can extend the height function of the region to the interior points of the region. We have already determined how a height function must act around a black square and a white square. Since each domino covers both one black and one white square, we can determine the height of any point on the border of a domino and thus any vertex on the integer lattice on the interior of the Aztec diamond. Notice that there is a height difference of three units across the center of any domino. As an example of the height function on a region inherited from a tiling, see Figure 1.4. The large range for the height function of an Aztec diamond puts large restrictions on the structure of tilings that can be placed in the region. In particular, a random tiling of an Aztec diamond has an intriguing structure as mentioned in Section 5.4.

For a nice visualization of the three-dimensional nature of height functions in domino tilings, see Thurston's article [41]. Height functions appear once again in Chapter 2 where they are used to determine a workable definition for Aztec pillows. Height functions also arise in lozenge tilings directly from the correspondence between tilings and the plane partitions — the height above the bottom of the "box" that the unit cubes fill is considered to be the

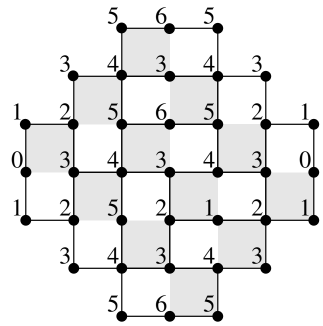

Figure 1.4: The height function of AD_3 given a particular tiling

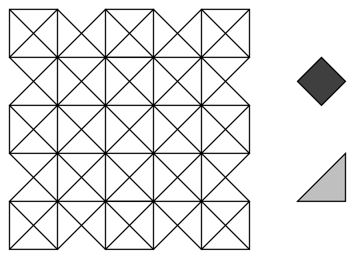

Figure 1.5: A fortress and its diforms

height of points on the interior of the region. For more information on height functions, see [8, 22, 37].

Diform tiling regions whose diforms are not always congruent are also studied. One example of such a region is called a fortress (see Figure 1.5).

One common aspect to all these regions is that the graphs are all bipartite. Limited research has been done in the non-bipartite case, but it is also based on matrix methods introduced by Kasteleyn.

1.4 Current Lines of Approach

Various useful techniques have been created by the domino community, and we are always on the lookout for more.

In counting matchings on graphs directly, sometimes it is useful to reduce one graph to another whose number of tilings is known. A tool in this vein is called Urban Renewal, presented by Jim Propp [36]. It uses the idea that we can replace one set of eight weighted edges by another set of four differently weighted edges, and when we count the weighted matchings of the first graph, it equals the number of weighted matchings of the second graph. This is a nice combinatorial technique that sometimes proves useful.

Kasteleyn uses 0-$\pm$1-$\pm i$ matrices in his work, a technique that is the basis for much work in the subject. Helfgott exploits this in his bachelor thesis work, and his result is presented in Section 3.4. Kuperberg uses representation theory in his 1998 and 2001 articles [25, 26]. Jockusch uses combinatorial methods that exploit 2-fold and 4-fold rotational symmetry in his 1994 article [18]. Ciucu uses matching generating functions in graphs with reflective symmetry in his 1996 article [7]. Kuo uses graphical condensation in his 2003 article [24].

A number of tools that have been created to take advantage of the bipartite nature of the graph. One that is often useful is called vaxmacs, a customized emacs environment written by David Wilson, into which you input a graph. This graph is written in VAX format, so called because it is full of V's, A's, and X's. It passes the corresponding Kasteleyn-Percus matrix to Maple, which takes the determinant, giving the number of tilings of the region. All the above types of graphs are representable in VAX-code, so creating a sequence of graphs to feed into vaxmacs makes data collection easier. The software and documentation for vaxmacs can be found at http://www.math.wisc.edu/~propp/software.html.

Once one collects the data, it is nice to be able to find a pattern in the data, and a couple of options are available to that end. The most famous is the On-Line Encyclopedia of Integer Sequences ([38]), but a second option exists in a Mathematica program called RATE (German for guess), where you can input the first terms of a sequence, and it will guess the next terms. The code can be found at http://www.mat.univie.ac.at/~kratt/rate/rate.html. Prime decomposition calculations have been quickened using software called PARI/GP, available for download at http://pari.math.u-bordeaux.fr/. Combinatorial arguments from Concrete Mathematics [15] and Proofs That Really Count [4] have been especially useful in the proofs provided.

Chapter 2

AZTEC PILLOWS

In this chapter, we define the central region of study whose domino tilings we enumerate and explain some tools that we will use in future chapters.

2.1 Aztec Pillows

An Aztec pillow, as it was initially presented in [35], is a rotationally symmetric region in the plane that has boundary constraints like those of Aztec diamonds. On the top left diagonal however, the steps are composed of three squares to the right for every square up. As an example, Figure 2.1 presents AP_7 and AP_{10}. The subscript on the Aztec pillow has to do with how many squares there are in the central rows; there are always $2n$ squares in each of the central rows in AP_n. This is exactly analogous to Aztec diamonds.

Because the step lengths are 3 instead of 1, this implies that the last step is either of length 2 or of length 4 depending on the parity of n. This is why when Aztec pillows were introduced in [35], they were broken into two types, "2 mod 4 pillows" and "0 mod 4 pillows", indexed by their order, or number of steps taken. The Aztec pillows in Figure 2.1 would be called a 2 mod 4 pillow of order 4 and a 0 mod 4 pillow of order 5.

Aztec pillows were singled out as interesting regions because the number of tilings appears to have an intriguing formula, as described in the following conjecture.

Propp's Conjecture. *The number of tilings of an Aztec pillow AP_n is a larger number squared times a smaller number. We write $\#AP_n = \ell_n^2 s_n$. In addition, depending on the parity of n, the smaller number s_n satisfies a simple generating function. For AP_{2m+1}, the*

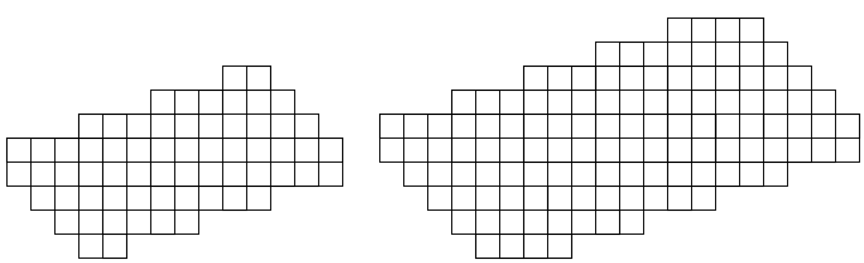

Figure 2.1: Two Aztec pillows

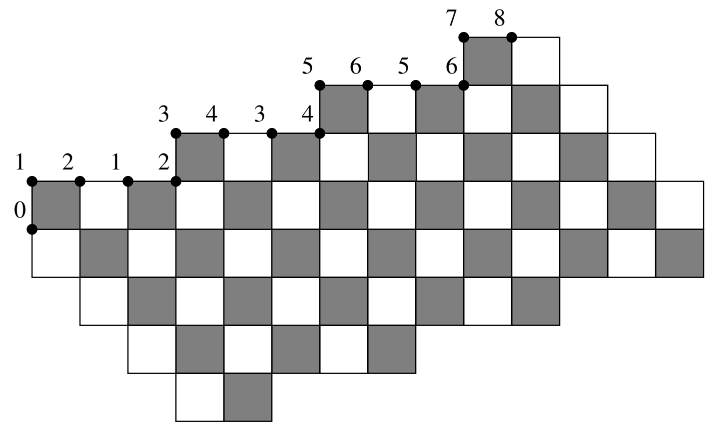

Figure 2.2: The boundary height function of the Aztec pillow AP_7

generating function is

$$\sum_{m=0}^{\infty} s_{2m+1}x^m = (5+6x+3x^2-2x^3)/(1-2x-2x^2-2x^3+x^4). \tag{2.1}$$

while for AP_{2m+2}, the generating function is

$$\sum_{m=0}^{\infty} s_{2m+2}x^m = (5+3x+x^2-x^3)/(1-2x-2x^2-2x^3+x^4), \tag{2.2}$$

Remark. The value s_n is not simply the squarefree part of $\#AP_n$. See Appendix A for a table of values for the factorization of $\#AP_n$ and the corresponding values s_n.

As described in Section 1.3, the height functions of the boundaries of Aztec diamonds increase along every step on the upper-left boundary. We might expect Aztec pillows to have such a nice formula for their number of tilings since the height function of the boundary restricts the structure of tilings similarly. Since the steps are of odd length, the height function increases as you climb each step. (See Figure 2.2.) This suggests that Aztec pillows are the next natural region that we should consider to try to understand domino tilings of regions more fully.

2.2 Generalized Aztec Pillows

After experimental calculation, it becomes clear that the above notion of a pillow can be generalized to encompass a larger family of pillows. In particular, taking the height function as a clue, we can define a generalized Aztec pillow. Hoping to increase our height function at each step, we realize that this only occurs when the steps are of odd length. We define a generalized Aztec pillow using the following definitions.

Definition. *A region R is said to be* horizontally convex *if each horizontal line meets R in a single line segment, not at all. Similarly, a region R is said to be* vertically convex *if each vertical line meets R in a single line segment or not at all. We define a region R to be* block-convex *if R is both horizontally and vertically convex.*

Definition. *A block-convex union of squares is said to satisfy the* odd-step property *if both the northern and southern boundaries of the region are composed of odd steps. For the northern boundary of the region, ensure that every up-step is composed of following one square up and an odd number of squares to the right and every down-step is composed of following an odd number of squares to the right and one square down. For the southern boundary, rotate the region 180 degrees and apply the same restriction.*

Definition. *A block-convex union of squares R is said to have a* central $m \times n$ belt *if the widest rectangle that can fit in R is of width n, the largest rectangle of width n that can fit in R has height m, and removing this $m \times n$ rectangle from R disconnects the region into two (possibly empty) subregions with maximum width $n - 1$.*

The *center* of the region with an $m \times n$ central belt will be defined to be the centroid of the $m \times n$ rectangle.

Definition. *A* generalized Aztec pillow *P is a block-convex union of squares with a central $2 \times 2n$ belt and that satisfies the odd-step property.*

Remark. This implies that a pillow will have a top half and a bottom half split through the central belt and that the plateaus on the top and the bottom of P are of even length. This also implies that on both the top half and on the bottom half, there are the same number of up-steps as down-steps. Note that when we talk about "up-steps" on the bottom half, we are talking about the up-steps on the 180-degree-rotated bottom half.

In Chapter 3, we will consider rotationally symmetric pillows with steps of length one on the upper right boundary (and symmetrically on the bottom left boundary). Otherwise, results in Sections 2.6, 3.2, 3.3, and all of Chapter 4 apply to generalized Aztec pillows.

We need a notation to discuss the more well-behaved, rotationally symmetric Aztec pillows with steps of length one on the upper right boundary. We reference the boundary information of generalized Aztec pillows by a vector of the odd step lengths and an extra index to clarify the length of the vector. We subtract 1 from the length of the top plateau so that the last entry in the vector is odd as well. For example, AP_{2n} pillows are of the form $(3, \ldots, 3, 3)_n$, while AP_{2n-1} are written $(3, \ldots, 3, 1)_n$. Note that Aztec diamonds can be also be written using this notation — $AD_n = (1, \ldots, 1)_n$.

The original Aztec pillows that Propp introduced will be referenced as 3-pillows, since their steps are all of length three (except perhaps the last step). Similarly, we will call vectors of the form $(5, \ldots, 5, i)_n$ for $i \in \{1, 3, 5\}$ the 5-pillows, and define other "odd pillows" similarly. If q is odd, we denote the n-th q pillow by AP^q_n. Through experimental calculations using vaxmacs, Maple, and PARI, it appears that odd pillows all share the form of a smaller number times the square of a larger number for their number of tilings, as discussed in Section 5.1.

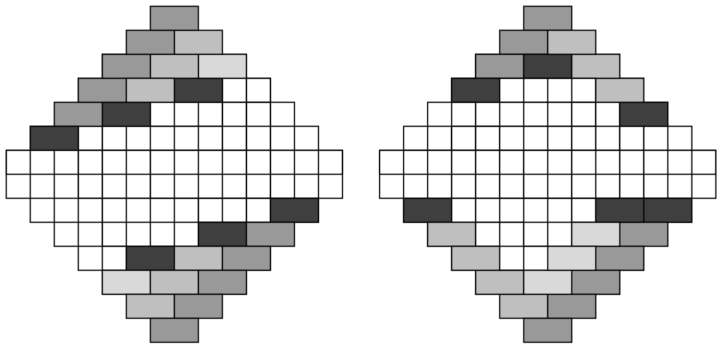

Figure 2.3: Restricting Aztec diamonds to generalized Aztec pillows

2.3 A Coordinate System for Aztec Diamonds

A useful property of generalized Aztec pillows is that they can be constructed from Aztec diamonds by placing initial dominoes in strategic positions and considering the region that results once dominoes forced by the initial dominoes are placed. We present a visualization of this property in the case of AP_7 and an arbitrary generalized Aztec pillow in Figure 2.3. The lightly shaded dominoes are the dominoes that are forced by the initial placement of the darker dominoes and thus would be included in any tiling of the pillow that includes the darker dominoes.

We need not place many dominoes to arrive at a pillow. To restrict AD_n to AP_n, we need $n-1$ dominoes if n is odd and n dominoes if n is even. In general, if the generalized Aztec pillow P is of type $(i_1, \ldots, i_k)_k$, then we can construct P from the Aztec diamond of order $n = \left(k + \sum_{j=1}^{k} i_j\right)/2$ by placing $n-k$ dominoes in both the top and the bottom halves of AD_n. For example, in Figure 2.3a, we see how to create the pillow AP_7 from AD_7 using 3 pairs of dominoes (the ones that are darkly shaded).

To be able to refer to specific blocks in an Aztec diamond, we need a coordinate system. For an illustrating example, consider the Aztec diamond of order 4 shown in Figure 1.3 in Chapter 1. We will label and give coordinates to both the black and white squares as shown in Figure 2.4. In general, for the Aztec diamond of size n, there are $n(n+1)$ squares of each color. The coordinates (x, y) of white squares satisfy all values $1 \leq x \leq n+1$, and $1 \leq y \leq n$; whereas the coordinates (x', y') of black squares satisfy all values $1 \leq x' \leq n$ and $1 \leq y' \leq n+1$. These coordinates will be of particular use in Sections 3.4 – 3.6, as will the Krawtchouk polynomials presented in the next section.

2.4 The Binary Krawtchouk Polynomials

The *Krawtchouk polynomial* $\mathrm{kr}(j, n, k)$ is the coefficient of x^j in the polynomial expression $(1-x)^k(1+x)^{n-k}$. Two references for these polynomials are [23, 29].

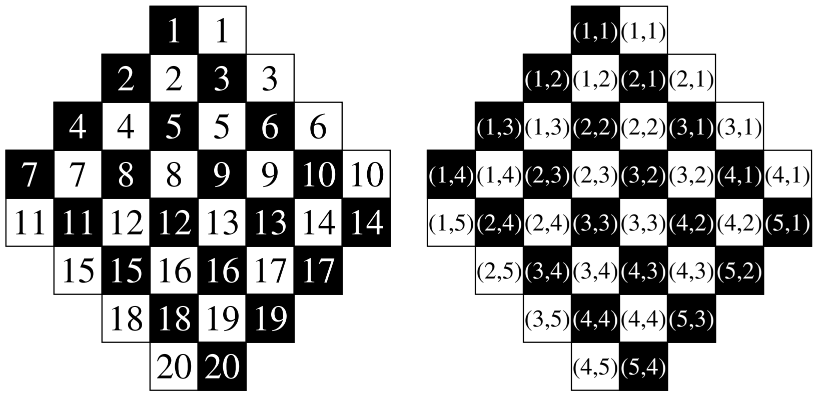

Figure 2.4: Square positions and coordinates

Some useful manipulations that Krawtchouk polynomials satisfy include

$$\operatorname{kr}(a, n, c) = (-1)^c \operatorname{kr}(n-a, n, c), \tag{2.3}$$

$$\operatorname{kr}(a, n, c) = (-1)^a \operatorname{kr}(a, n, n-c), \tag{2.4}$$

which are useful for symmetric arguments,

$$\operatorname{kr}(a, n, c) = \operatorname{kr}(a-1, n-1, c) + \operatorname{kr}(a, n-1, c), \tag{2.5}$$

which is useful for recurrences, and

$$\sum_{i=0}^{n} \operatorname{kr}(a, n, i) \operatorname{kr}(i, n, b) = \delta_{ab} 2^n, \tag{2.6}$$

which exhibits one of their orthogonality properties. These are all taken from [23].

2.5 *The Gessel-Viennot Method*

The Gessel-Viennot method was introduced in [13, 14], and has its roots in works by Karlin and McGregor [20] and Lindström [27]. A nice exposition of the method is given in [1]. The Gessel-Viennot method is a determinantal method to count vertex-disjoint path systems in an acyclic directed graph G with k sources s_i and k sinks t_j for $1 \leq i, j \leq k$. An example of such a system is given in Figure 2.5.

A vertex-disjoint path system $\mathcal{P}$ is a collection of k vertex-disjoint paths from s_i to $t_{\sigma(i)}$ for some $\sigma \in S_k$ (where S_k is the symmetric group on k elements). Call a path system $\mathcal{P}$ positive if the sign of this permutation σ satisfies $\operatorname{sgn}(\sigma) = +1$ and negative if $\operatorname{sgn}(\sigma) = -1$. Let p^+ be the number of positive vertex-disjoint path systems and p^- be the number of negative vertex-disjoint path systems.

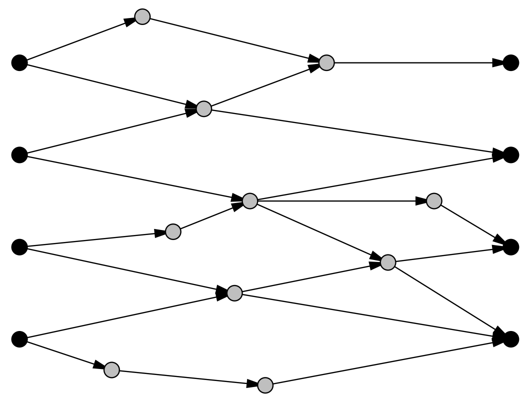

Figure 2.5: A directed graph with four sources and four sinks

Corresponding to this graph G is a $k \times k$ matrix $A = (a_{ij})$ where a_{ij} is the number of paths from s_i to t_j. The result of Gessel and Viennot states that $\det A = p^+ - p^-$. For the example in Figure 2.5, the matrix A is

$$A = \begin{bmatrix} 2 & 1 & 0 & 0 \\ 1 & 2 & 2 & 0 \\ 0 & 1 & 3 & 3 \\ 0 & 0 & 1 & 3 \end{bmatrix}.$$

The determinant of A is 8. This corresponds the eight path systems in Figure 2.6. Notice that there are no negative path systems in this example since the only permutation occurring in a path system to be (1234), an even permutation of (1234). For some additional applications of the Gessel-Viennot method, see [9, 13, 30].

In Chapter 4, we prove an analogue of the Gessel-Viennot method for counting cycle systems on a type of graph we call a hamburger graph, which has applications to counting domino tilings of generalized Aztec pillows.

2.6 Non-Intersecting Lattice Paths in Generalized Aztec Pillows

Given a generalized Aztec pillow region R with k_1 steps in the upper half and k_2 steps in the lower half, we can apply the Gessel-Viennot method to count the number of domino tilings of R in four distinct ways.

We create a bijection between domino tilings of the region R and non-intersecting lattice paths determined by the structure of R.

Overlaying the standard "chessboard" coloring of the squares in R on any domino tiling, the dominoes break into four classes depending on their color scheme. To each class we associate one or zero edges inside. The classes and their associated interior edges are presented in Figure 2.7. By construction, the interior edges link together to form paths that enter the region R on the left of the region at white squares and leave R on the right at

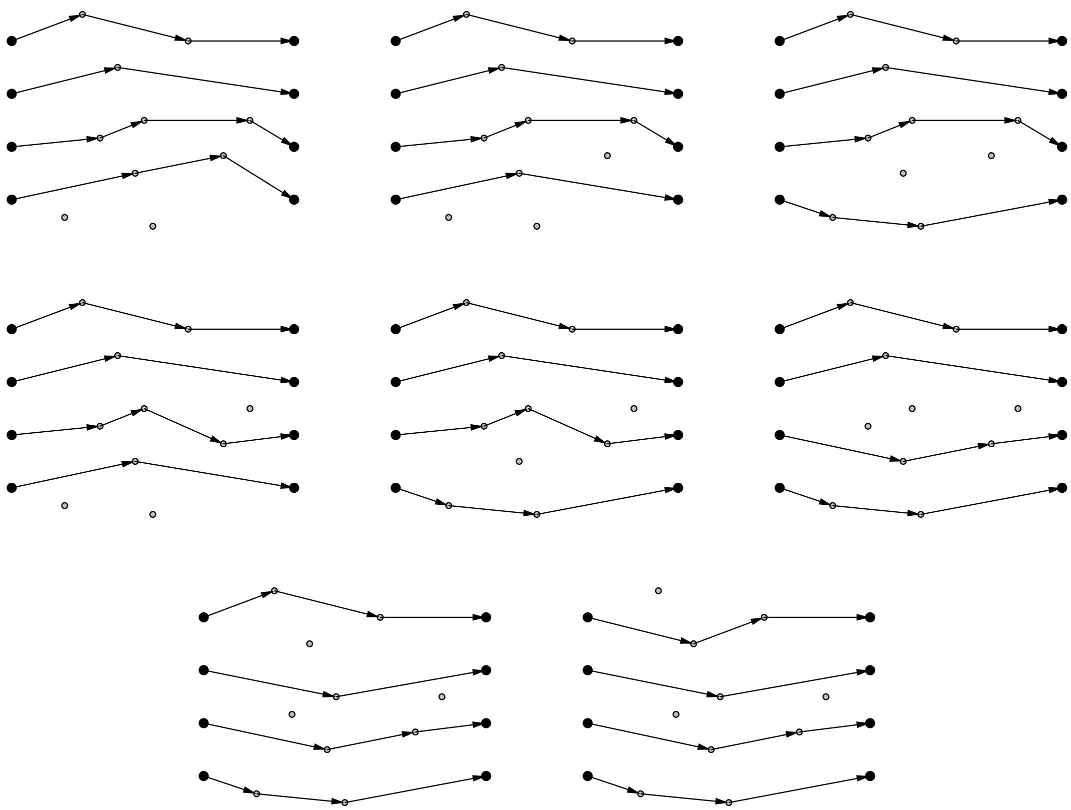

Figure 2.6: The eight path systems for the directed graph in Figure 2.5

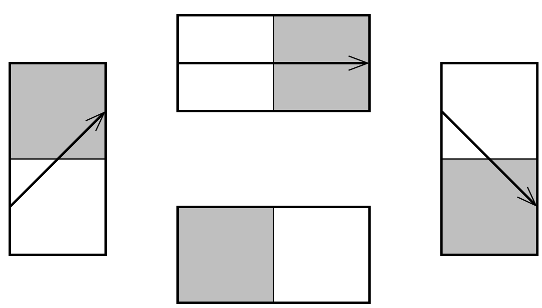

Figure 2.7: The four classes of colored dominoes and their associated edges

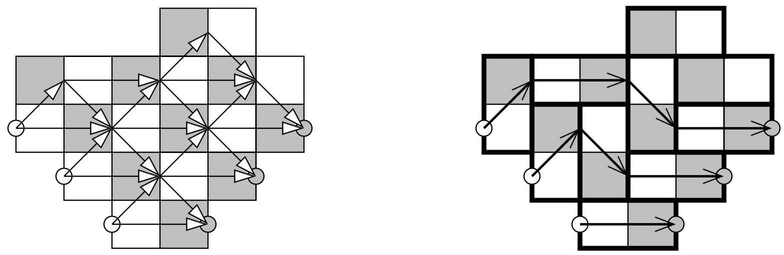

Figure 2.8: The horizontal lattice in a generalized Aztec pillow and a path system example

black squares and are non-intersecting. In this way, we associate to each domino tiling of R a path system of k_2 paths on the lattice of all possible paths. See Figure 2.8 for an example of a generalized Aztec pillow, its associated lattice, and the correspondence between a domino tiling and its path system.

Rotating the region 90 degrees and reversing the coloring produces a region to which we can apply the same method and find path systems of n paths. We will call the former application of Gessel-Viennot the *horizontal case* and the latter application the *vertical case.* If there is no rotational symmetry, we can rotate and invert colors twice more, giving four distinct ways to apply the Gessel-Viennot method to one region. In particular, we can calculate the number of tilings of R by taking the determinant of a $k \times k$ matrix, where $k = \min(k_1, k_2)$.

Analysis of the experimental results found using this method are presented in Section 5.2.

2.7 The Schur Complement

The Schur complement calculation is a nice way to reduce the size of the calculation of a determinant in question. For any $n \times n$ block matrix of the form

$$A = \begin{bmatrix} A_1 & A_{12} \\ A_{21} & A_2 \end{bmatrix}$$

with A_1 a $k \times k$ matrix and A_2 a $(n-k) \times (n-k)$ matrix, we can derive a matrix C of the form

$$C = \begin{bmatrix} I_k & 0 \\ -A_{21}A_1^{-1} & I_{n-k} \end{bmatrix}$$

that has determinant 1. This implies that the determinant of

$$CA = \begin{bmatrix} A_1 & A_{12} \\ 0 & A_2 - A_{21}A_1^{-1}A_{12} \end{bmatrix}$$

has the same determinant as A. The matrix $A_2 - A_{21}A_1^{-1}A_{12}$ is called the *Schur complement* of A_1 in A.

We will use this handy calculation in Section 4.5.

Chapter 3

COMBINATORIAL AND MATRIX THEORETICAL RESULTS

In this chapter, we discuss purely combinatorial results and matrix theoretical results about generalized Aztec pillows. In Section 3.1, we explain the limited combinatorial results available using the method of inclusion-exclusion. In addition to the combinatorial approaches to Aztec pillows, matrix theoretical results appear as well. In Section 3.2, a prevalent type of matrix is introduced. This type of matrix allows us to prove a special case of a theorem of Jockusch, which we do from the Kasteleyn matrix in Section 3.3. An additional matrix theoretical line of approach uses Helfgott's Theorem. This theorem is presented in Section 3.4 and is used to prove additional explicit results about generalized Aztec pillows in the final sections of this chapter.

3.1 Combinatorial Approaches to Aztec Pillows

Domino tilings of Aztec pillows are combinatorial objects, yet an intuitive combinatorial approach does not produce many results. One can quickly prove a formula for $\#(1,\ldots,1,3)_n$, but the $\#(1,\ldots,1,3,1)_n$ case is elusive, and any more complicated pillow seems unthinkable.

The region $R = (1,\ldots,1,3)_{n-1}$ can be thought of as the Aztec diamond AD_n with a horizontal domino forced in the top and bottom positions. There is a nice combinatorial argument to prove the formula for $\#R$.

Consider tiling AD_n in any way. There are $2^{n(n+1)/2}$ ways to do this, by Equation 1.2. On the other hand, we can break down the number of tilings of AD_n into cases. We can place a horizontal domino in both the top and bottom rows in $\#R$ ways. Otherwise, there would be some vertical tile in either the top or the bottom rows. By Inclusion-Exclusion, we can count the number of ways to tile AD_n with some vertical tile in the top row, add the

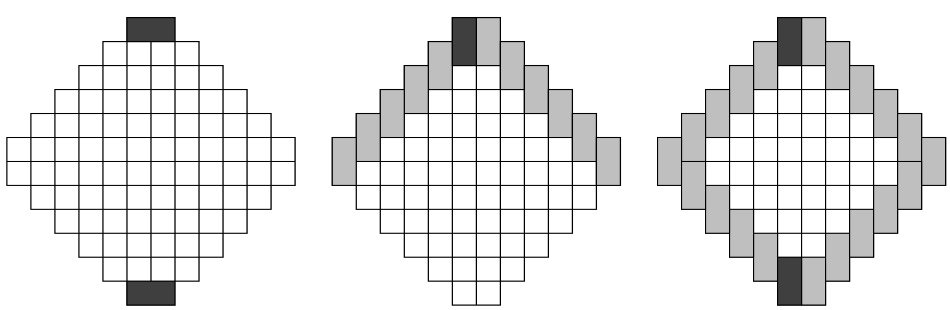

Figure 3.1: Combinatorial proof of $\#(1,\ldots,1,3)_n$ formula

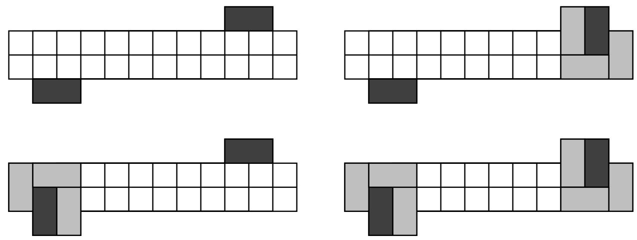

Figure 3.2: Combinatorial proof of $\#AP^q_{(q+3)/2}$ formula

number of ways to tile with some vertical tile in the bottom row (each produces an AD_{n-1}), and subtract the overcounting of the cases when you place vertical dominoes in both the top and the bottom rows of AD_n, which results in an AD_{n-2}. (See Figure 3.1.)

This implies that

$$\#(1,\dots,1,3)_{n-1} = 2^{n(n+1)/2} - 2\cdot 2^{(n-1)n/2} + 2^{(n-2)(n-1)/2} = 2^{(n-1)(n-2)/2}\left(2^{2n-1} - 2^n + 1\right). \tag{3.1}$$

Trying to use the same approach for $(1,\dots,1,3,1)_{n-1}$ runs into problems because the resulting regions do not decompose into Aztec diamonds.

Another region that lends itself to combinatorial analysis is the region $AP^q_{(q+3)/2}$. Remember that one interpretation of the n-th Fibonacci numbers f_n (Sequence A000045 in [38]) is the number of domino tilings of the $2\times 2n$ rectangle. Since for $1 \le n \le \frac{q+1}{2}$, the region AP^q_n is a $2\times 2n$ rectangle, the formula $\#AP^q_n = f_n$ holds. It is perhaps mysterious however that the Fibonacci numbers appear in the next term $AP^q_{(q+3)/2}$ — we have that $\#AP^q_{(q+3)/2} = 2^2 f_{q+1}$. We prove this result combinatorially.

We condition on the position of the dominoes covering the top right square and the bottom left square. Consulting Figure 3.2, there are four cases. When the two dominoes are horizontal, the number of ways to tile the board is f_{q+3}. When one of the two dominoes is horizontal, the number of ways to tile the board is f_q; this happens twice. When both of the two dominoes are vertical, the number of ways to tile the board is f_{q-3}. Simplifying the sum $f_{q+3} + 2f_q + f_{q-3}$ using the Fibonacci recurrence $f_n = f_{n-1} + f_{n-2}$ gives the desired result, $\#AP^q_{(q+3)/2} = 2^2 f_{q+1}$. Similar analyses for other simple boards do not yield Fibonacci numbers so their formulas are not as simple.

3.2 Alternating Centrosymmetric Matrices

Define J to be the *exchange matrix* with 1's along the cross-diagonal. Matrices A such that $JAJ = A$ are called *centrosymmetric* and have been studied in much detail because of their applications in wavelets and other areas (see [31, 42]). A matrix such that $JAJ = -A$ is called *skew-centrosymmetric*. In the article by Tao and Yasuda, they define a generalization of these matrices for any involutory matrix K ($K^2 = I$), where a *generalized* *centrosymmetric K-matrix* A is a matrix such that $KAK = A$ (see [2, 40]). Generalized skew-centrosymmetric K-matrices are defined to be matrices such that $KAK = -A$.

In the study of generalized Aztec pillows, a related type of matrix arises. Define a matrix K to be *anti-involutory* if $K^2 = -I$. If K is an $n \times n$ matrix for $n = 2k$ even, we can write

$$K = \begin{pmatrix} K_1 & K_2 \\ K_3 & K_4 \end{pmatrix},$$

with each submatrix K_i being of size $k \times k$. Extend the definition of generalized centrosymmetric matrices to include these matrices, i.e., a matrix is a generalized centrosymmetric K-matrix if $KAK = A$, and similarly for skew matrices.

A simple case of such an anti-involutory matrix is when $K_1 = K_4 = 0$. In this case, $K_3 = -K_2^{-1}$, so we can write

$$K = \begin{pmatrix} 0 & K_2 \\ -K_2^{-1} & 0 \end{pmatrix}. \tag{3.2}$$

For such a matrix K, a matrix A that is a generalized centrosymmetric K-matrix has a simple form for its determinant.

Theorem 1. *If K is an anti-involutory matrix of the form in Equation 3.2, and the $2k \times 2k$ matrix A is a generalized centrosymmetric K-matrix, then A has the form*

$$A = \begin{pmatrix} B & CK_2 \\ K_2^{-1}C & -K_2^{-1}BK_2 \end{pmatrix}.$$

In addition, $\det A = (-1)^{m+1} \det(B + iC) \det(B - iC)$

Proof: Calculating the conditions for which a matrix

$$A = \begin{pmatrix} A_1 & A_2 \\ A_3 & A_4 \end{pmatrix}$$

is a generalized centrosymmetric K-matrix for matrices K of the form given in Equation 3.2 gives us that $K_2^{-1}A_2 = A_3K_2$ and $A_4 = -K_2^{-1}A_1K_2$. This means we can write

$$A = \begin{pmatrix} B & CK_2 \\ K_2^{-1}C & -K_2^{-1}BK_2 \end{pmatrix},$$

for $B = A_1$ and $C = -A_2K_2^{-1}$. With this rewriting, $\det A$ is simple to compute:

$$\begin{aligned}
\det A &= \det \begin{pmatrix} B & CK_2 \\ K_2^{-1}C & -K_2^{-1}BK_2 \end{pmatrix} \\
&= \det \begin{pmatrix} I & 0 \\ -iK_2^{-1} & I \end{pmatrix} \det \begin{pmatrix} B & CK_2 \\ K_2^{-1}C & -K_2^{-1}BK_2 \end{pmatrix} \det \begin{pmatrix} I & 0 \\ -iK_2^{-1} & I \end{pmatrix} \\
&= \det \begin{pmatrix} B - iC & CK_2 \\ 0 & -K_2^{-1}(B + iC)K_2 \end{pmatrix} \\
&= (-1)^k \det(B + iC) \det(B - iC).
\end{aligned}$$

•

$$\begin{pmatrix} a_1 & a_2 & a_3 & a_4 & a_5 & a_6 \\ a_7 & a_8 & a_9 & a_{10} & a_{11} & a_{12} \\ a_{13} & a_{14} & a_{15} & a_{16} & a_{17} & a_{18} \\ a_{18} & -a_{17} & a_{16} & -a_{15} & a_{14} & -a_{13} \\ -a_{12} & a_{11} & -a_{10} & a_9 & -a_8 & a_7 \\ a_6 & -a_5 & a_4 & -a_3 & a_2 & -a_1 \end{pmatrix}$$

Figure 3.3: The general form of a 6×6 alternating centrosymmetric matrix

Corollary 2. *The determinant of such a matrix A is the sum of two squares (perhaps up to a sign), where the two squares are the real and imaginary parts of* $\det(B + iC)$.

In the case of a generalized skew-centrosymmetric K-matrix A, the analogous result states that A has the form

$$A = \begin{pmatrix} B & CK_2 \\ -K_2^{-1}C & K_2^{-1}BK_2 \end{pmatrix}$$

and that $\det A = \det(B + iC)\det(B - iC)$, with no sign term.

Consider the specific case when the $2k \times 2k$ matrix K is the *alternating exchange matrix* — the matrix with its cross-diagonal populated with alternating 1's and -1's, starting in the upper-right corner. Such a matrix K is anti-involutory. Had K been square of odd order, this matrix would be involutory instead of anti-involutory.

Definition. *Let K be the alternating exchange matrix. We define an $n \times n$ matrix A to be* alternating centrosymmetric *if $KAK = A$ or* alternating skew-centrosymmetric *if $KAK = -A$.*

Another classification of $n \times n$ alternating centrosymmetric matrices is that their entries satisfy $a_{i,j} = (-1)^{i+j+1} a_{n+1-i,n+1-j}$. An $n \times n$ alternating skew-centrosymmetric matrix has entries that satisfy $a_{i,j} = (-1)^{i+j} a_{n+1-i,n+1-j}$. For an example of such a matrix, see Figure 3.3.

By Theorem 1, we know that the determinant of an alternating centrosymmetric matrix is the sum of two squares. We now present a different version of its determinant with additional symmetry built in.

We first define a set of k-member subsets of $[2k]$. Take a subset I of $[k]$. Create $\widetilde{I}$ by taking $I \cup I'$, where $i \in I'$ if $2k + 1 - i \in [k] \setminus I$. In this way, each $\widetilde{I}$ has k members. We will call subsets of $[2k]$ of this form *complementary*. We will define the sets S, S', T, and T' of subsets of $[2k]$. If I has ℓ elements,

$$\text{place } \widetilde{I} \text{ into set } \begin{cases} S & \text{if } \ell \equiv 0 \mod 4, \\ T & \text{if } \ell \equiv 1 \mod 4, \\ S' & \text{if } \ell \equiv 2 \mod 4, \text{ or} \\ T' & \text{if } \ell \equiv 3 \mod 4. \end{cases}$$

Given a $2k \times 2k$ matrix N, we define $M(\widetilde{I})$ to be the $k \times k$ submatrix of N with columns restricted to $j \in \widetilde{I}$, and rows restricted to the first k rows of N.

Theorem 3. *The formula for the determinant of an alternating centrosymmetric matrix A satisfies*

$$(-1)^k \det A = \left[\sum_{\widetilde{I}\in S} \det(M(\widetilde{I})) - \sum_{\widetilde{I}\in S'} \det(M(\widetilde{I}))\right]^2 + \left[\sum_{\widetilde{I}\in T} \det(M(\widetilde{I})) - \sum_{\widetilde{I}\in T'} \det(M(\widetilde{I}))\right]^2. \tag{3.3}$$

Proof: Let L be the upper-right $k \times k$ submatrix of the alternating exchange matrix K. As in the proof of Theorem 1, we write $\det A = \det(B + iC)\det(B - iC)$, where $B = A_1$ and $C = -A_2 L^{-1}$. We calculate the real and imaginary parts of $\det(B + iC)$. Writing out explicitly $B + iC$ gives

$$B + iC = \begin{pmatrix} a_{1,1} + ia_{1,2k} & a_{1,2} - ia_{1,2k-1} & \dots & a_{1,k} + (-1)^{k+1} ia_{1,k+1} \\ a_{2,1} + ia_{2,2k} & a_{2,2} - ia_{2,2k-1} & \dots & a_{2,k} + (-1)^{k+1} ia_{2,k+1} \\ \vdots & \vdots & & \vdots \\ a_{k,1} + ia_{k,2k} & a_{k,2} - ia_{k,2k-1} & \dots & a_{k,k} + (-1)^{k+1} ia_{k,k+1} \end{pmatrix}. \tag{3.4}$$

Define b_j to be the column $b_j = (a_{1,j}, a_{2,j}, \dots, a_{k,j})^T$. By linearity of determinants, $\det(B + iC)$ is the sum of 2^k determinants of matrices M with dimensions $k \times k$, where in column j we can choose to place either b_j or $i(-1)^{j+1} b_{2k+1-j}$. Given any determinant of this form, we can convert it into a form where the indices of the columns are increasing: $\widetilde{I} = i_1 < \dots < i_r < k + 1/2 < i_{r+1} < \dots < i_k$. Note that $\widetilde{I}$ is complementary as defined above. When we do this and account for changes of sign by interchanging columns, the matrix M becomes

$$M = \begin{pmatrix} a_{1,i_1} & \dots & a_{1,i_r} & i(-1)^{k+1} a_{1,i_{r+1}} & \dots & i(-1)^{k+1} a_{1,i_k} \\ a_{2,i_1} & \dots & a_{2,i_r} & i(-1)^{k+1} a_{2,i_{r+1}} & \dots & i(-1)^{k+1} a_{2,i_k} \\ \vdots & & \vdots & \vdots & & \vdots \\ a_{k,i_1} & \dots & a_{k,i_r} & i(-1)^{k+1} a_{k,i_{r+1}} & \dots & i(-1)^{k+1} a_{k,i_k} \end{pmatrix}. \tag{3.5}$$

The determinant of this matrix is $(i(-1)^{k+1})^{k-r}$ times $\det(M(\widetilde{I}))$. In particular, matrices such that $(k-r) \equiv 0 \mod 2$ contribute to the real part of $\det(B+iC)$, while matrices such that $(k-r) \equiv 1 \mod 2$ contribute to the imaginary part of $\det(B + iC)$. In addition, the value of $(k - r)$ mod 4 determines the sign of the matrix in the sum.

This establishes the theorem. •

A similar approach gives an analogous statement for alternating skew-centrosymmetric matrices — The formula for the determinant of an alternating skew-centrosymmetric matrix A satisfies

$$\det A = \left[\sum_{\widetilde{I}\in S} \det(M(\widetilde{I})) - \sum_{\widetilde{I}\in S'} \det(M(\widetilde{I}))\right]^2 + \left[\sum_{\widetilde{I}\in T} \det(M(\widetilde{I})) - \sum_{\widetilde{I}\in T'} \det(M(\widetilde{I}))\right]^2. \tag{3.6}$$

Just as in the analogous statement of Theorem 1, there is no $(-1)^k$ term that appears.

3.3 Jockusch's Theorem and Rotationally Symmetric Generalized Aztec Pillows

A certain symmetry property of a bipartite graph allows us to say something about its number of matchings.

Definition. *A 2-even symmetric graph G is a connected planar bipartite graph such that a 180 degree rotation R_2 about the origin maps G to itself and the length of a path between v and $R_2(v)$ is even.*

A result of William Jockusch states that if a graph is 2-even symmetric then the number of matchings of the graph is a sum of squares [18]. Jockusch's result produces a weighted labeling function u of the quotient graph G_2 involving complex numbers. Counting the number of weighted matchings associated to u, denoted $M_u(G_2)$, gives a value such that the number of matchings of G is $M_u(G_2)\overline{M_u(G_2)}$, resulting in a sum of two squares.

In the specific case of 2-even symmetric graphs that can be embedded in the square lattice in a 2-even symmetric way, Theorem 1 allows us to prove this result in a new way that relies only on the structure of the Kasteleyn-Percus matrix of the region.

Our representation of the square lattice in the standard x-y coordinates will place vertices at $(2k+1, 2\ell+1)$ for $k, \ell \in \mathbb{Z}$, so that the center of rotation $(0,0)$ is the centroid of some square in the lattice. We color the vertices white if $k+\ell$ is even and black if $k+\ell$ is odd.

The Kasteleyn-Percus matrix A of a bipartite graph $G=(V,E)$ has $|V|/2$ rows representing the white vertices and $|V|/2$ columns representing the black vertices. The non-zero entries a_{ij} of A are exactly those that have an edge between white vertex w_i and black vertex b_j. These entries are all $+1$ or -1 depending on the position of the edges they represent in the graph — the restriction is that closed cycles have a net -1 product. In the case of the square lattice above, this condition corresponds most nicely to giving entries the value -1 if they correspond to edges that are of the form $e=(v_1\,v_2)$ with $v_1=(2k-1, 2\ell+1)$ and $v_2=(2k+1, 2\ell+1)$ and such that v_1 is black. This is most easily understood by giving orientations to the edges of the lattice as in Figure 3.4, and assigning an edge the value $+1$ if the edge goes from black to white and the value -1 if the edge goes from white to black.

With this definition of the Kasteleyn-Percus matrix, we formulate our theorem.

Theorem 4. *The Kasteleyn-Percus matrix A of a 2-symmetric graph G embedded in the square lattice is alternating centrosymmetric.*

Proof: We label the black and white vertices to determine the positions of the $+1$ and -1 entries in A. After an initial labeling, we interchange rows and columns as necessary to manipulate the matrix into being alternating centrosymmetric.

Embedded in this lattice, half the vertices of G lie above the horizontal line through the origin. Coloring the vertices of G the color they inherit from the lattice coloring above, R_2 takes vertices to counterparts of the same color so m vertices of each color are in the upper half of the graph and there are $4m$ vertices in all.

Label all white vertices v in the upper half of graph with values 1 to m, and do the same for black vertices w. For each vertex x with value i, label $R_2(x)$ with value $2m+1-i$.

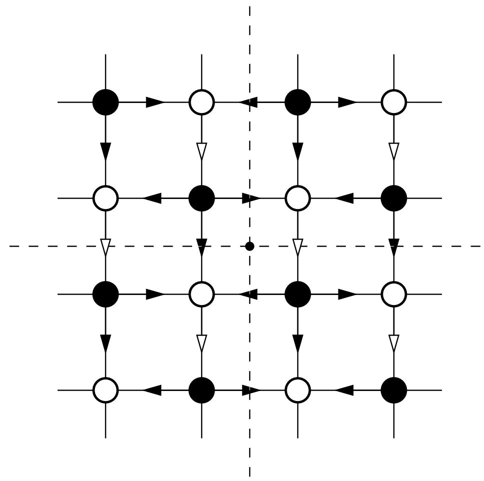

Figure 3.4: The canonical orientation of edges on the square lattice

From this initial numbering of vertices, we wish to modify some labels so that the labels in each row of the square lattice are of the same parity. Note that each vertex and its counterpart have opposite parity. Start with the top row. For each vertex that is labeled with an even number, switch its label with its counterpart. In this way, all elements in the top row will have an odd value. For the second row, exchange a vertex's label with its counterpart's if it has an odd value. Continue in this fashion until all odd rows have vertices with odd labels and all even rows have vertices with even values. After determining all rows above the horizontal line through the origin, the rest of the rows come for free.

By this construction, for any horizontal edge (v_i, w_j) in G', we know that i and j are of the same parity. Similarly, we know that any vertical edge (v_i, w_j) has i and j of opposite parity. In addition, this implies that the rotation of a vertical edge by R_2 results in the opposite sign appearing in the Kasteleyn-Percus matrix.

Since (v_i, w_j) is a horizontal edge if and only if (v_{2m+1-i}, w_{2m+1-j}) is a horizontal edge, a $+1$ appears in position $a_{(i,j)}$ for $i+j$ even if and only if $a_{(2m+1-i,2m+1-j)}$ is $+1$. Similarly, if (v_i, w_j) is a vertical edge, then so is (v_{2m+1-i}, w_{2m+1-j}), and their entries in A are opposite. This occurs exactly where $i+j$ is odd. All other entries are zero, so for those $a_{i,j}$ we have $a_{(i,j)} = \pm a_{(2m+1-i,2m+1-j)}$.

These conditions imply that entry $a_{(i,j)}$ equals $(-1)^{i+j} a_{(2m+1-i,2m+1-j)}$, which implies A is alternating centrosymmetric, as desired. •

From Theorem 1, we have the following corollary.

Corollary 5 (Jockusch). *The number of matchings of a 2-even-symmetric graph embedded in the square lattice is a sum of two squares.*

Since the dual graph of a rotationally symmetric generalized Aztec pillow is 2-even-symmetric and is already a subgraph of the square lattice, the following corollary also holds.

Corollary 6. *The number of tilings of a rotationally-symmetric Aztec pillow embedded in the square lattice is a sum of two squares.*

3.4 Helfgott's Theorem

Given a subregion S of a tiling region R such that the complement $R \setminus S$ of S in R is tilable, Rick Kenyon wrote an article that explained how to calculate the ratio of $\#(R \setminus S)/\#R$ [22]. In particular, S must be made up of an equal number of black and white vertices. The basic idea is that a certain subdeterminant of the inverse of a Kasteleyn matrix gives this ratio, so knowing how to calculate the entries of this matrix allows determination of the ratio $\#S/\#R$ with relatively few calculations.

In his Bachelor thesis [17], Harald Helfgott calculated what these matrix entries are explicitly for when R is the Aztec diamond. In this way, using the coordinate system from Figure 2.4, he proved that there is a formula involving a determinant for the ratio of the number of tilings of the restricted region over the number of tilings of the Aztec diamond. He gives the following result:

> The probability of a pattern covering white squares $v_1, \dots, v_k$, and black squares $w_1, \dots, w_k$ of an Aztec diamond of order n is equal to the absolute value of $|c(v_i, w_j)|_{i,j=1,\dots,k}$. The coupling function $c(v, w)$ at white square v and black square w is
>
> $$2^{-n} \sum_{j=0}^{x_i-1} \mathrm{kr}(j, n, y_i - 1)\, \mathrm{kr}(y'_i - 1, n-1, n-(j+x'_i - x_i)) \tag{3.7}$$
>
> for $x'_i > x_i$ and
>
> $$-2^{-n} \sum_{j=x_i}^{n} \mathrm{kr}(j, n, y_i - 1)\, \mathrm{kr}(y'_i - 1, n-1, n-(j+x'_i - x_i)) \tag{3.8}$$
>
> for $x'_i \leq x_i$, where (x_i, y_i) and (x'_i, y'_i) are the coordinates of v and w in the coordinate system in Figure 2.4, and $\mathrm{kr}(j, n, k)$ is the Krawtchouk polynomial.

This coupling function is difficult to manipulate but it has some nice properties. The coupling matrix that arises from the placement of dominoes to form an Aztec pillow has a particularly nice form.

Theorem 7. *The coupling matrix of an Aztec pillow is alternating centrosymmetric or alternating skew-centrosymmetric.*

Proof: An Aztec pillow can be derived from an Aztec diamond by a placement of dominoes that is symmetric with respect to a rotation by 180 degrees. In essence, this means that for every white square in position $v_1 = (x_1, y_1)$ and black square in position

$w_1 = (x'_1, y'_1)$ in the coordinates of Figure 2.4, there is a white square in position $v_2 = (n+1-x_1, n+2-y_1)$ and a black square in position $w_2 = (n+2-x'_1, n+1-y'_1)$. (Note that we do not require v_1 and w_1 to be in the same domino.)

Given this relation, we can calculate the relationship between $c(v_1, w_1)$ and $c(v_2, w_2)$. Without loss of generality, assume that $x'_1 \leq x_1$ (or else switch the v_i's and w_i's). This implies that $-x_1 \leq -x'_1$, which implies that $x_2 = n+1-x_1 < n+2-x'_1 = x'_2$, so we know which of Equations 3.7 or 3.8 we need to apply in the various cases.

Making extensive use of Equations 2.3 and 2.4, we have that $c(v_2, w_2)$ is equal to

$$\begin{aligned}
&= 2^{-n} \sum_{j=0}^{n-x_1} \mathrm{kr}(j, n, n+1-y_1)\, \mathrm{kr}(n-y'_1, n-1, n-(j+(n+2-x'_1)-(n+1-x_1))) \\
&= 2^{-n} \sum_{j=0}^{n-x_1} \mathrm{kr}(j, n, n-(y_1-1))\, \mathrm{kr}(n-1-(y'_1-1), n-1, n-1-(j-x'_1+x_1)) \\
&= 2^{-n} \sum_{j=x_1}^{n} \mathrm{kr}(n-j, n, n-(y_1-1))\, \mathrm{kr}(n-1-(y'_1-1), n-1, n-1-(n-(j+x'_1-x_1))) \\
&= 2^{-n} \sum_{j=x_1}^{n} (-1)^{n-(y_1-1)}(-1)^j\, \mathrm{kr}(j, n, y_1-1) \cdot \\
&\qquad\qquad (-1)^{n-1-(y'_1-1)}(-1)^{n-(j+x'_1-x_1)}\, \mathrm{kr}(y'_1-1, n-1, n-(j+x'_1-x_1)) \\
&= (-1)^{n+x_1+x'_1+y_1+y'_1} \left(-2^{-n} \sum_{j=x_1}^{n} \mathrm{kr}(j, n, y_1-1)\, \mathrm{kr}(y'_1-1, n-1, n-(j+x'_1-x_1)) \right) \\
&= (-1)^{n+x_1+x'_1+y_1+y'_1}\, c(v_1, w_1). \qquad (3.9)
\end{aligned}$$

Notice that for $v_i = (x_i, y_i)$ and $w_j = (x'_j, y'_j)$, we have that

$$(-1)^{x_i+y_i+x'_j+y'_j} = -1 \cdot (-1)^{x_i+y_i+x'_{2d+1-j}+y'_{2d+1-j}}$$

and therefore for fixed v_i, the sequence $Q(j) = (-1)^{x_i+y_i+x'_j+y'_j}$ is antisymmetric, in that $Q(j) = -Q(2d+1-j)$. Therefore we can relabel the vertices w_j such that the sequence $Q(j)$ becomes $(1, -1, \ldots, 1, -1)$ by exchanging w_j and w_{2d+1-j} if necessary. Relabeling the vertices v_i in the same way gives us that $(-1)^{x_i+y_i} = (-1)^i$ and $(-1)^{x'_j+y'_j} = (-1)^j$. This means that Equation 3.9 implies that the entries in the newly indexed coupling matrix satisfy $a_{2d+1-i,2d+1-j} = (-1)^{n+i+j} a_{i,j}$, implying that the coupling matrix is either alternating centrosymmetric or alternating skew-centrosymmetric, depending on the parity of n. •

This proof also provides for a new proof of Jockusch's Theorem, now restricted to the case when the region is a subgraph of an Aztec diamond graph.

Corollary 8. *The number of matchings of a rotationally symmetric subgraph of an Aztec diamond is the sum of two squares.*

Notice that there are no signs multiplying the sum of squares because Helfgott's Theorem includes an absolute value term. Since any 2-symmetric region that can be embedded in the square lattice can be thought of as a subgraph of a large enough Aztec diamond graph, this also reproves Theorem 4.

3.5 Calculating $\#(1,\dots,1,3)_n$ using Helfgott's Theorem

The simplest application of Helfgott's theorem is when there are only two dominoes restricting positions in the Aztec diamond. One example of those cases is when the dominoes are placed at the very top and bottom of AD_n. In this case, we find the region $(1,\dots,1,3)_n$, of which we calculated the number of tilings in Section 3.1. We can now verify this formula independently using Helfgott's theorem.

We calculate $(1,\dots,1,3)_{n-1}$. The coordinates from Figure 2.4 of the white and black squares covered by the dominoes (cells numbered 1 and $n(n+1)$ in AD_n) are:

$$\begin{array}{cc} (x_1,y_1)=(1,1) & (x_1',y_1')=(1,1) \\ (x_2,y_2)=(n,n+1) & (x_2',y_2')=(n+1,n) \end{array}$$

This implies that the formulas for calculating the values $c(v_i,w_j)$ are as follows:

For $c(v_1,w_1)$, we note $x_1'\le x_1$, so we apply 3.8:

$$\begin{aligned} c(v_1,w_1) &= -2^{-n}\sum_{j=1}^{n}\mathrm{kr}(j,n,0)\,\mathrm{kr}(0,n-1,n-j) \\ &= -2^{-n}\sum_{j=1}^{n}\binom{n}{j}\cdot 1 \\ &= -2^{-n}(2^n-1) \end{aligned}$$

For $c(v_1,w_2)$, we note $x_2'>x_1$, so we apply 3.7:

$$\begin{aligned} c(v_1,w_2) &= 2^{-n}\sum_{j=0}^{0}\mathrm{kr}(j,n,0)\,\mathrm{kr}(n-1,n-1,-j) \\ &= 2^{-n}\,\mathrm{kr}(0,n,0)\,\mathrm{kr}(n-1,n-1,0) \\ &= 2^{-n}(1\cdot 1) \end{aligned}$$

We can now use Equation 3.9 to establish that the determinant of the Helfgott matrix for $(1,\dots,1,3)_{n-1}$ is

$$\begin{vmatrix} -2^{-n}(2^n-1) & 2^{-n} \\ -2^{-n}(-1)^n & 2^{-n}(-1)^{n-1}(2^n-1) \end{vmatrix} = 2^{-2n}\left[(2^n-1)^2+1\right]. \tag{3.10}$$

This will be the probability that the dominoes are placed in the top and bottom positions of the Aztec diamond. This was to be expected because we calculated combinatorially (in Section 3.1) the number of tilings of $(1,1,\dots,1,3)_{n-1}$ to be $2^{(n-1)(n-2)/2}(2^{2n-1}-2^n+1)$. With this information, we expect the above probability to be

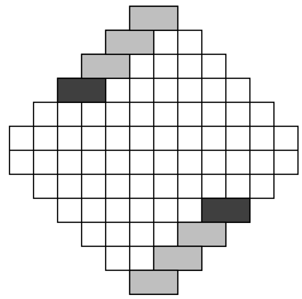

Figure 3.5: A $(1,3,1,1,1)_5$ pillow from AD_6

$$
\begin{aligned}
\frac{\#(1,1,\ldots,1,3)_{n-1}}{\#AD_n} &= \frac{2^{(n-1)(n-2)/2}(2^{2n-1}-2^n+1)}{2^{n(n+1)/2}} \\
&= \frac{2^{n(n+1)/2}2^{-2n}(2^{2n}-2^{n+1}+2)}{2^{n(n+1)/2}} \\
&= 2^{-2n}\left[(2^n-1)^2+1\right]. \qquad (3.11)
\end{aligned}
$$

3.6 Calculating $\#(1,\ldots,1,3,1,\ldots,1)_n$ using Helfgott's Theorem

Another region that is determined by the placement of only two dominoes is a pillow of the form $(1,\ldots,1,3,\overbrace{1,\ldots,1}^{\ell})_n$. Figure 3.5 shows an example where $n=5$ and $\ell=3$.

To get $\#(1,\ldots,1,3,\overbrace{1,\ldots,1}^{\ell})_{n-1}$ from AD_n, we put two dominoes on the board, in positions $(\ell)(\ell-1)/2+1$ and $n(n+1)/2-\ell(\ell-1)/2$. Calculating the coupling functions,

$$
\begin{aligned}
c(v_1,w_2) &= 2^{-n}\sum_{j=0}^{0}\mathrm{kr}(j,n,\ell)\,\mathrm{kr}(n-1-\ell,n-1,-j) \\
&= 2^{-n}\,\mathrm{kr}(0,n,\ell)\,\mathrm{kr}(n-1-\ell,n-1,0) \\
&= 2^{-n}\binom{n-1}{n-1-\ell} \\
&= 2^{-n}\binom{n-1}{\ell}.
\end{aligned}
$$

The calculation of $c(v_2,w_2)$ presents a more difficult challenge. On the next page, we show $c(v_2,w_2)=2^n-\binom{n+1}{\ell}-\cdots-(n+1)-1$.

$$\begin{aligned}
c(v_2,w_2) &= 2^{-n}\sum_{j=0}^{n-1}\mathrm{kr}(j,n,n-\ell)\,\mathrm{kr}(n-1-\ell,n-1,n-1-j)\\
&= 2^{-n}\sum_{j=0}^{n-1}(-1)^j\,\mathrm{kr}(j,n,\ell)(-1)^{n-1-\ell}(-1)^j\,\mathrm{kr}(\ell,n-1,j)\\
&= 2^{-n}(-1)^{n-1-\ell}\sum_{j=0}^{n-1}\mathrm{kr}(j,n,\ell)\,[\,\mathrm{kr}(\ell,n,j)-\,\mathrm{kr}(\ell-1,n-1,j)]\\
&= 2^{-n}(-1)^{n-1-\ell}\sum_{j=0}^{n-1}\mathrm{kr}(j,n,\ell)\,[\,\mathrm{kr}(\ell,n,j)-\,\mathrm{kr}(\ell-1,n,j)+\,\mathrm{kr}(\ell-2,n-1,j)]\\
&= 2^{-n}(-1)^{n-1-\ell}\sum_{j=0}^{n-1}\mathrm{kr}(j,n,\ell)\left[\sum_{k=1}^{\ell}(-1)^{\ell-k}\,\mathrm{kr}(k,n,j)+(-1)^{\ell}\,\mathrm{kr}(0,n-1,j)\right]\\
&= 2^{-n}(-1)^{n-1-\ell}\sum_{j=0}^{n-1}\mathrm{kr}(j,n,\ell)\left[\sum_{k=0}^{\ell}(-1)^{\ell-k}\,\mathrm{kr}(k,n,j)\right]\\
&= 2^{-n}(-1)^{n-1-\ell}\sum_{k=0}^{\ell}(-1)^{\ell-k}\sum_{j=0}^{n-1}\mathrm{kr}(k,n,j)\,\mathrm{kr}(j,n,\ell)\\
&= 2^{-n}(-1)^{n-1-\ell}\sum_{k=0}^{\ell}(-1)^{\ell-k}\left(\sum_{j=0}^{n}\mathrm{kr}(k,n,j)\,\mathrm{kr}(j,n,\ell)-\,\mathrm{kr}(k,n,n)\,\mathrm{kr}(n,n,\ell)\right)\\
&= 2^{-n}(-1)^{n-1-\ell}\sum_{k=0}^{\ell}(-1)^{\ell-k}\left(\sum_{j=0}^{n}\mathrm{kr}(k,n,j)\,\mathrm{kr}(j,n,\ell)-(-1)^k\binom{n}{k}(-1)^{\ell}\right)\\
&= 2^{-n}(-1)^{n-1-\ell}\sum_{k=0}^{\ell}\left((-1)^{\ell-k}\delta_{k\ell}2^n-\binom{n}{k}\right)\\
&= 2^{-n}(-1)^{n-1-\ell}\left[2^n-\sum_{k=0}^{\ell}\binom{n}{k}\right]\\
&= 2^{-n}(-1)^{n-1-\ell}\left[\sum_{k=\ell+1}^{n}\binom{n}{k}\right].
\end{aligned}$$

The determinant now gives

$$2^{-2n}\left[\left(2^n-\binom{n}{\ell}-\cdots-(n)-1\right)^2+\binom{n-1}{k}^2\right]$$

$$=2^{-2n}\left[\left(\sum_{j=\ell+1}^{n}\binom{n}{j}\right)^2+\binom{n-1}{\ell}^2\right]$$

This is be the probability that the dominoes are placed in the correct positions of the Aztec diamond, so multiplying by $2^{n(n+1)/2}$ gives

$$\#(1,\ldots,1,3,\overbrace{1,\ldots,1}^{\ell})_{n-1} = 2^{(n-1)(n-2)/2}\frac{1}{2}\left[\left(\sum_{j=\ell+1}^{n}\binom{n}{j}\right)^2 + \binom{n-1}{\ell}^2\right]. \tag{3.12}$$

This formula looks very combinatorial, but a purely combinatorial proof of Equation 3.12 has been elusive. Consider two special cases of Equation 3.12. When $\ell = 0$, this reduces to the result from Section 3.5. When $\ell = n-1$, we obtain the following verification of an experimental result:

$$\#(3,1,\ldots,1)_n = 2^{n(n-1)/2}\left[\frac{(n+1+1)^2+(n)^2}{2}\right] = 2^{n(n-1)/2}\left[(n+1)^2+1\right]. \tag{3.13}$$

Again, this formula seems to lend itself to a nice combinatorial proof, but none has been found to date. Appendix B contains a table of values for $(1,\ldots,1,3,\overbrace{1,\ldots,1}^{\ell})_n$ for different values of n and ℓ.

Chapter 4

THE HAMBURGER THEOREM

In this chapter, the focus changes from combinatorial and matrix-theoretical results to counting matchings of the dual graph, which are in one-to-one correspondence with cycle systems in related directed graphs. The main result of this chapter is an analogue of the Gessel-Viennot method for counting cycle systems on a type of graph we call a hamburger graph.

4.1 Hamburger Graphs

A hamburger graph H is made up of two acyclic graphs G_1 and G_2 and a connecting edge set E_3 with the following properties. The graph G_1 has k distinguished vertices $\{v_1, \cdots, v_k\}$ with directed paths from v_i to v_j only if $i < j$. The graph G_2 has k distinguished vertices $\{w_{k+1}, \cdots, w_{2k}\}$ with directed paths from w_i to w_j only if $i > j$. The edge set E_3 connects each vertex v_i to vertex w_{k+i} and vice versa. (See Figure 4.1 for a visualization.)

We present a determinantal method for counting vertex-disjoint cycle systems in a hamburger graph H. A vertex-disjoint cycle system $\mathcal{C}$ is a collection of vertex-disjoint edge cycles in H. Let ℓ be the number of edges in $\mathcal{C}$ that travel from G_2 to G_1 and let m be the number of vertex-disjoint edge cycles in $\mathcal{C}$.

Call a cycle system positive if $(-1)^{\ell+m} = +1$ and negative if $(-1)^{\ell+m} = -1$. Let c^+ be the number of positive vertex-disjoint cycle systems and c^- be the number of negative vertex-disjoint cycle systems.

Throughout this chapter, the following simple example will serve to guide us. Consider the two graphs $G_1 = (V_1, E_1)$ and $G_2 = (V_2, E_2)$, where $V_1 = \{v_1, v_2, v_3\}$, $V_2 = \{w_4, w_5, w_6\}$,

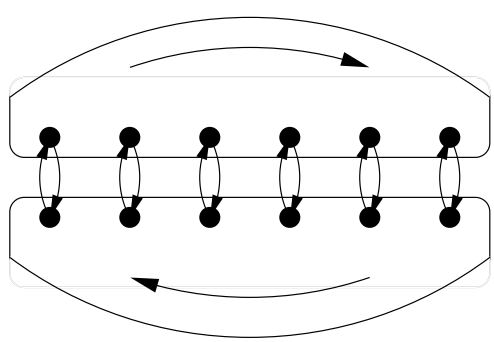

Figure 4.1: A hamburger graph

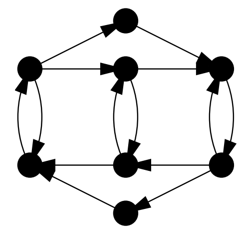

Figure 4.2: A simple hamburger graph H

$E_1 = \{v_1 \to v_2, v_2 \to v_3, v_1 \to v_3\}$, and $E_2 = \{w_6 \to w_5, w_5 \to w_4, w_6 \to w_4\}$. Our hamburger graph H will be the union of G_1, G_2, and the edge set E_3 consisting of edges $e_i : v_i \to w_{k+i}$ and $e_i' : w_{k+i} \to v_i$. In this example we have that $k = 3$. Figure 4.2 gives the graphical representation of H.

Corresponding to each hamburger graph H is a $2k \times 2k$ block matrix M_H of the form

$$M_H = \begin{bmatrix} A & I_k \\ -I_k & B \end{bmatrix},$$

where the upper triangular matrix $A = (a_{ij})$ represents the number of paths from v_i to v_j in G_1 and the lower triangular matrix $B = (b_{ij})$ represents the number of paths from w_{k+i} to w_{k+j} in G_2. The main result of this chapter — the "Hamburger Theorem" — proves that $\det M_H = c^+ - c^-$.

In terms of the example above, the hamburger matrix M_H equals

$$M_H = \begin{bmatrix} 1 & 1 & 2 & 1 & 0 & 0 \\ 0 & 1 & 1 & 0 & 1 & 0 \\ 0 & 0 & 1 & 0 & 0 & 1 \\ -1 & 0 & 0 & 1 & 0 & 0 \\ 0 & -1 & 0 & 1 & 1 & 0 \\ 0 & 0 & -1 & 2 & 1 & 1 \end{bmatrix}.$$

The determinant of M_H is 17, corresponding to the seventeen cycle systems (each with weight $+1$) in Figure 4.3.

The initial graph that inspired the hamburger graph comes from the work of Brualdi and Kirkland [6] in which they give a new proof that the number of tilings of the Aztec diamonds is $2^{n(n+1)/2}$.

The Hamburger Theorem applies to the enumeration of domino tilings of Aztec diamonds and generalized Aztec pillows. To illustrate this connection, we count domino tilings of the Aztec diamond by enumerating an equivalent quantity, the number of matchings on the dual graph G of the Aztec diamond. The natural matching N of horizontal neighbors in G as exemplified in Figure 4.4a on AD_4 is a reference point. Given any other matching M on G, such as in Figure 4.4b, their symmetric difference is a union of cycles in the graph,

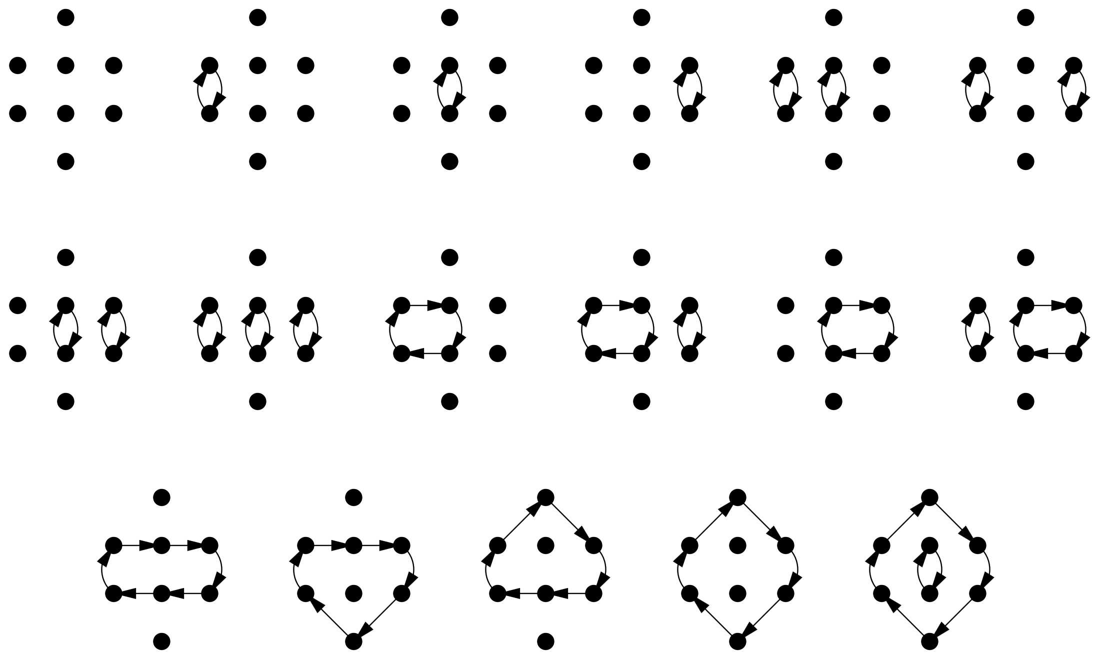

Figure 4.3: The seventeen cycle systems for the hamburger graph in Figure 4.2

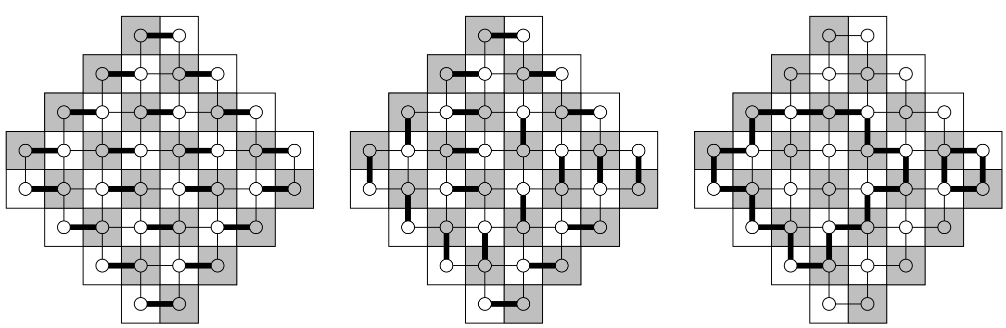

Figure 4.4: The symmetric difference of two matchings gives a cycle system

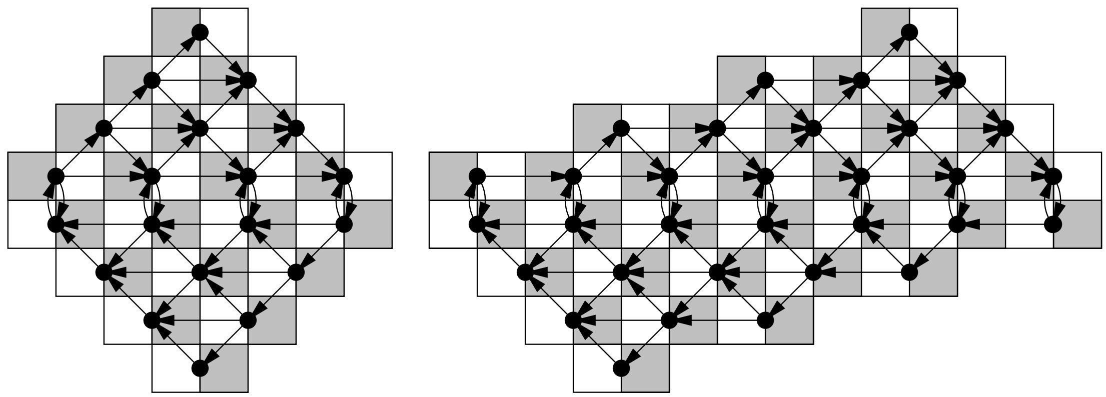

Figure 4.5: The hamburger graph for an Aztec diamond and an Aztec pillow

such as in Figure 4.4c. When we orient the edges in N from black vertices to white vertices and in M from white vertices to black vertices, the symmetric difference becomes a union of directed cycles. Notice that edges in the upper half of G all go from left to right and the edges in the bottom half of G go from right to left.

We can contract the edges of N to points and the graph retains its structure in terms of the cycle systems it produces. This new graph H is of the form in Figure 4.5a. This argument shows that the number of domino tilings of an Aztec diamond equals the number of cycle systems of this new condensed graph, called the region's *digraph*. In the case of generalized Aztec pillows, the region's digraph is always a hamburger graph. We discuss the explicit matrices determined from the Hamburger Theorem in Section 4.5.

Brualdi and Kirkland's proof used the Kasteleyn-Percus matrix of this directed graph to enumerate its cycle systems. The Hamburger Theorem allows us to now enumerate domino tilings by taking the determinant of a $2n \times 2n$ matrix. An analogous reduction in determinant size occurs in all regions to which this theorem applies. In addition, whereas Kasteleyn theory applies only to planar graphs, there is no restriction of planarity for hamburger graphs. For this reason, the Hamburger Theorem introduces a new counting method for cycle systems in some non-planar graphs.

The proof of the Hamburger Theorem, like the proof of the Gessel-Viennot method, hinges on terms canceling in the permutation decomposition of the determinant of M_H. If a cycle system arising from the permutation decomposition of the determinant is M_H is not vertex-disjoint, there are four possibilities. First, the cycle system may contain a cycle that is self-intersecting. Second, the cycle system may have two intersecting cycles, neither of which is a 2-cycle. If either of these first two properties hold, there is some notion of order to determine which holds first. This vertex of first intersection is the basis for a family of cycle systems that all intersect for the first time at this vertex. We show that this family contributes a net zero weight in the determinantal expansion of M_H.

When calculating the number of cycle systems, we notice that the determinantal expansion of M_H has various summands that may represent the same cycle system. Consider the second cycle system in the third row of Figure 4.3. Since the solitary edge cycle visits vertices v_1, v_2, v_3, w_6, and w_4 in order, this cycle contributes a non-zero weight in the permutation expansion of the determinant corresponding to the permutation cycle (12364) in S_6. Notice that this cycle will also contribute a non-zero weight in the permutation expansion of the determinant corresponding to the permutation cycle (1364) since the edge cycle follows a path from v_1 to v_3 (by way of v_2), returning to v_1 via w_6 and w_4. Because of this ambiguity, we must introduce the idea of a minimal permutation cycle and a minimal cycle system, and realize that the determinant of M_H counts minimal vertex-disjoint cycle systems. The minimal permutation cycle for this second cycle system in the third row of Figure 4.3 is (1364).

In the case when neither the first nor second properties hold and that the cycle system is not vertex-disjoint or not minimal, at least one of two additional properties hold. The third property is that two cycles intersect and one of the cycles is a two-cycle. The fourth property is that the cycle system may not be minimal. We can determine where the two-cycle intersections and non-minimalities occur, and corresponding to this set of violations, we create a family of cycle systems each with this set of violations. We show that this family contributes a net zero weight in the determinantal expansion of M_H.

The cancellation from the above sets of families gives us that only minimal vertex-disjoint cycle systems contribute to the determinantal expansion of M_H. This contribution is the signed weight of each cycle system determined above, implying that the determinant of M_H exactly equals $c^+ - c^-$.

In Section 4.2, we present the definitions necessary to state the Hamburger Theorem. In Section 4.3, we present the definitions necessary for the proof of the Hamburger Theorem; we prove this result in Section 4.4. Lastly, we present applications of the theorem to Aztec diamonds and Aztec pillows in Section 4.5.

4.2 Definitions and Statement of the Hamburger Theorem

Definition. *A* hamburger graph $H = (V, E)$ *is a directed graph composed of two acyclic subgraphs* $G_1 = (V_1, E_1)$ *and* $G_2 = (V_2, E_2)$ *with additional edges* E_3*, described below. Choose* k *vertices* v_i *from* G_1 *and* k *vertices* w_{k+i} *from* G_2 *with the restriction that there are no directed paths from* v_i *to* v_j *in* G_1 *if* $i > j$ *or from* w_{k+i} *to* w_{k+j} *in* G_2 *if* $i < j$*. We call the vertices* $\{v_1, \ldots, v_k, w_{k+1}, \ldots, w_{2k}\}$ *the* distinguished vertices *of* H*. The additional edge set* E_3 *consists of* k *pairs of edges* $e_i : v_i \to w_{k+i}$ *and* $e_i' : w_{k+i} \to v_i$ *for* $1 \leq i \leq k$*.*

This leads to a visualization of the graph as in Figure 4.1, hence the name. We allow weights on the hamburger by introducing weights $\mathrm{wt}(e)$ on every edge $e \in E$; the simplest weighting which allows for counting the number of cycle systems is $\mathrm{wt}(e) \equiv 1$. We only require that $\mathrm{wt}(e_i)\mathrm{wt}(e_i') = 1$ for all $2 \leq i \leq k-1$, and do not require this condition for $i = 1$ nor for $i = k$.

Associated to the hamburger graph H, we define the $2k \times 2k$ *hamburger matrix* M_H to be the block matrix

$$M_H = \begin{bmatrix} A & D_1 \\ -D_2 & B \end{bmatrix}. \tag{4.1}$$

The upper triangular $k \times k$ matrix $A = (a_{ij})$ represents the sum of the products of the weights of edges over all paths from v_i to v_j in G_1 and the lower triangular $k \times k$ matrix $B = (b_{ij})$ represents the sum of the products of the weights of edges over all paths from w_{k+i} to w_{k+j} in G_2. The diagonal $k \times k$ matrix D_1 has as its entries $d_{ii} = \mathrm{wt}(e_i)$ and the diagonal $k \times k$ matrix D_2 has as its entries $d_{ii} = \mathrm{wt}(e_i')$. Note that when the weights of the edges in E_3 are all 1, these matrices satisfy $D_1 = D_2 = I_k$.

In our hamburger graph H, there are two possible types of edge cycles. There are k 2-*cycles*

$$c : v_i \xrightarrow{e_i} w_{k+i} \xrightarrow{e_i'} v_i$$

and many more *general edge cycles* in H that alternate between G_1 and G_2. We can think of an edge cycle of this form as a path P_1 in G_1 connected by an edge $e_{1,1} \in E_3$ to a path Q_1 in G_2, which in turn connects to a path P_2 in G_1 by an edge $e_{1,2}'$, continuing in this fashion until arriving at a final path Q_ℓ in G_2 whose terminal vertex is adjacent to the initial vertex of P_1. We write

$$c : P_1 \xrightarrow{e_{1,1}} Q_1 \xrightarrow{e_{1,2}'} P_2 \xrightarrow{e_{2,1}} \cdots \xrightarrow{e_{\ell,1}} P_\ell \xrightarrow{e_{\ell,2}'} Q_\ell.$$

To each edge cycle c, we define the weight $\mathrm{wt}(c)$ of c to be the product of all the weights of the edges traversed by c:

$$\mathrm{wt}(c) = \prod_{e \in c} \mathrm{wt}(e).$$

We define a *cycle system* to be a collection $\mathcal{C}$ of m edge cycles. We define the sign of an cycle system to be $\mathrm{sgn}(\mathcal{C}) = (-1)^{\ell+m}$, where ℓ is the total number of edges from G_2 to G_1 in $\mathcal{C}$. We say that a cycle system $\mathcal{C}$ is *positive* if $\mathrm{sgn}(\mathcal{C}) = +1$ and *negative* if $\mathrm{sgn}(\mathcal{C}) = -1$.

For a hamburger graph H, let c^+ be the sum of the weights of positive vertex-disjoint cycle systems, and c^- be the sum of the weights of negative vertex-disjoint cycle systems.

Theorem 9. *The determinant of the hamburger matrix M_H equals $c^+ - c^-$.*

The proof of this "Hamburger Theorem" is based on cancellation in the permutation expansion of the determinant of M_H, and will be proved after acquiring some additional machinery.

4.3 Additional Definitions

In the proof of the Hamburger Theorem, there are two distinct mathematical objects that have the name "cycle". We have already mentioned the type of cycle that appears in graph theory. There, an (elementary) cycle in a directed graph is a closed path with no repeated vertices.

Secondly, there is a notion of cycle when we talk about permutations. If $\sigma \in S_n$ is a permutation, we can write σ as the product of disjoint cycles $\sigma = \chi_1 \chi_2 \cdots \chi_\tau$, where χ_ι is a cycle $\chi_\iota = (\rho_{\iota 1}\ \rho_{\iota 2}\ \cdots\ \rho_{\iota \eta_\iota})$ for integers $1 \le \rho_{\iota\kappa} \le n$. Recall that the *order* $|\chi|$ of a cycle χ is its length.

To distinguish between these two types of cycles when there is possible confusion, we call the former kind an *edge cycle* and the latter kind a *permutation cycle*. Notation-wise, we will use roman letters when discussing edge cycles and Greek letters when discussing permutation cycles.

We recall that the *permutation expansion* of the determinant of an $n \times n$ matrix M is the decomposition of the matrix as

$$\det M = \sum_{\sigma \in S_n} (\operatorname{sgn} \sigma) m_{1,\sigma(1)} \cdots m_{n,\sigma(n)}. \tag{4.2}$$

We will be considering non-zero summands in the permutation expansion of the determinant of the hamburger matrix M_H. Because of the special block form of the hamburger matrix in Equation 4.1, the permutations σ that have non-zero contributions to this sum are products of disjoint cycles of either of two forms — the simple transposition

$$\chi = (\varphi_{11}\ \omega_{11})$$

or the more general permutation cycle

$$\chi = (\varphi_{11}\ \varphi_{12}\ \cdots\ \varphi_{1\mu_1}\ \omega_{11}\ \omega_{12}\ \cdots\ \omega_{1\nu_1}\ \varphi_{21}\ \cdots\cdots\ \varphi_{\lambda\mu_\lambda}\ \omega_{\lambda 1}\ \cdots\ \omega_{\lambda\nu_\lambda}). \tag{4.3}$$

In both cases, $1 \leq \varphi_{\iota\kappa} \leq k$, $k+1 \leq \omega_{\iota\kappa} \leq 2k$, $\varphi_{\iota\kappa} < \varphi_{\iota,\kappa+1}$, and $\omega_{\iota\kappa} > \omega_{\iota,\kappa+1}$ for all $1 \leq \iota \leq \lambda$ and relevant κ. Another piece of information that comes out of the matrix is that $\varphi_{\iota\mu_\iota} + k = \omega_{\iota 1}$ and $\omega_{\iota\nu_\iota} - k = \varphi_{\iota+1,1}$. We also have that $\omega_{\lambda\nu_\lambda} - k = \varphi_{11}$. So that this permutation cycle is well-defined, we make sure that $\varphi_{11} = \min_{\iota,\kappa} \varphi_{\iota\kappa}$. In order to reference this value later, define $\Phi(\chi) = \varphi_{11}$.

Given a permutation $\sigma = \chi_1\chi_2\cdots\chi_\tau$, each number φ_ι or ω_ι appears only once in all permutation cycles of σ. The function Φ defines an ordering on cycles in a cycle system — we say that the associated edge cycle c_χ comes before the associated edge cycle $c_{\chi'}$ if $\Phi(\chi) < \Phi(\chi')$. We call this the *initial term order*.

We call a permutation cycle χ *minimal* if it is a transposition or if $\mu_\iota = \nu_\iota = 2$ for all ι. This condition implies we can write our more general permutation cycles χ in the form

$$\chi = (\varphi_{11}\ \varphi_{12}\ \omega_{11}\ \omega_{12}\ \varphi_{21}\ \cdots\ \varphi_{\lambda 2}\ \omega_{\lambda 1}\ \omega_{\lambda 2}), \tag{4.4}$$

with the same conditions as before. We call a permutation $\sigma = \chi_1 \cdots \chi_\tau$ *minimal* if each of its disjoint cycles χ_ι is minimal.

To each permutation cycle $\chi \in S_{2k}$, we can associate one or more edge cycles c_χ in H. If χ is the transposition $\chi = (\varphi_{11}\ \omega_{11})$, then we associate the edge 2-cycle $c_\chi : v_{\varphi_{11}} \to w_{\omega_{11}} \to v_{\varphi_{11}}$ to χ.

To any permutation cycle χ that is not a transposition, we can associate multiple edge cycles c_χ in the following way. If χ has the form of Equation 4.3, then for each $1 \leq i \leq \lambda$, let P_i be any path in G_1 that visits each of the vertices $v_{\varphi_{i1}}$, $v_{\varphi_{i2}}$, all the way through $v_{\varphi_{i\mu_i}}$ in order. Similarly, let Q_i be any path in G_2 that visits each of the vertices $w_{\omega_{i1}}$, $w_{\omega_{i2}}$, through $w_{\omega_{i\nu_i}}$ in order. For each choice of paths P_i and Q_i, we have an additional possibility for the edge cycle c_χ; we can set

$$c_\chi : P_1 \xrightarrow{e_{\omega_{11}}} Q_1 \xrightarrow{e'_{\varphi_{21}}} P_2 \xrightarrow{e_{\omega_{21}}} \cdots\cdots \xrightarrow{e'_{\varphi_{\lambda 1}}} P_\lambda \xrightarrow{e_{\omega_{\lambda 1}}} Q_\lambda. \tag{4.5}$$

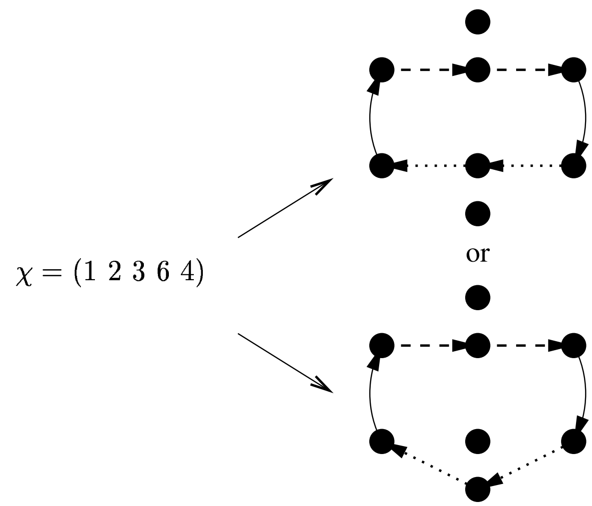

Figure 4.6: A permutation cycle χ and two edge cycles in H associated to χ

See Figure 4.6 for an example in the hamburger graph in Figure 4.2. We call λ the *number of P-paths* in c_χ.

We defined cycle systems earlier in Section 4.2, but we will see that the proof of Theorem 9 requires us to think of the cycle systems first as a permutation and second as a collection of edge cycles determined by the permutation. In terms of vertex-disjoint minimal cycle systems, we show that this characterization is the same.

If H is a hamburger graph with k pairs of distinguished vertices, we define a cycle system-permutation pair as follows.

Definition. *A* cycle system-permutation pair *(or* CSP-pair *for short) is a pair $(\mathcal{C}, \sigma)$, where $\sigma \in S_{2k}$ is a permutation and $\mathcal{C}$ is a collection of edge cycles $c \in \mathcal{C}$ with the following property. If the disjoint cycle representation of σ is $\sigma = \chi_1 \cdots \chi_\tau$, then $\mathcal{C}$ is a union of τ edge cycles c_{χ_ι} for $1 \leq \iota \leq \tau$ such that c_{χ_ι} is an edge cycle associated to the permutation cycle χ_ι.*

This definition of CSP-pair implies that each permutation σ yields many unions of edge cycles $\mathcal{C}$, that collections of edge cycles $\mathcal{C}$ may be associated to many permutations σ, but that any vertex-disjoint union of edge cycles $\mathcal{C}$ corresponds to one and only one minimal permutation σ_m. This is because given any path as in Equation 4.5, we can read off the initial and terminal vertices of each P_i and Q_i in order producing a permutation cycle. Since the edge cycles are disjoint, there can be no repeated vertex from each edge cycle, so indeed the minimal permutation cycles are disjoint as well. We define a CSP-pair $(\mathcal{C}, \sigma)$ to be *minimal* if σ is a minimal permutation.

Each CSP-pair appears once in the permutation expansion of the determinant of M_H. We break down the contribution of each CSP-pair into its weight and its sign. The weight of a CSP-pair is dependent on its cycle system, whereas its sign is dependent on both its

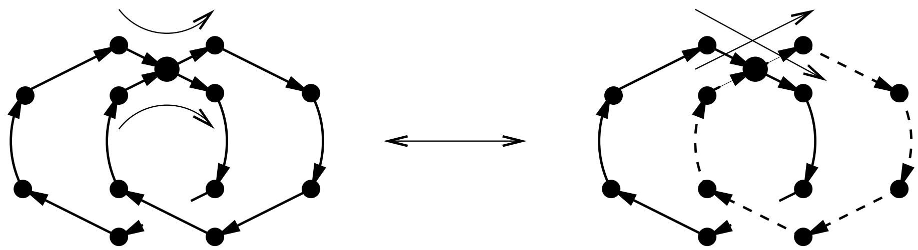

Figure 4.7: A self-intersecting cycle and its corresponding pair of intersecting cycles

permutation and its cycle system because of the -1-terms in the lower left block of the hamburger matrix. We define the *weight* of a CSP-pair $(\mathcal{C}, \sigma)$ to be the product of the weights of the associated edge cycles $c_\chi \in \mathcal{C}$.

For a CSP-pair $(\mathcal{C}, \sigma)$, where $\sigma = \chi_1 \cdots \chi_\tau$, we define the *sign* of the CSP-pair $\operatorname{sgn}(\mathcal{C}, \sigma)$ to be $(-1)^\ell \operatorname{sgn}(\sigma)$, where $\ell = \sum_{c_\chi \in \mathcal{C}} \lambda_\chi$ and where λ_χ is the number of P-paths in c_χ. We can think about the sign of $(\mathcal{C}, \sigma)$ as being equal to the product of the signs of the associated edge cycles c_χ in $\mathcal{C}$, where the sign of c_χ would be $\operatorname{sgn}(c_\chi) = (-1)^{\lambda_\chi} \operatorname{sgn}(\chi)$.

Note that if $(\mathcal{C}, \sigma)$ is a minimal CSP-pair then $\operatorname{sgn}(c_\chi) = +1$ for a transposition χ and $\operatorname{sgn}(c_\chi) = (-1)^{\lambda+1}$ if χ is of the form in Equation 4.4. In particular, a vertex-disjoint CSP-pair is consistent with the definition of a vertex-disjoint cycle system given in Section 4.2 when $(\mathcal{C}, \sigma)$ is minimal.

We say that a CSP-pair $(\mathcal{C}, \sigma)$ is *positive* if $\operatorname{sgn}(\mathcal{C}, \sigma) = +1$ and is *negative* if $\operatorname{sgn}(\mathcal{C}, \sigma) = -1$.

4.4 Proof of the Hamburger Theorem

We create families $\mathcal{F}$ of not vertex-disjoint or not-minimal CSP-pairs $(\mathcal{C}, \sigma)$ whose net contribution to the permutation expansion of the determinant of M_H is zero. In this way, only the minimal vertex-disjoint CSP-pairs contribute their weight to the determinant so $\det M_H = c^+ - c^-$.

We consider first the possibility that in the collection of edge cycles $\mathcal{C}$, there is either a self-intersecting edge cycle or two general edge cycles that intersect (i.e. neither is a 2-cycle) or both. If neither of these occurs, skip to the next section of the proof.

The idea to prove the argument comes from the picture presented in Figure 4.7. When you have a self-intersecting edge cycle, changing the direction in which you traverse the edges at the self-intersection vertex leads to breaking the one self-intersecting cycle into two cycles that intersect at that same vertex. Since the edge set of the collection of edge cycles has not changed, the weight of the two CSP-pairs is the same. Note that we have introduced a transposition into the sign of the permutation cycle of the CSP-pair which changes the sign of the CSP-pair, so that these two CSP-pairs cancel in the permutation expansion of the determinant of M_H.

One can imagine that this means to every self-intersecting CSP-pair you can associate one CSP-pair with two cycles intersecting. However, more than one self-intersection may occur at the same vertex, and there may be additional edge cycles that pass through that same vertex. Exactly to what this corresponds is not clear. Do we break one of the self-intersections or sew together two of the intersecting cycles? If we were to break all the self-intersections so that we have some number N of cycles through our vertex, it is not clear in what order we must sew the cycles back together. One starts to get the idea that we must consider all possible ways of sewing back together. Once we do just that, we have a family of CSP-pairs, all of the same weight, whose net contribution to the permutation expansion of the determinant is zero.

This idea is conceptually simple but the proof is notationally complicated.

In terms of the initial term order, we want to determine the first general edge cycle $c_{\chi_\alpha} \in \mathcal{C}$ that satisfies one of the following two properties:
(i) The edge cycle c_{χ_α} is self-intersecting.
(ii) The edge cycle c_{χ_α} intersects some other edge cycle c_{χ_β}, where $\chi_\beta \in \sigma$ is not a transposition.

To determine which of these conditions appears first, follow the paths P_i and Q_i starting at $\Phi(c_{\chi_\alpha})$:

$$c_{\chi_a} : P_1 \to Q_1 \to P_2 \to \cdots \to P_m \to Q_m,$$

and see which of the following happens first. While traversing the path, you cross a vertex that you are going to meet again later or while traversing the path, you cross a vertex that is a vertex of some other edge cycle, and the cycle happens not to be a transposition. This vertex is well-defined and unique and is the basis for the family we create.

In our discussion, we make the assumption that this vertex is a vertex v^* in G_1. A similar argument exists if the first appearance occurs in G_2. Notice that at v^* there may be multiple self-intersections and/or multiple cycle crossings. We will create a family $\mathcal{F}$ of CSP-pairs that takes into account each of these possibilities.

If we want to rigorously define the breaking of a self-intersecting edge cycle, we need to specify many different components of the CSP-pair (C, σ). First, we need to specify on which edge cycle in $\mathcal{C}$ we are acting. Next, we need to specify the vertex of self-intersection. Since this self-intersection vertex may occur in multiple paths, we need to specify which two paths we interchange in the breaking process.

In the following paragraphs, we will define an operation "break" on CSP-pairs, which takes in a CSP-pair $(\mathcal{C}, \sigma)$, one of σ's disjoint permutation cycles χ_α, the associated edge cycle c_{χ_α}, paths P_y and P_z in c_{χ_α}, and the vertex v^* in both P_y and P_z where c_{χ_α} has a self-intersection. For simplicity, we assume that v^* is not a distinguished vertex, but the argument still holds in this case. The inverse of this operation will be the operation "sew".

In this framework, c_{χ_α} has the form

$$c_{\chi_\alpha} : P_1 \to Q_1 \to P_2 \to \cdots \to P_y \to Q_y \to \cdots \to P_z \to Q_z \to \cdots \to P_\ell \to Q_\ell,$$

where P_y and P_z can be separated into two halves as

$$P_y : P_y^{(1)} \to v^* \to P_y^{(2)}$$

and

$$P_z : P_z^{(1)} \to v^* \to P_z^{(2)}.$$

Remember that P_y and P_z are paths that stop over at various vertices depending on the permutation χ_α. The vertex v^* must have adjacent stop-over vertices in each of the two paths P_y and P_z. Let the adjacent stop-over vertices in P_y be v_{φ_y} and $v_{\varphi_{y+1}}$ and the adjacent stop-over vertices in P_z be v_{φ_z} and $v_{\varphi_{z+1}}$.

This implies χ_α has the form

$$\chi_\alpha = (\varphi_{11} \ \cdots \ \varphi_{1\mu_1} \ \omega_{11} \ \cdots \ \varphi_y \ \varphi_{y+1} \ \cdots \ \varphi_z \ \varphi_{z+1} \ \cdots \ \varphi_{\lambda\mu_\lambda} \ \omega_{\lambda 1} \ \cdots \ \omega_{\lambda\nu_\lambda}).$$

We can now properly define the output of the operation "break". We define χ_β and χ_γ by splitting χ_α as follows:

$$\chi_\beta = (\varphi_{11} \ \cdots \ \varphi_y \ \varphi_{z+1} \ \cdots \ \omega_{\lambda\nu_\lambda})$$

and

$$\chi_\gamma = (\varphi_{y+1} \ \cdots \ \varphi_z),$$

with the necessary rewriting of χ_γ to have as its initial entry the value $\Phi(\chi_\gamma)$. Define c_{χ_β} and c_{χ_γ} to be

$$c_{\chi_\beta} : P_1 \to Q_1 \to P_2 \to \cdots \to P_y^{(1)} \to v^* \to P_z^{(2)} \to Q_z \to \cdots \to P_\ell \to Q_\ell,$$

and

$$c_{\chi_\gamma} : P_z^{(1)} \to v^* \to P_y^{(2)} \to Q_y \to \cdots \to Q_{z-1},$$

again changing the starting vertex of c_{χ_γ} to $v_{\Phi(c_{\chi_\gamma})}$.

We define the break of the CSP-pair with the above inputs to be the CSP-pair $(\mathcal{C}', \sigma')$ such that

$$\mathcal{C}' = \mathcal{C} \cup \{c_{\chi_\beta}, c_{\chi_\gamma}\} \setminus \{c_{\chi_\alpha}\}$$

and

$$\sigma' = \sigma\chi_\alpha^{-1}\chi_\beta\chi_\gamma = \sigma \cdot (\varphi_{y+1} \ \varphi_{z+1}).$$

The edge set of $\mathcal{C}$ is equal to the edge set of $\mathcal{C}'$, so the weight of the modified cycle systems is the same as the original. Since we changed σ to σ' by only multiplying by a transposition, the sign of the modified CSP-pair is opposite that of the original.

Having defined break and sew, we continue the proof of Theorem 9. To any CSP-pair $(\mathcal{C}, \sigma)$ that has a cycle that satisfies either property (i) or (ii), let c_{χ_α} be the first such cycle in the initial term order. Let v^* be the first vertex of intersection in c_{χ_α}. Then for all edge cycles c that have one or more self-intersections at v^*, break c at v^*. Define the CSP-pair $(\mathcal{C}_s, \sigma_s)$ that results to be the *simple CSP-pair* associated to $(\mathcal{C}, \sigma)$. There will be some number N of general cycles that intersect at vertex v^*. There may be a 2-cycle that intersects v^* as well, but this does not matter.

For any permutation $\xi \in S_N$, let $\xi = \zeta_1\zeta_2\cdots\zeta_\eta$ be its disjoint cycle representation, where each ζ_ι represents a disjoint cycle. For each $1 \le \iota \le \eta$, sew together edge cycles in order. If $\zeta_\iota = (\delta_{\iota 1} \ \cdots \delta_{\iota\varepsilon_\iota})$, sew together $c_{\chi_{\delta_{\iota 1}}}$ and $c_{\chi_{\delta_{\iota 2}}}$ at v^*. Sew that result together with $c_{\chi_{\delta_{\iota 3}}}$, and so on through $c_{\chi_{\delta_{\iota\varepsilon_\iota}}}$. Note that the result of these sewings is unique, and that every CSP-pair $(\mathcal{C}, \sigma)$ that has $(\mathcal{C}_s, \sigma_s)$ as its simple CSP-pair can be obtained in this way and no others. We can perform this procedure for any $\xi \in S_N$, and the sign of the resulting system (C_ξ, σ_ξ) is $\operatorname{sgn}(C_\xi, \sigma_\xi) = \operatorname{sgn}(\xi) \operatorname{sgn}(\mathcal{C}_s, \sigma_s)$. This means that the contributions of the weights of all CSP-pairs in the family $\mathcal{F}$ to the determinant is

$$\sum_{\xi \in S_N} \operatorname{sgn}(\xi) \operatorname{sgn}(\mathcal{C}_s, \sigma_s) \operatorname{wt}(\mathcal{C}_s, \sigma_s) = \operatorname{sgn}(\mathcal{C}_s, \sigma_s) \operatorname{wt}(\mathcal{C}_s, \sigma_s) \sum_{\xi \in S_N} \operatorname{sgn}(\xi) = 0. \tag{4.6}$$

So elements of the same family cancel out in the determinant of M_H.

If there is no such self-intersection or intersection of two general cycles, then for the CSP-pair to be not vertex-disjoint or not minimal, one of the following must be true for the CSP-pair $(\mathcal{C}, \sigma)$.
(iii) There is a transposition $\chi_\alpha = (\varphi, \omega) \in \sigma$ such that $c = c_{\chi_\alpha} : v_\varphi \to w_\omega \to v_\varphi$ intersects some other edge cycle $c' = c_{\chi_\beta}$, where $\chi_\beta \in \sigma$.
(iv) There is some permutation cycle $\chi_\alpha \in \sigma$ that is not minimal.

We will show that each CSP-pair having a cycle c satisfying either condition (iii) or condition (iv) can be grouped into a family $\mathcal{F}$ of CSP-pairs, each with the same weight.

Define a set of indices $I \subset [k]$, of which an element can become a member in one of two ways. If $(\mathcal{C}, \sigma)$ is not minimal, there is permutation cycle χ_α with more than two consecutive φ's or ω's in its cycle notation. For any intermediary ι between two φ's or $\iota + k$ between two ω's, place ι in I. For example, if $\chi_\alpha = (\cdots \ \varphi' \ \iota \ \varphi'' \ \cdots)$, we place $\iota \in I$. If $(\mathcal{C}, \sigma)$ satisfies condition (iii) at some point, there is a 2-cycle $c : v_i \to w_{k+i} \to v_i$ such that either v_i is in some other cycle c_{χ_β} or w_{k+i} is in some other cycle c_{χ_γ}, or both. We also declare this i to be in I.

Note that any CSP-pair $(\mathcal{C}, \sigma)$ satisfying one of conditions (iii) or (iv) will have a non-empty set I. From our original CSP-pair, create the associated minimal CSP-pair $(\mathcal{C}_m, \sigma_m)$ by removing any transposition χ_α from σ and its corresponding 2-cycle c_{χ_α} from $\mathcal{C}$, and also removing any intermediary φ's or ω's from σ. We do not change the associated edge paths in $\mathcal{C}$ since they still correspond to this minimized permutation cycle.

Let i be any element in I. Since $i \in I$, the 2-cycle $c_i : v_i \to w_{k+i} \to v_i$ intersects another edge cycle either at v_i, at w_{k+i}, or both. So there are four cases:
(1) c_i intersects some edge cycle c_{χ_β} at v_i and no cycle at w_{k+i}.
(2) c_i intersects some edge cycle c_{χ_γ} at w_{k+i} and no cycle at v_i.
(3) c_i intersects some edge cycle c_{χ_β} at v_i and the same cycle again at w_{k+i}.
(4) c_i intersects some edge cycle c_{χ_β} at v_i and some other cycle c_{χ_γ} at w_{k+i}.

See Figure 4.8 for a visual reference.

Define a set of two or four options $\mathcal{O}_i$ for each i.

In case (1), there are two options. Let o_1 be the option to include the edge cycle c_i in $\mathcal{C}_m$ and its corresponding transposition χ_α in σ_m. Let o_2 be the option to include the intermediary $\varphi = i$ in χ_β in the position where c_{χ_β} passes through v_i.

[Note that we could not apply both options at the same time since then the χ_α and χ_β would not be disjoint cycle permutations and so would not appear in the permutation expansion of the determinant.]

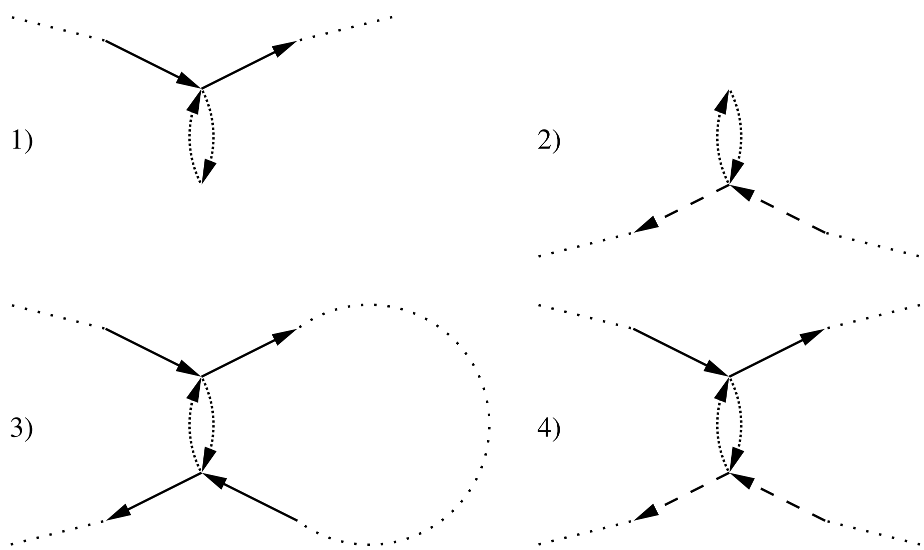

Figure 4.8: The four cases for general edge cycles to intersect with a 2-cycle

Similarly in case (2), there are two options. Let o_1 be the option to include the edge cycle c_i in $\mathcal{C}_m$ and its corresponding transposition χ_α in σ_m. Let o_2 be the option to include the intermediary $\omega = i + k$ in χ_γ in the position where c_{χ_γ} passes through w_{k+i}.

In case (3), there are four options. Let o_1 be the option to include the edge cycle c_i in $\mathcal{C}_m$ and its corresponding transposition χ_α in σ_m. Let o_2 be the option to include the intermediary $\varphi = i$ in χ_β in the position where c_{χ_β} passes through v_i. Let o_3 be the option to include the intermediary $\omega = i + k$ in χ_β in the position where c_{χ_β} passes through w_{k+i}. Let o_4 be the option to include both intermediaries $\varphi = i$ and $\omega = i + k$ in χ_β in the respective positions where c_{χ_β} passes through v_i and w_{k+i}.

In case (4), there are four options. Let o_1 be the option to include the edge cycle c_i in $\mathcal{C}_m$ and its corresponding transposition χ_α in σ_m. Let o_2 be the option to include the intermediary $\varphi = i$ in χ_β in the position where c_{χ_β} passes through v_i. Let o_3 be the option to include the intermediary $\omega = i + k$ in χ_γ in the position where c_{χ_γ} passes through w_{k+i}. Let o_4 be the option to include intermediary $\varphi = i$ in χ_β in the position where c_{χ_β} passes through v_i and intermediary $\omega = i + k$ in χ_γ in the position where c_{χ_γ} passes through w_{k+i}.

Corresponding to the associated minimal CSP-pair $(\mathcal{C}_m, \sigma_m)$ and index set I, define the family $\mathcal{F}$ to be the set of CSP-pairs $(\mathcal{C}_f, \sigma_f)$ where we exercise some set of options $o_j \in \mathcal{O}_i$ on $(\mathcal{C}_m, \sigma_m)$ for every i. Note that every CSP-pair derived in this fashion is in fact a CSP-pair that satisfies either condition (iii) or (iv) and is such that its associated minimal CSP-pair is $(\mathcal{C}_m, \sigma_m)$. There is also no other CSP-pair $(\mathcal{C}', \sigma')$ that has $(\mathcal{C}_m, \sigma_m)$ as its minimal CSP-pair.

Every member CSP-pair in $\mathcal{F}$ has the same weight since each option changes the edge set of $\mathcal{C}$ by at most a 2-cycle $v_i \to w_{k+i} \to v_i$, where $2 \leq i \leq k - 1$ and each of those two cycles contributes a multiplicative 1 to the weight of the CSP-pair. Note that the peculiar bounds are because no permutation σ could ever include two cycles through v_1, w_{k+1}, v_k, or w_{2k}. Also notice that in each option set $\mathcal{O}_i$, the sign changes induced by the options $\mathrm{sgn}(o_j)$ are $\mathrm{sgn}(o_1) = +1$, $\mathrm{sgn}(o_2) = -1$, and $\mathrm{sgn}(o_3) = -1$ and $\mathrm{sgn}(o_4) = +1$ if they exist. In this way, any non-vertex disjoint or non-minimal CSP-pair is a member of one of these families, and the cumulative weight from a family $\mathcal{F}$ is zero.

Since every CSP-pair appears once in the permutation expansion of $\det M_H$, the only CSP-pairs that do not cancel each other out are those that are vertex-disjoint and come from minimal permutation cycles. Therefore $\det M_H$ is the sum over such CSP-pairs of $\mathrm{wt}(\mathcal{C}, \sigma)$ times their signs $\mathrm{sgn}(\mathcal{C}, \sigma)$. •

4.5 Applications of the Hamburger Theorem

As mentioned in Section 4.1, hamburger graphs arise in the study of all generalized Aztec pillows. We discuss first the application of the Hamburger Theorem in the case when the region is an Aztec diamond, mirroring results of Brualdi and Kirkland. Then we discuss the results from the case when the region is a 3-pillow, and lastly we explain how to implement the Hamburger Theorem when our region is any generalized Aztec pillow.

We wish to concretize the notion of a digraph of the Aztec diamond AD_n. Given the natural tiling of an Aztec diamond consisting solely of horizontal dominoes, we place a vertex in the center of every domino. The edges of this digraph are made up of three families of edges. From every vertex in the top half of the diamond, create edges to the east, to the northeast, and to the southeast whenever there is a vertex there. From every vertex in the bottom half of the diamond, form edges to the west, to the southwest, and to the northwest whenever there is a vertex there. Additionally, label the bottom vertices in the top half v_1 through v_n from west to east and the top vertices in the bottom half w_{n+1} through w_{2n}. For all i between 1 and n, create a directed edge from v_i to w_{n+i} and from w_{n+i} to v_i. The result when this construction is applied to AD_4 is a graph of the form in Figure 4.5a.

Since both the upper half of the digraph and the lower half of the digraph are both planar, there are no negative cycle systems, so the determinant of the corresponding hamburger matrix counts exactly the number of cycle systems in the digraph.

To apply Theorem 9 to count the number of tilings of AD_n, we need to find the number of paths in the upper half of D from v_i to v_j and the number of paths in the lower half of D from w_{n+j} to w_{n+i}. The key observation is that by the equivalence in Figure 4.9, we are in effect counting the number of paths from (i, i) to (j, j) using steps of size $(0, 1)$, $(1, 0)$, or $(1, 1)$ that do not pass above the line $y = x$. This is exactly a combinatorial interpretation for the $(j - i)$-th large Schröder number. The first six large Schröder numbers are $1, 2, 6, 22, 90, 394$, and are referenced as A006318 in the Encyclopedia of Integer Sequences [38].

The Hamburger Theorem implies that the number of tilings of the Aztec diamond AD_n is equal to $\det \begin{bmatrix} S_n & I_n \\ -I_n & S_n^T \end{bmatrix}$, where S_n is an upper triangular matrix with the i-th Schröder

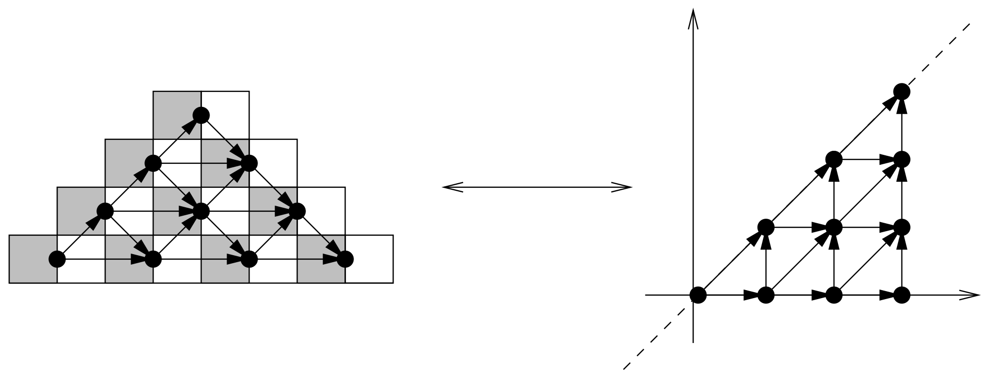

Figure 4.9: The equivalence between paths in D and lattice paths in the first quadrant

number on its ith superdiagonal:

$$S_6 = \begin{bmatrix} 1 & 2 & 6 & 22 & 90 & 394 \\ 0 & 1 & 2 & 6 & 22 & 90 \\ 0 & 0 & 1 & 2 & 6 & 22 \\ 0 & 0 & 0 & 1 & 2 & 6 \\ 0 & 0 & 0 & 0 & 1 & 2 \\ 0 & 0 & 0 & 0 & 0 & 1 \end{bmatrix},$$

Brualdi and Kirkland prove a similar determinantal formula for the number of tilings of an Aztec diamond in a matrix-theoretical fashion based on the Kasteleyn matrix of the graph H and a Schur complement calculation. The Hamburger Theorem gives a purely combinatorial way to reduce the calculation of the $n(n+3)\times n(n+3)$ Kasteleyn determinant to the calculation of a $2n\times 2n$ Hamburger determinant. Following the cues from Brualdi and Kirkland, we can reduce this to an $n \times n$ determinant via a Schur complement calculation, which was described in Section 2.7.

In the case of the block matrix M_H in Equation 4.1, taking the Schur complement of A in M_H gives that

$$\det M_H = \det A \cdot \det(B + D_2 A^{-1} D_1) = \det(B + D_2 A^{-1} D_1), \tag{4.7}$$

since A is an upper triangular matrix with 1's on the diagonal. In this way, every hamburger determinant can be reduced to a smaller determinant of a Schur complement matrix. In the case of a simple hamburger graph where $D_2 = D_1 = I$, the determinant calculation reduces further to $\det(B + A^{-1})$. Lastly, in the case where the hamburger graph is rotationally symmetric, $B = JAJ$, where J is the exchange matrix. This implies we can write the determinant only in terms of the submatrix A, i.e., $\det(A^{-1} + JAJ) = \det(A + JA^{-1}J)$ since J has determinant ± 1.

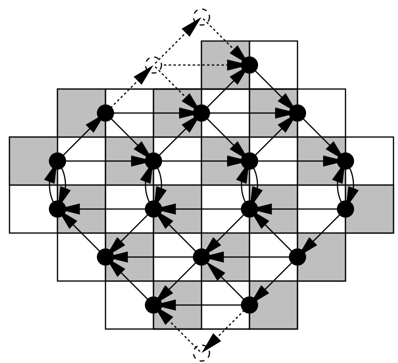

Figure 4.10: The digraph of a generalized Aztec pillow from the digraph of an Aztec diamond

In terms of the Aztec diamond graph example above, we can thus calculate the number of tilings of the Aztec diamond AD_6 as follows. The inverse of S_6 is

$$S_6^{-1} = \begin{bmatrix} 1 & -2 & -2 & -6 & -22 & -90 \\ 0 & 1 & -2 & -2 & -6 & -22 \\ 0 & 0 & 1 & -2 & -2 & -6 \\ 0 & 0 & 0 & 1 & -2 & -2 \\ 0 & 0 & 0 & 0 & 1 & -2 \\ 0 & 0 & 0 & 0 & 0 & 1 \end{bmatrix},$$

which implies that the determinant of the reduced hamburger matrix M_6

$$M_6 = \begin{bmatrix} 2 & 2 & 6 & 22 & 90 & 394 \\ -2 & 2 & 2 & 6 & 22 & 90 \\ -2 & -2 & 2 & 2 & 6 & 22 \\ -6 & -2 & -2 & 2 & 2 & 6 \\ -22 & -6 & -2 & -2 & 2 & 2 \\ -90 & -22 & -6 & -2 & -2 & 2 \end{bmatrix},$$

gives the number of tilings of AD_6.

Brualdi and Kirkland were the first to find such a determinantal formula for the number of tilings of an Aztec Diamond [6]. They were able to calculate the sequence of determinants $\{M_n\}$ using a J-fraction expansion, which only works when matrices are Toeplitz or Hankel.

Since generalized Aztec pillows (and 3-pillows as a special case) all can be created from Aztec diamonds by placement of dominoes, we define the digraph of a generalized Aztec pillow to be the restriction of the digraph of an Aztec diamond to the vertices that are on the interior of the pillow. For a visualization, see the example of Figure 4.10.

The underlying hope going into the Hamburger Theorem was that it would allow us to prove Propp's Conjecture. The same reasoning as above implies that domino tilings of generalized Aztec pillows can be counted using the Hamburger Theorem.

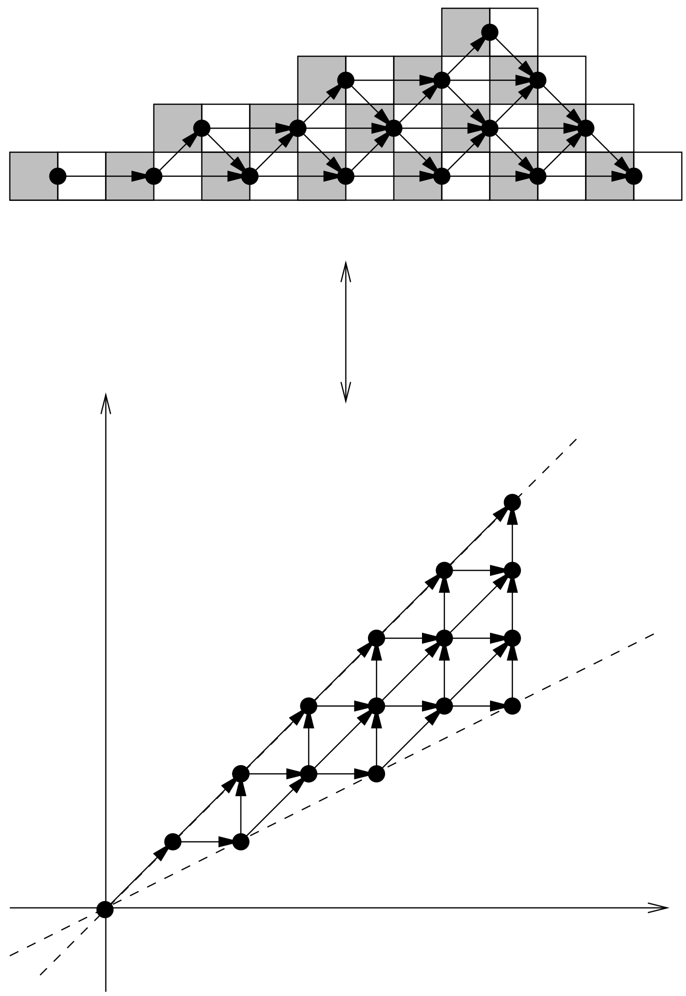

Figure 4.11: The equivalence between paths in D and lattice paths in the first quadrant

Creating the hamburger graph H that corresponds to the Aztec pillow in Figure 2.2 gives Figure 4.5b. Counting the number of paths from v_i to v_j and from w_{k+j} to w_{k+i} in successively larger Aztec pillows gives us the infinite upper-triangular array $S = (s_{i,j})$ of "modified Schröder numbers" defined by the following combinatorial interpretation. Let $s_{i,j}$ be the number of paths from (i,i) to (j,j) using steps of size $(0,1)$, $(1,0)$, and $(1,1)$, not passing above the line $y = x$ nor below the line $y = x/2$. This equivalence is shown in Figure 4.11. The principal 7×7 minor matrix S_7 of S is

$$S_7 = \begin{bmatrix} 1 & 1 & 2 & 5 & 16 & 57 & 224 \\ 0 & 1 & 2 & 5 & 16 & 57 & 224 \\ 0 & 0 & 1 & 2 & 6 & 21 & 82 \\ 0 & 0 & 0 & 1 & 2 & 6 & 22 \\ 0 & 0 & 0 & 0 & 1 & 2 & 6 \\ 0 & 0 & 0 & 0 & 0 & 1 & 2 \\ 0 & 0 & 0 & 0 & 0 & 0 & 1 \end{bmatrix}.$$

The Hamburger Theorem proves that the number of domino tilings of an Aztec pillow of order n is given by the determinant of the $2n \times 2n$ matrix $M_H = \begin{bmatrix} S_n & I_n \\ -I_n & J_n S_n J_n \end{bmatrix}$, where S_n is the $n \times n$ principal submatrix of S and J_n is the $n \times n$ exchange matrix. As in the case of Aztec diamonds, we can calculate the reduced hamburger matrix through a Schur calculation. The inverse of S_6 is

$$S_6^{-1} = \begin{bmatrix} 1 & -1 & 0 & 0 & 0 & 0 \\ 0 & 1 & -2 & -1 & -2 & -5 \\ 0 & 0 & 1 & -2 & -2 & -5 \\ 0 & 0 & 0 & 1 & -2 & -2 \\ 0 & 0 & 0 & 0 & 1 & -2 \\ 0 & 0 & 0 & 0 & 0 & 1 \end{bmatrix}$$

and the resulting reduced hamburger matrix for AP_6 is

$$M_6 = \begin{bmatrix} 2 & 1 & 2 & 5 & 16 & 57 \\ -2 & 2 & 2 & 5 & 16 & 57 \\ -2 & -2 & 2 & 2 & 6 & 21 \\ -5 & -2 & -2 & 2 & 2 & 6 \\ -5 & -2 & -1 & -2 & 2 & 2 \\ 0 & 0 & 0 & 0 & -1 & 2 \end{bmatrix}.$$

This gives us a much faster way to calculate the number of domino tilings of an Aztec pillow than was known previously. We have reduced the calculation of the $O(n^2) \times O(n^2)$ Kasteleyn-Percus determinant to an $n \times n$ reduced hamburger matrix. To be fair, the Kasteleyn-Percus matrix has -1, 0, and $+1$ entries while the reduced hamburger matrix may have very large entries, which makes running time comparisons difficult theoretically. Experimentally, when calculating the number of domino tilings of AP_{14} using Maple 8.0 on a 447 MHz Pentium III processor, the determinant of the 112×112 Kasteleyn-Percus matrix takes 25.3 seconds while the determinant of the 14×14 reduced hamburger matrix takes less than 0.1 seconds.

Whereas we now have a very understandable determinantal formula for the number of tilings of the region, this does not translate into a proof of Propp's Conjecture because we can not calculate the determinant of the sequence of matrices $\{M_n\}$ explicitly. We can not apply a J-fraction expansion as Brualdi and Kirkland did since the reduced hamburger matrix is not Toeplitz or Hankel.

An intriguing consequence of the Schur calculations is the pattern that is apparent between the modified Schröder matrix S_n and its inverse S_n^{-1}. In particular, the same

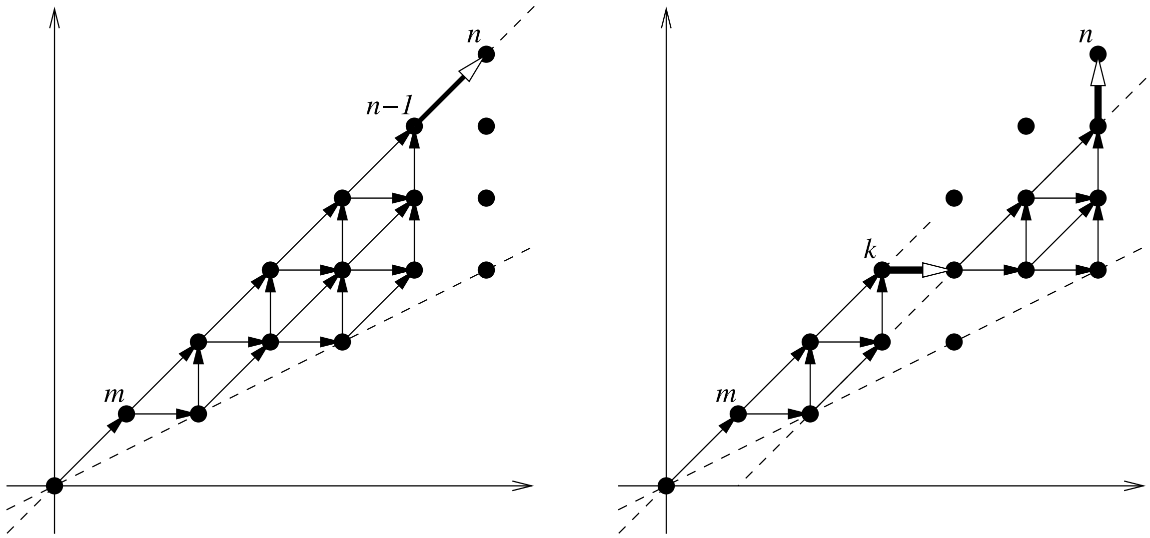

Figure 4.12: Proof of the recurrence in the modified Schröder numbers

terms appear in both, even if shifted by a row and a column. This implies that there is a (two-dimensional) recurrence to determine the array of modified Schröder numbers and that we do not need to calculate them via their combinatorial lattice path definition which can be computationally complicated. The recurrence to calculate $s_{m,n}$ in terms of values $s_{i,j}$ with $j < n$ is given by the following theorem.

Theorem 10. *For $m, n \geq 0$, let $s_{m,n}$ be the number of $(0,1)$, $(1,0)$, $(1,1)$ paths from (m,m) to (n,n) that do not pass above the line $y = x$ nor below the line $y = x/2$. When $m < n$, the terms $s_{m,n}$ satisfy the recurrence*

$$s_{m,n} = s_{m,n-1} + \sum_{k=m}^{n-1} s_{m,k} s_{k-1,n-2}$$

if $m \geq 1$ and

$$s_{0,n} = s_{0,n-1} + \sum_{k=1}^{n-1} s_{0,k} s_{k-1,n-2}$$

if $m = 0$.

Proof: We provide a combinatorial proof. The left-hand side counts the number of paths from (m,m) to (n,n) in our restricted lattice. For the right hand side, we count this quantity in a second way. Conditioning on the last step of a path, we either have that the last step is diagonal or is vertical. (See Figure 4.12.) By definition, there are $s_{m,n-1}$ paths such that the last step is diagonal. Otherwise, the last step is vertical, in which case the path must cross the line $y = x - \frac{1}{2}$ horizontally at some last time. Let this last horizontal step be of the

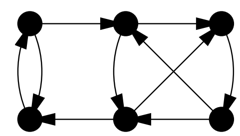

Figure 4.13: A simple generalized hamburger graph

form $(k,k) \to (k+1,k)$. Then the number of paths from (m,m) to (k,k) in our restricted lattice is $s_{m,k}$ while the number of paths from $(k+1,k)$ to $(n,n-1)$ without crossing the line $y = x-1$ nor $y = x/2$ is $s_{k-1,n-2}$. (Notice that the indices are off since the origin of the newly restricted lattice has moved.) Summing over all valid values of k proves the recurrence. •

In terms of more exotic generalized Aztec pillows P with a $2 \times 2n$ central belt, it is clear that the Hamburger Theorem produces a $2n \times 2n$ matrix whose determinant is the number of tilings of P. The discussion about Schur complements implies that we can find an $n \times n$ reduced hamburger matrix. Future examination of these hamburger matrices may help derive an explicit formula for the enumeration of domino tilings of Aztec pillows and other related regions.

4.6 Counterexamples to Possible Extensions of the Hamburger Theorem

The structure of the hamburger graph as presented in Section 4.2 seems restrictive, so the question naturally arises whether it is somehow necessary. Can the edge set E_3 between G_1 and G_2 be an arbitrary bipartite graph? The answer in general is no. Take for example the simple graph H in Figure 4.13. As one can count by hand, there are 10 distinct cycle systems in H, as enumerated in Figure 4.14. Creating the hamburger matrix that would correspond to this graph gives

$$M_H = \begin{bmatrix} 1 & 1 & 1 & 1 & 0 & 0 \\ 0 & 1 & 1 & 0 & 1 & 0 \\ 0 & 0 & 1 & 0 & 0 & 1 \\ -1 & 0 & 0 & 1 & 0 & 0 \\ 0 & 0 & -1 & 1 & 1 & 0 \\ 0 & -1 & 0 & 1 & 1 & 1 \end{bmatrix}.$$

This seems the most logical extension of the matrix since the lower left block of the matrix describes paths from w_4, w_5, and w_6 to v_1, v_2, and v_3 and we have changed no other block of the matrix.

The determinant of this matrix is -5. Even though one might expect there to be a new sign convention on cycle systems in generalized hamburger graphs, any sign convention would necessarily conserve the parity of the number of cycle systems. Therefore there is no $+1/-1$ labeling of the cycle systems in Figure 4.14 that would allow $\det M_H = \sum_{c \in \mathcal{C}} \operatorname{sgn}(c)$.

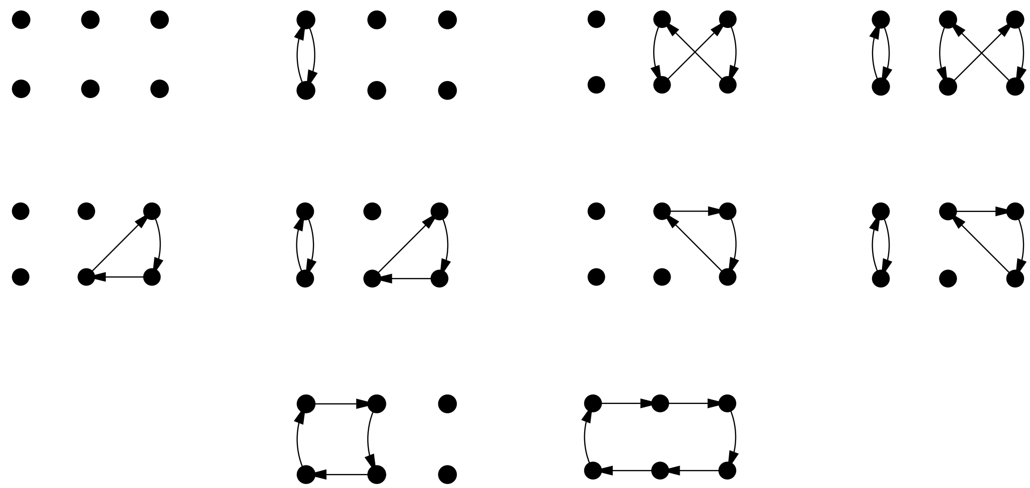

Figure 4.14: The ten cycle systems for the generalized hamburger graph in Figure 4.13

This means that either the matrix for this generalized hamburger graph is not correct or that the theorem does not hold in general.

The only hope that exists is what happens when one considers the difference between even and odd permutations. In the given counterexample, the edge set E_3 sends vertex w_4 to vertex v_1, w_5 to v_3, and w_6 to v_2. This can be thought of as an odd permutation of the natural edge set (sending w_4 to v_1, w_5 to v_2, and w_6 to v_3). In all the calculations so far, whenever the permutation of the natural edge set is even, the parity of the hand-counted cycle systems is equal to the parity of the determinant of the matrix. A sign convention for these graphs has not been found that explains the calculated determinant, but being equal in parity allows for hope of a possible extension to the Hamburger Theorem.

Chapter 5

FUTURE WORK

There are various avenues of future study available. Many of them are based in experimental results which have not led to completely explicit conjectures. In Section 5.1, we present a generalization of Propp's Conjecture. Experimental results and conjectures are presented in Sections 5.2 and 5.3. Lastly, Section 5.4 deals with the random tilings of Aztec Pillows. Each of these areas has the possibility of producing additional fruitful lines of research.

5.1 Generalizing Propp's Conjecture

The motivation of the study of Aztec pillows was Propp's Conjecture for 3-pillows, as presented in Section 2.1. Through experimental calculations, we can expand and extend the conjecture.

For one, we can extend the conjecture to odd pillows. As mentioned in 2.1, we use the notation AP_n^q to represent the n-th q-pillow for q odd. This is a centrally-symmetric region with steps of length q and central belt of size $2 \times 2n$. Calculating the number of tilings of AP_n^5 for n up to 70, and the number of tilings of AP_n^7 and AP_n^9 up to 40 gives strong evidence that $\#AP_n^q$ for q odd is always a larger number squared times a smaller number.

Additional structure in these "smaller numbers" also appears. Propp's Conjecture gives an explicit recurrence for the smaller number values when $q = 3$. In the case of $q = 5$, there is no linear, constant coefficient k-th degree recurrence for any k up to 20. However in each case ($q = 5$, $q = 7$, and $q = 9$) the structure is undeniable. Plotting the values of $\#AP_n^q/\#AP_{n-2}^q$ gives a remarkable damped sinusoidal graph converging to some number ρ. In addition, plotting the values of $\#AP_n^q/\#AP_{n-1}^q$ depending on whether n is even or odd gives two damped sinusoidal graphs that converge to some values τ and 2τ respectively. This implies $\rho = 2\tau^2$. Approximate values for ρ are given in Table 5.1. We have included the values for Aztec diamonds ($q = 1$) and the original Aztec pillows ($q = 3$).

n	Approximate limit of s_n/s_{n-2}
1	2
3	2.890053636
5	3.0821372
7	3.145
9	3.18

Table 5.1: ρ values for various values of q

Appendices C and D contain the raw data.

Even more appears to be true. Since odd pillows are rotationally symmetric, we can apply Corollary 6 and learn that the number of tilings of such a region is the sum of two squares. Calculating the squares via Theorem 1 gives us a better understanding of the larger numbers that appear in Propp's Conjecture. In particular it appears that the larger number divides both the squares in the sum of squares. This implies that the smaller number is also a sum of squares, which may lend some insight into its recurrence formula.

This allows us to formulate a new and improved conjecture about odd pillows.

Conjecture 11. *The number of tilings of AP_n^q is a larger number squared times a smaller number. Write $\#AP_n^q = \ell_n^2 s_n$. Then s_n satisfies the following structure. The ratio of s_{2n+1}/s_{2n} to s_{2n+2}/s_{2n+1} is exactly 2 in the limit. In addition, we know that $\#AP_n^q = a_n^2 + b_n^2$ for explicit values a_n and b_n given by Theorem 1. The value ℓ_n from above divides both a_n and b_n.*

Remark. This conjecture only appears to apply in its most general form to the so-called "odd pillows". The next nicest regions that one might consider would be the generalized Aztec pillows such that steps on all borders are of size 3, which we will denote $AP_n^{3,3}$. The first few values give the data in Table 5.2. From these figures it is clear that the number of tilings can not be written generally as a larger number squared times a smaller number since there are no relatively large square factors.

n	$\#AP_n^{3,3}$
1	2
2	5
3	13
4	61
5	$2^2 \cdot 101$
6	$5 \cdot 615$
7	$2^3 \cdot 4877$
8	$5 \cdot 17 \cdot 8329$
9	$2 \cdot 7773253$
10	$1601 \cdot 344269$

Table 5.2: Values of $\#AP_n^{3,3}$ are not of the form $\ell_n^2 s_n$

Remark. It is unclear how we might determine the regions we might consider "even" pillows, such as $(2, 2, \ldots, 2)_k$. In particular, the pillow $(2, 2)_2$ is untilable since there are more squares of one color than another. This is the case for all even k . In addition, pillows such as $(2, 2, 2)_3$ restrict the structure of tilings greatly. Starting in the bottom right, the dominoes covering the three white squares must also cover three of the four adjacent black squares. The remaining black square is covered by a domino that also covers one of the four

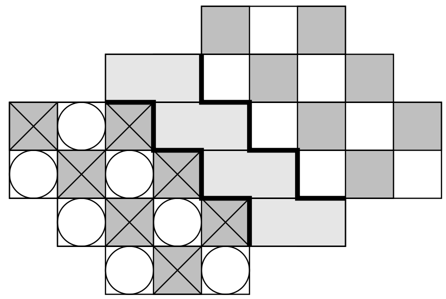

Figure 5.1: A $(2, 2, 2)_3$ pillow breaks into two independent halves

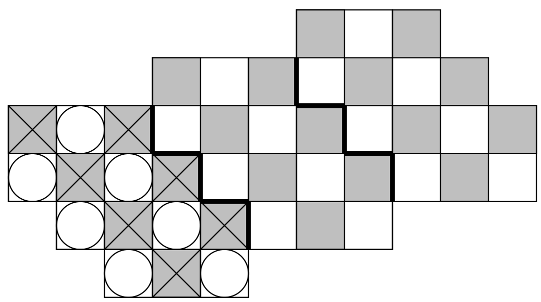

Figure 5.2: A $(3, 3, 2)_3$ pillow breaks into three independent pieces

adjacent white squares. The remaining three squares have no choice but to be paired with the three adjacent black squares. This breaks the region into pieces, each which must be tiled independently. This argument is presented visually in Figure 5.1.

A similar argument proves that the number of tilings of a $(3, 3, \ldots, 3, 2)_k$ "pillow" is $(2k+1)^k$ for $k \geq 2$ by breaking down the "pillow" into k pieces that must be tiled independently. (See Figure 5.2.) This is why we do not consider such pillows in our study. We also note that the number of tilings of a $(3, 3, \ldots, 3, 0)_k$ "pillow" is exactly one since all dominoes are forced by the boundary conditions.

One last interesting combinatorial piece of information that appears experimentally deals with the reduced hamburger matrix presented in Section 4.5.

Conjecture 12. *Any $(n-1) \times (n-1)$ submatrix of the $n \times n$ reduced hamburger matrix for an ordinary Aztec pillow AP_n^3 has as a factor of its determinant the value ℓ_n from above. In addition, ℓ_n^2 does not divide this minor.*

This tells us that the combinatorial structure is intertwined with this ℓ_n, so ℓ_n is not as mysterious as before.

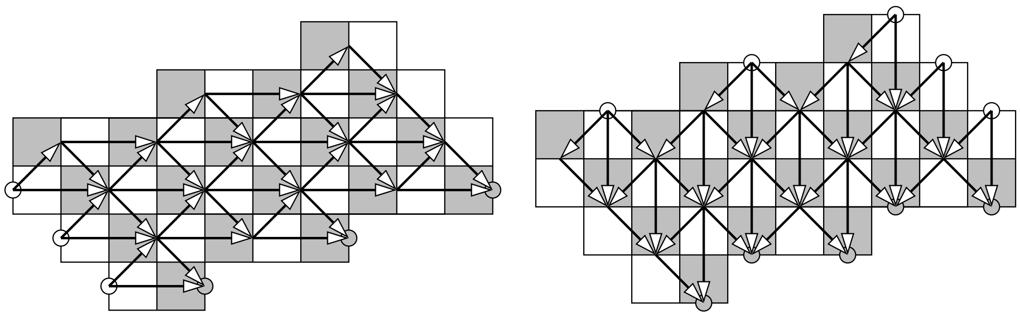

Figure 5.3: Two applications of the Gessel-Viennot method to AP_5

5.2 *Experimental Results from the Gessel–Viennot Method*

The combinatorial approach using the Gessel-Viennot Method presented in Section 4.5 leads to two determinantal formulas for the number of tilings of an Aztec pillow. In this section, we discuss these results.

Given an ordinary Aztec pillow, the vertical and the horizontal approaches (Figure 5.3) give two distinct determinantal formulas for the number of tilings of the region. For the Aztec pillow AP_n, we call the former matrix the *vertical Gessel-Viennot matrix* and denote it V_n; whereas, we call the latter matrix the *horizontal Gessel-Viennot matrix* and denote it H_n.

The (larger) $n \times n$ vertical Gessel-Viennot matrix has a very nice structure related to crystal ball sequences. Let $D = (d_{ij})$ be the matrix

$$D = \begin{bmatrix} 2 & 2 & 2 & 2 & 2 & 2 \\ 1 & 4 & 8 & 12 & 16 & 20 \\ 0 & 2 & 10 & 26 & 50 & 82 \\ 0 & 1 & 8 & 32 & 88 & 192 \\ 0 & 0 & 2 & 18 & 82 & 258 \\ 0 & 0 & 1 & 12 & 72 & 292 \\ 0 & 0 & 0 & 2 & 26 & 170 \\ 0 & 0 & 0 & 1 & 16 & 128 \\ 0 & 0 & 0 & 0 & 2 & 34 \\ 0 & 0 & 0 & 0 & 1 & 20 \\ 0 & 0 & 0 & 0 & 0 & 2 \\ 0 & 0 & 0 & 0 & 0 & 1 \end{bmatrix},$$

and $E = (e_{ij})$ be the matrix

$$E = \begin{bmatrix} 1 & 1 & 1 & 1 & 1 & 1 & 1 & 1 & 1 \\ 2 & 3 & 4 & 5 & 6 & 7 & 8 & 9 & 10 \\ 1 & 2 & 5 & 8 & 13 & 18 & 25 & 32 & 41 \\ 0 & 1 & 2 & 7 & 12 & 25 & 38 & 63 & 88 \\ 0 & 0 & 1 & 2 & 9 & 16 & 41 & 66 & 129 \\ 0 & 0 & 0 & 1 & 2 & 11 & 20 & 61 & 102 \\ 0 & 0 & 0 & 0 & 1 & 2 & 13 & 24 & 85 \\ 0 & 0 & 0 & 0 & 0 & 1 & 2 & 15 & 28 \\ 0 & 0 & 0 & 0 & 0 & 0 & 1 & 2 & 17 \\ 0 & 0 & 0 & 0 & 0 & 0 & 0 & 1 & 2 \\ 0 & 0 & 0 & 0 & 0 & 0 & 0 & 0 & 1 \end{bmatrix}.$$

Notice that the i-th row d_i of D starting at the first non-zero entry has the generating function

$$\sum_{j=0}^{\infty} d_{i,j}x^i = \begin{cases} 2(1+x)^i/(1-i)^{i+1} & \text{if } i \text{ is even} \\ (1+x)^{i+1}/(1-i)^{i+1} & \text{if } i \text{ is odd} \end{cases},$$

and that the i-th diagonal e_i of E (starting at the diagonal of 1's and going upwards) has the generating function

$$\sum_{j=0}^{\infty} e_{i,j}x^i = \begin{cases} (1+x)^{i/2}/(1-i)^{i/2+1} & \text{if } i \text{ is even} \\ (1+x)^{(i+1)/2}/(1-i)^{(i+1)/2} & \text{if } i \text{ is odd} \end{cases}.$$

For any n, define k to be $k = \lceil \frac{n}{2} \rceil$. Define B_n to be the principal $n \times k$ submatrix of D. Define C_n to be the $n \times n - k$ matrix such that its ℓ-th column is of the form $[0, \ldots, 0, e_{1,n}, e_{2,n}, \ldots, e_{2\lfloor \frac{n}{2} \rfloor - 2\ell + 2, n}]$.

Theorem 13. *The vertical Gessel-Viennot matrix V_n for AP_n has the form $V_n = [B_n | C_n]$.*

As an example, when $n = 7$, we have

$$V_7 = \left[\begin{array}{cccc|ccc} 2 & 2 & 2 & 2 & 0 & 0 & 0 \\ 1 & 4 & 8 & 12 & 1 & 0 & 0 \\ 0 & 2 & 10 & 26 & 8 & 0 & 0 \\ 0 & 1 & 8 & 32 & 25 & 1 & 0 \\ 0 & 0 & 2 & 18 & 38 & 8 & 0 \\ 0 & 0 & 1 & 12 & 41 & 25 & 1 \\ 0 & 0 & 0 & 2 & 20 & 38 & 8 \end{array}\right].$$

Proof: We consider the lattice in Figure 5.4, where starting at $(0,0)$, you can take steps in the directions $(1,0)$, $(0,1)$, and $(1,1)$. These steps are called *right*, *up*, and *diagonal* steps. The number of paths from $(0,0)$ to (i,j) in this lattice is the Delannoy number $D(i,j)$, with generating function

$$\sum_{n \geq 0, k \geq 0} D(n,k)x^n y^k = \frac{1}{1-x-y-xy},$$

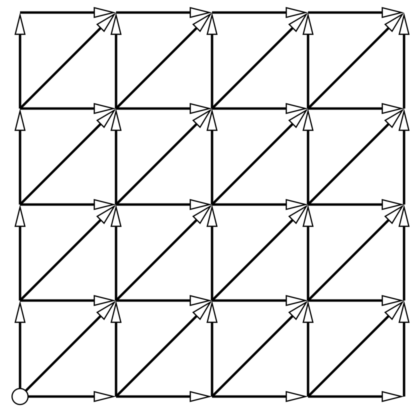

Figure 5.4: The underlying base lattice in Aztec pillows

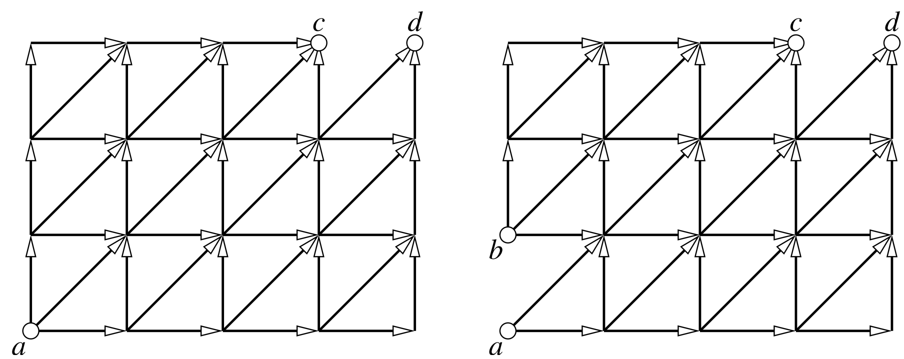

Figure 5.5: Two particular sublattices of the base lattice in Figure 5.4

and is referenced as Sequence A008288 in the Online Encyclopedia of Integer Sequences [38].

We determine subsets of this base lattice that appear while counting lattice paths in the vertical implementation of the Gessel-Viennot method to Aztec pillows. From their combinatorial interpretations, the entries in the matrices D and E will then be proved. The key idea is that paths starting from the vertices on the up-steps of length three will translate to paths in sublattices of the form in Figure 5.5a; whereas, paths starting from the vertices on the down-steps of length one will translate to paths in sublattices of the form in Figure 5.5b.

In Figure 5.5a, we consider a rectangular subset of the lattice with one edge removed and vertices marked a, c, and d. We will determine the number of paths from a to either c or d. A path from a to c in this sublattice can be seen as a path from $(0,0)$ to (i,j) in the base lattice for some i and j. In our example, these values are $i = 3$ and $j = 3$. In particular, the number of paths from a to c is $D(i,j)$ for the correct values of i and j.

On the other hand, placing a at the origin in the base lattice and considering the number of paths to the representation of d overcounts the number of paths from a to d in the sublattice by exactly the number of paths from a to c. In particular, if i and j are defined as in the previous paragraph, the number of paths from a to d is $D(i+1,j) - D(i,j)$.

In Figure 5.5b, we consider a rectangular subset of the lattice with two edges removed and vertices marked a, b, c, and d. We will determine the number of paths from a to either c or d. As before, we can lay this sublattice over the lattice from Figure 5.4 so that a is on $(0,0)$ and c is on some lattice point (i,j) for some values of i and j. (Again, in our example $i = 3$ and $j = 3$). The number of paths from $(0,0)$ to (i,j) now overcounts the number of paths from a to c by exactly the number of paths from b to c. This implies that the number of paths from a to c is $D(i,j) - D(i,j-1)$.

To count the number of paths from a to d, we realize that we can use similar arguments to the above cases and inclusion-exclusion. We have that the number of paths from a to d in our sublattice is $D(i+1,j) - D(i,j) - D(i+1,j-1) + D(i,j-1)$.

The entries of V come directly from overlaying these sublattices on an Aztec pillow. Concretely, the number of paths from initial vertex i to terminal vertex j for $1 \le i \le k$ and $1 \le j \le 2i-1$ is

$$V_{i,j} = \begin{cases} D(j,i) - D(j,i-1) & \text{if } j \text{ is odd} \\ D(j+1,i) - D(j,i) - D(j+1,i-1) + D(j,i-1) & \text{if } j \text{ is even} \end{cases}.$$

When $j = 2i$, the number of paths from initial vertex i to terminal vertex j is 1.

The other half of V_n depends on whether n is even or odd. If n is even, the number of paths from an initial vertex i to terminal vertex j for $k+1 \le i \le n$ and $2(i-k) \le j \le n$ is

$$V_{i,j} = \begin{cases} D(j-2(i-k)+1, i-j/2) & \text{if } j \text{ is even} \\ D(j-2(i-k)+1, i-(j-1)/2) - D(j-2(i-k), i-(j-1)/2) & \text{if } j \text{ is odd} \end{cases}.$$

When $j = 2(i-k)-1$, the number of paths from initial vertex i to terminal vertex j is 1. If n is odd, the number of paths from an initial vertex i to terminal vertex j for $k+1 \le i \le n$ and $2(i-k) \le j \le n$ is

$$V_{i,j} = \begin{cases} D(j-2(i-k), i-j/2) & \text{if } j \text{ is even} \\ D(j-2(i-k), i-(j-1)/2) - D(j-2(i-k)-1, i-(j-1)/2) & \text{if } j \text{ is odd} \end{cases}.$$

This gives explicit formulas for the entries of the vertical Gessel-Viennot matrices V_n. •

Remark. Very similar arguments can give explicit formulas for the entries of vertical Gessel-Viennot matrices for any odd pillow, not just the 3-pillows.

An interesting phenomenon is how these vertical Gessel-Viennot matrices relate to the horizontal Gessel-Viennot matrices. Unlike its vertical counterpart, the (smaller) $k \times k$ horizontal Gessel-Viennot matrix does not have a predictable form. For example, when $n = 7$, the 4×4 horizontal Gessel-Viennot matrix H_7 is

$$H_7 = \begin{bmatrix} 8266 & 846 & 68 & 2 \\ 4498 & 488 & 46 & 2 \\ 1372 & 170 & 22 & 2 \\ 238 & 34 & 6 & 2 \end{bmatrix}.$$

However, it appears that the horizontal Gessel-Viennot matrix can be derived from the vertical Gessel-Viennot matrix with judiciously chosen row and column operations.

When $n = 7$, the operations that transform the vertical determinant into the horizontal determinant are as follows. Writing r_i as the i-th row and r_j as the j-th column, the elementary row operation of adding k times the j-th row to the i-th row will be represented by $(r_i + kr_j)$.

$$V_7 \xrightarrow{\substack{c_5 - 11c_4 \\ c_6 - 25c_4 \\ c_7 - 7c_4 \\ c_6 - 7c_5 \\ c_7 - 5c_5 \\ c_7 - 3c_6}} \begin{bmatrix} 2 & 2 & 2 & 2 & -22 & 104 & -216 \\ 1 & 4 & 8 & 12 & -131 & 617 & -1280 \\ 0 & 2 & 10 & 26 & -278 & 1296 & -2680 \\ 0 & 1 & 8 & 32 & -327 & 1490 & -3059 \\ 0 & 0 & 2 & 18 & -160 & 678 & -1360 \\ 0 & 0 & 1 & 12 & -91 & 362 & -714 \\ 0 & 0 & 0 & 2 & -2 & 2 & -2 \end{bmatrix}$$

$$\xrightarrow{\substack{r_5 - 2r_6 \\ r_4 - 8r_6 \\ r_3 - 10r_6 \\ r_2 - 8r_6 \\ r_1 - 2r_6 \\ r_3 - 2r_4 \\ r_2 - 4r_4 \\ r_1 - 2r_4 \\ r_1 - 2r_2}} \begin{bmatrix} 0 & 0 & 0 & -238 & 1372 & -4498 & 8266 \\ 1 & 0 & 0 & 172 & -1007 & 3345 & -6180 \\ 0 & 0 & 0 & 34 & -170 & 488 & -846 \\ 0 & 1 & 0 & -64 & 401 & -1406 & 2653 \\ 0 & 0 & 0 & -6 & 22 & -46 & 68 \\ 0 & 0 & 1 & 12 & -91 & 362 & -714 \\ 0 & 0 & 0 & 2 & -2 & 2 & -2 \end{bmatrix}.$$

Expanding the determinant about its first, second, and third columns yields

$$\begin{bmatrix} -238 & 1372 & -4498 & 8266 \\ 34 & -170 & 488 & -846 \\ -6 & 22 & -46 & 68 \\ 2 & -2 & 2 & -2 \end{bmatrix}.$$

Multiplying the first and third rows and the second and fourth columns by -1 yields a matrix that clearly has the same determinant as H_7. Notice that the coefficients in the row and column operations are all integers arising in crystal ball sequences. A similar set of elementary row operations reduces V_n to H_n when $n = 6$ and $n = 8$. This leads us to state the following conjecture for ordinary Aztec pillows in general.

Conjecture 14. *The vertical Gessel-Viennot determinant calculation reduces to horizontal Gessel-Viennot determinant calculation.*

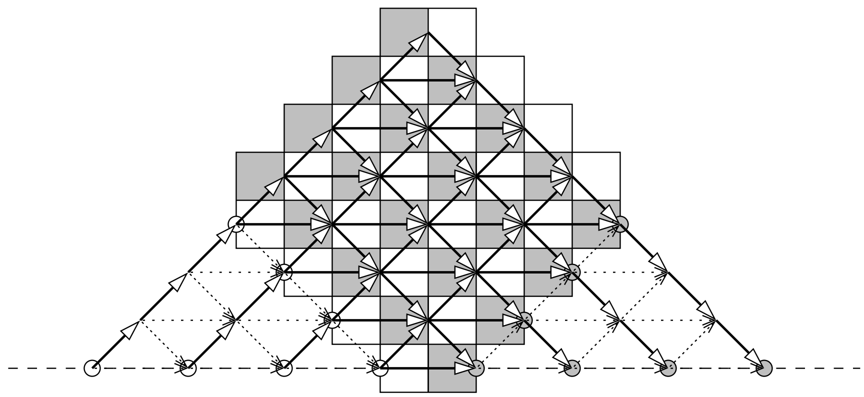

Figure 5.6: Extending lattice paths to the horizontal axis

An interesting variant of the Gessel-Viennot approach is used for the case of an Aztec diamond in the work of Eu and Fu [11]. Consider drawing a horizontal axis so that it coincides with the bottom edge in the lattice arising in the horizontal application of the Gessel-Viennot method. Extending the other $n-1$ paths down to this horizontal axis, there is a new interpretation of the paths we are constructing. We now count the number of sets of n non-intersecting paths from $1-2i$ to $2i-1$ using steps of length $(1,1)$, $(1,-1)$, or $(2,0)$. See Figure 5.6 for reference.

By the Gessel-Viennot method on this new lattice, the large Schröder numbers appear again; the number of non-intersecting paths is the determinant of a Hankel matrix:

$$\det \begin{bmatrix} s_1 & s_2 & \cdots & s_{n-1} & s_n \\ s_2 & s_3 & & s_n & s_{n+1} \\ \vdots & & \ddots & & \vdots \\ s_{n-1} & s_n & & s_{2n-2} & s_{2n-1} \\ s_n & s_{n+1} & \cdots & s_{2n-1} & s_{2n} \end{bmatrix},$$

where s_i is the i-th large Schröder number. Notice that this matrix is different from the matrix Brualdi and Kirkland found since the entries are all positive.

We can apply the same method to any non-symmetric generalized Aztec pillow such that the bottom half is of the form of an Aztec diamond. The top half may be of any shape. Notice by removing the symmetry the values in the matrix will no longer be predictable as with the case of the Aztec diamond, however our matrix will have entries that are all positive. The only thing we know is that the upper left half of the matrix (including the skew diagonal and everything above) will have the same entries as the corresponding Hankel matrix with large Schröder number values since the bottom half of the pillow is like an Aztec diamond.

As an example, the number of tilings of the region in Figure 5.7 can be calculated by the following determinant of with positive integral entries

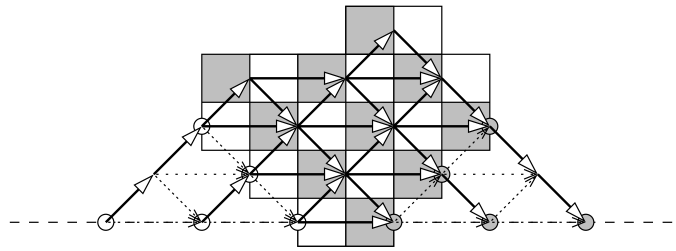

Figure 5.7: Applying Eu and Fu's method to a generalized Aztec pillow

$$\det \begin{bmatrix} 2 & 6 & 22 \\ 6 & 22 & 90 \\ 22 & 89 & 384 \end{bmatrix}.$$

The determinant of this matrix is 32, which is the number of tilings of the corresponding generalized Aztec pillow.

This method will not apply directly if we have a generalized Aztec pillow that does not have a bottom half with the form of an Aztec diamond. The lattice paths from the horizontal application of the Gessel-Viennot method do not lift uniquely to paths in the new lattice.

5.3 Experimental Results from the LU Decomposition of a Kasteleyn-Percus Matrix

As discussed in Section 3.3, the Kasteleyn-Percus matrix for an Aztec pillow is alternating centrosymmetric. This implies that $\#AP_n = \det(B+iC)\det(B-iC)$. For the Aztec Pillow AP_6, the matrix $B+iC$ equals

$$B+iC = \begin{bmatrix}
1 & 0 & 0 & i & 0 & 0 & 0 & 0 & 0 & 0 & 0 & 0 \\
i & -1 & 0 & 0 & i & 0 & 0 & 0 & 0 & 0 & 0 & 0 \\
0 & 0 & 1 & 0 & 0 & 0 & 0 & -i & 0 & 0 & 0 & 0 \\
0 & 0 & i & -1 & 0 & 0 & 0 & 0 & -i & 0 & 0 & 0 \\
-1 & 0 & 0 & i & 1 & 0 & 0 & 0 & 0 & -i & 0 & 0 \\
0 & 1 & 0 & 0 & i & -1 & 0 & 0 & 0 & 0 & -i & 0 \\
0 & 0 & 0 & 0 & 0 & 0 & 1 & 0 & 0 & 0 & 0 & -1 \\
0 & 0 & 0 & 0 & 0 & 0 & i & -1 & 0 & 0 & -1 & 0 \\
0 & 0 & 1 & 0 & 0 & 0 & 0 & i & 1 & -1 & 0 & 0 \\
0 & 0 & 0 & -1 & 0 & 0 & 0 & 0 & -1+i & -1 & 0 & 0 \\
0 & 0 & 0 & 0 & 1 & 0 & 0 & -1 & 0 & i & 1 & 0 \\
0 & 0 & 0 & 0 & 0 & -1 & -1 & 0 & 0 & 0 & i & -1
\end{bmatrix}$$

Taking the LU factorization of $B+iC$ we get the following values for L and U.

$$L = \begin{bmatrix}
1 & 0 & 0 & 0 & 0 & 0 & 0 & 0 & 0 & 0 & 0 & 0 \\
i & 1 & 0 & 0 & 0 & 0 & 0 & 0 & 0 & 0 & 0 & 0 \\
0 & 0 & 1 & 0 & 0 & 0 & 0 & 0 & 0 & 0 & 0 & 0 \\
0 & 0 & i & 1 & 0 & 0 & 0 & 0 & 0 & 0 & 0 & 0 \\
-1 & 0 & 0 & -2i & 1 & 0 & 0 & 0 & 0 & 0 & 0 & 0 \\
0 & -1 & 0 & -1 & 2i & 1 & 0 & 0 & 0 & 0 & 0 & 0 \\
0 & 0 & 0 & 0 & 0 & 0 & 1 & 0 & 0 & 0 & 0 & 0 \\
0 & 0 & 0 & 0 & 0 & 0 & i & 1 & 0 & 0 & 0 & 0 \\
0 & 0 & 1 & 0 & 0 & 0 & 0 & -2i & 1 & 0 & 0 & 0 \\
0 & 0 & 0 & 1 & 0 & 0 & 0 & -1 & -1+2i & 1 & 0 & 0 \\
0 & 0 & 0 & 0 & 1 & 0 & 0 & 1-2i & -2 & 1 & 1 & 0 \\
0 & 0 & 0 & 0 & 0 & 1 & -1 & -5 & 5i & 3/4-7i/4 & -133/260-271i/260 & 1
\end{bmatrix},$$

$$U = \begin{bmatrix} 1 & 0 & 0 & i & 0 & 0 & 0 & 0 & 0 & 0 & 0 & 0 \\ 0 & -1 & 0 & 1 & i & 0 & 0 & 0 & 0 & 0 & 0 & 0 \\ 0 & 0 & 1 & 0 & 0 & 0 & 0 & -i & 0 & 0 & 0 & 0 \\ 0 & 0 & 0 & -1 & 0 & 0 & 0 & -1 & -i & 0 & 0 & 0 \\ 0 & 0 & 0 & 0 & 1 & 0 & 0 & -2i & 2 & -i & 0 & 0 \\ 0 & 0 & 0 & 0 & 0 & -1 & 0 & -5 & -5i & -2 & -i & 0 \\ 0 & 0 & 0 & 0 & 0 & 0 & 1 & 0 & 0 & 0 & 0 & -1 \\ 0 & 0 & 0 & 0 & 0 & 0 & 0 & -1 & 0 & 0 & -1 & i \\ 0 & 0 & 0 & 0 & 0 & 0 & 0 & 0 & 1 & -1 & -2i & -2 \\ 0 & 0 & 0 & 0 & 0 & 0 & 0 & 0 & 0 & -2+2i & -5-2i & -2+5i \\ 0 & 0 & 0 & 0 & 0 & 0 & 0 & 0 & 0 & 0 & 7-4i & -4-6i \\ 0 & 0 & 0 & 0 & 0 & 0 & 0 & 0 & 0 & 0 & 0 & -1311/260+133i/260 \end{bmatrix},$$

Taking clues from LU factorizations of larger $B + iC$ matrices we decide to factor the matrices a little differently. If we set L' and U' to be the nice parts of L and U and then calculate what matrix E we would have if we set $B + iC = L'EU'$, we see that E has an especially nice form. In terms of AP_6, if we set L' and U' to be:

$$L' = \begin{bmatrix} 1 & 0 & 0 & 0 & 0 & 0 & 0 & 0 & 0 & 0 & 0 & 0 \\ i & 1 & 0 & 0 & 0 & 0 & 0 & 0 & 0 & 0 & 0 & 0 \\ 0 & 0 & 1 & 0 & 0 & 0 & 0 & 0 & 0 & 0 & 0 & 0 \\ 0 & 0 & i & 1 & 0 & 0 & 0 & 0 & 0 & 0 & 0 & 0 \\ -1 & 0 & 0 & -2i & 1 & 0 & 0 & 0 & 0 & 0 & 0 & 0 \\ 0 & -1 & 0 & -1 & 2i & 1 & 0 & 0 & 0 & 0 & 0 & 0 \\ 0 & 0 & 0 & 0 & 0 & 0 & 1 & 0 & 0 & 0 & 0 & 0 \\ 0 & 0 & 0 & 0 & 0 & 0 & 0 & 1 & 0 & 0 & 0 & 0 \\ 0 & 0 & 0 & 0 & 0 & 0 & 0 & 0 & 1 & 0 & 0 & 0 \\ 0 & 0 & 0 & 0 & 0 & 0 & 0 & 0 & 0 & 1 & 0 & 0 \\ 0 & 0 & 0 & 0 & 0 & 0 & 0 & 0 & 0 & 0 & 1 & 0 \\ 0 & 0 & 0 & 0 & 0 & 0 & 0 & 0 & 0 & 0 & 0 & 1 \end{bmatrix},$$

$$U' = \begin{bmatrix} 1 & 0 & 0 & i & 0 & 0 & 0 & 0 & 0 & 0 & 0 & 0 \\ 0 & -1 & 0 & 1 & i & 0 & 0 & 0 & 0 & 0 & 0 & 0 \\ 0 & 0 & 1 & 0 & 0 & 0 & 0 & -i & 0 & 0 & 0 & 0 \\ 0 & 0 & 0 & -1 & 0 & 0 & 0 & -1 & -i & 0 & 0 & 0 \\ 0 & 0 & 0 & 0 & 1 & 0 & 0 & -2i & 2 & -i & 0 & 0 \\ 0 & 0 & 0 & 0 & 0 & -1 & 0 & -5 & -5i & -2 & -i & 0 \\ 0 & 0 & 0 & 0 & 0 & 0 & 1 & 0 & 0 & 0 & 0 & 0 \\ 0 & 0 & 0 & 0 & 0 & 0 & 0 & -1 & 0 & 0 & 0 & 0 \\ 0 & 0 & 0 & 0 & 0 & 0 & 0 & 0 & 1 & 0 & 0 & 0 \\ 0 & 0 & 0 & 0 & 0 & 0 & 0 & 0 & 0 & -1 & 0 & 0 \\ 0 & 0 & 0 & 0 & 0 & 0 & 0 & 0 & 0 & 0 & 1 & 0 \\ 0 & 0 & 0 & 0 & 0 & 0 & 0 & 0 & 0 & 0 & 0 & -1 \end{bmatrix},$$

then E becomes:

$$E = \begin{bmatrix} 1 & 0 & 0 & 0 & 0 & 0 & 0 & 0 & 0 & 0 & 0 & 0 \\ 0 & 1 & 0 & 0 & 0 & 0 & 0 & 0 & 0 & 0 & 0 & 0 \\ 0 & 0 & 1 & 0 & 0 & 0 & 0 & 0 & 0 & 0 & 0 & 0 \\ 0 & 0 & 0 & 1 & 0 & 0 & 0 & 0 & 0 & 0 & 0 & 0 \\ 0 & 0 & 0 & 0 & 1 & 0 & 0 & 0 & 0 & 0 & 0 & 0 \\ 0 & 0 & 0 & 0 & 0 & 1 & 0 & 0 & 0 & 0 & 0 & 0 \\ 0 & 0 & 0 & 0 & 0 & 0 & 1 & 0 & 0 & 0 & 0 & 1 \\ 0 & 0 & 0 & 0 & 0 & 0 & 0 & 1 & 0 & 0 & -1 & -i \\ 0 & 0 & 0 & 0 & 0 & 0 & 0 & 0 & 1 & 1 & -2i & 2 \\ 0 & 0 & 0 & 0 & 0 & 0 & 0 & 0 & -1 & 1-2i & -5 & -5i \\ 0 & 0 & 0 & 0 & 0 & 0 & 0 & 1 & -2i & 6 & 1-16i & 16 \\ 0 & 0 & 0 & 0 & 0 & 0 & -1 & -2i & -6 & -21i & -57 & 1-57i \end{bmatrix}.$$

The matrices L and U both have determinant 1. Notice that E is a block diagonal matrix so that its determinant reduces to a non-trivial determinant of a 6×6 matrix. Amazingly, the modified Schröder numbers from Section 4.5 make another appearance! This gives a further indication that the modified Schröder numbers are somehow embedded in the Kasteleyn-Percus matrix of an ordinary Aztec pillow. Or perhaps this implies that the LU decomposition of the Kasteleyn-Percus matrix gives some combinatorial information about the region itself.

Returning to this $n \times n$ submatrix E' of E, we see that $\det E = \det(B + iC)$, so that the number of tilings of the Aztec pillow AP_n is $\det E' \cdot \overline{\det E'}$. Let S_n be the $n \times n$ principal submatrix of the modified Schröder numbers S as described in Section 4.5 and let J_n be the $n \times n$ exchange matrix. We have the following conjecture.

Conjecture 15. *The number of tilings of the Aztec pillow AP_n is equal to* $\det E' \cdot \overline{\det E'}$, *where E' is the $n \times n$ matrix $S_n + iJ_n$.*

It is unclear how to prove what the form of the $L'EU'$ decomposition should be. It is also tantalizing that this matrix is so close to a triangular matrix yet its determinant seems difficult to calculate. If this problem were rectified, this would lead to a new and probably faster way to calculate the number of tilings of an ordinary Aztec pillow. It also gives hope that a similar formula would work in the case of any rotationally symmetric region, and that there is some sort of combinatorial interpretation similar to the Hamburger Theorem that is in play with this matrix. One piece of information that appears to be useful in terms of proving a general formula for the $L'EU'$ decomposition is that the triangular blocks of entries that appear off the diagonal in L (and thus L') are in absolute value modified Schröder matrices and the triangular blocks of entries off the diagonal in U are in absolute value the inverses of modified Schröder matrices.

5.4 Random Tilings of Aztec Pillows

A final subject of future research has to do with the idea of "random tilings". In terms of an Aztec diamond, if we consider the set of all tilings of AD_n and pick one uniformly at random, an interesting phenomenon appears. Consider the inscribed circle C_n in AD_n. As n goes to infinity, outside this circle C_n all the dominoes are fixed with probability tending to 1. That is, the squares in AD_n outside C_n to the right or to the left are all covered with vertical dominoes and the squares in AD_n outside C_n above or below are all covered with horizontal dominoes. For a visualization, see Figure 5.8. This property of random domino tilings of Aztec diamonds was first proved by Jockusch, Propp, and Shor in [19]; a slightly weaker result was proved for lozenge tilings of hexagons by Cohn, Larsen, and Propp in [8].

Given this framework, we wish to determine the properties of a random tiling of an Aztec pillow. Figure 5.9 gives an example of a randomly tiled AP_{100}. It appears to have a "frozen region" near the top and near the bottom of the pillow; however, the interior structure is not clear enough to even formulate a conjecture.

This concludes our study of Aztec pillows. We have learned many new things yet many mysteries remain for the curious pattern-seekers.

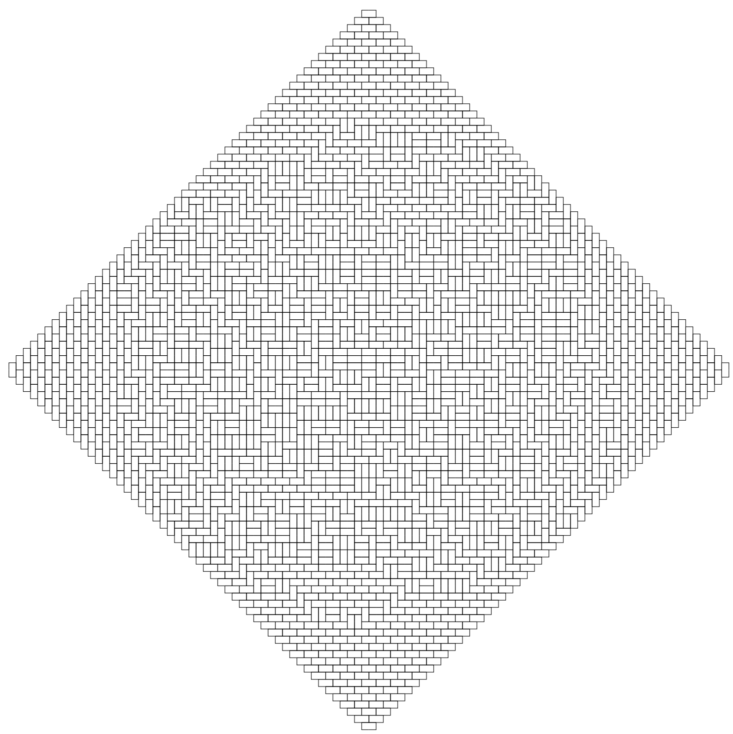

Figure 5.8: A randomly tiled AD_{50}

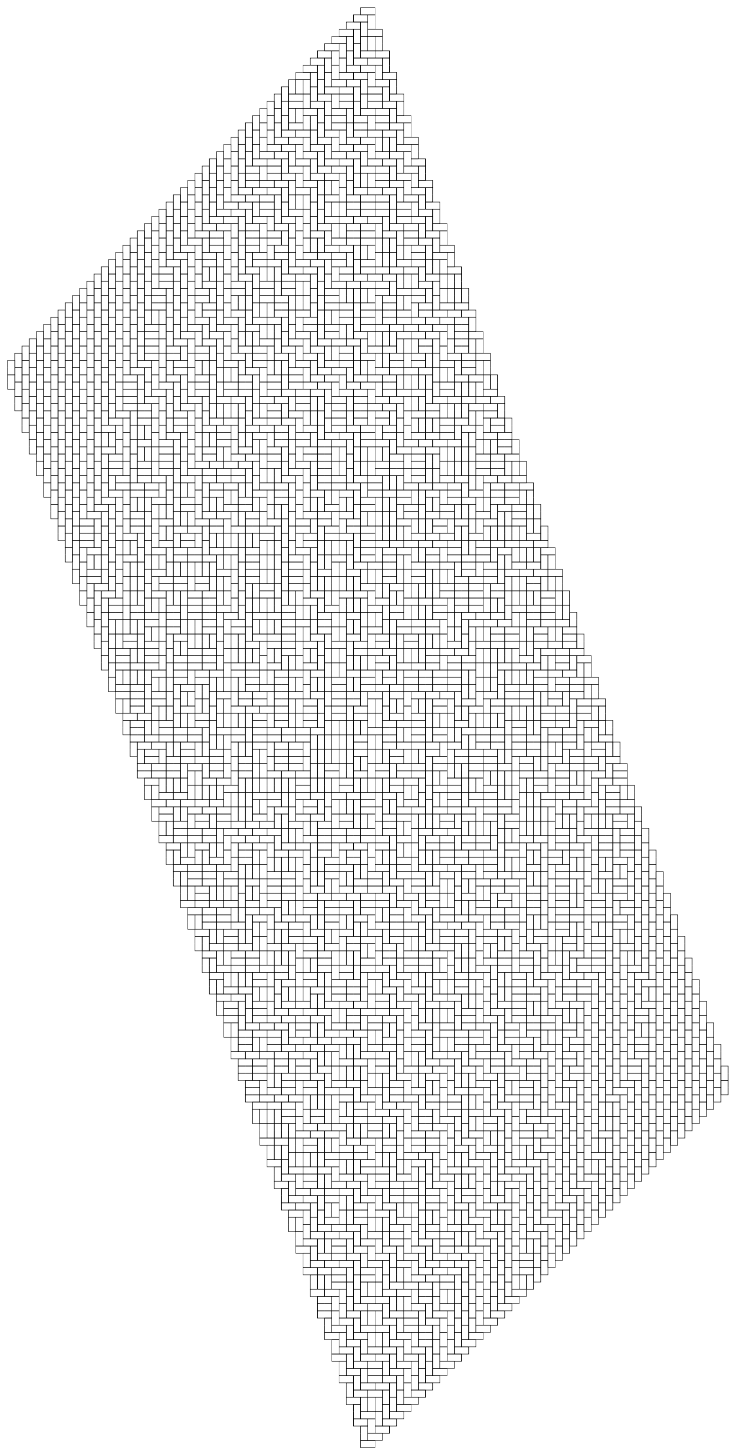

Figure 5.9: A randomly tiled AP_{100}

BIBLIOGRAPHY

[1] Martin Aigner. Lattice paths and determinants. In *Computational discrete mathematics*, volume 2122 of *Lecture Notes in Comput. Sci.*, pages 1–12. Springer, Berlin, 2001.

[2] A. L. Andrew. Eigenvectors of certain matrices. *Linear Algebra Appl.*, 7:151–162, 1973.

[3] M. Azaola and F. Santos. The number of triangulations of the cyclic polytope $C(n, n-4)$. *Discrete Comput. Geom.*, 27(1):29–48, 2002. Geometric combinatorics (San Francisco, CA/Davis, CA, 2000).

[4] A. T. Benjamin and J. J. Quinn. *Proofs That Really Count: The Art of Combinatorial Proof.* The Mathematical Association of America, Washington, D.C., 2003.

[5] Anders Björner and Richard P. Stanley. *A Combinatorial Miscellany.* Cambridge University Press, 1999.

[6] Richard Brualdi and Stephen Kirkland. Aztec diamonds and digraphs, and Hankel determinants of Schröder numbers, 2003. Available at http://www.math.wisc.edu/∼brualdi/aztec2.pdf.

[7] Mihai Ciucu. Enumeration of perfect matchings in graphs with reflective symmetry. *J. Combin. Theory Ser. A*, 77(1):67–97, 1997.

[8] Henry Cohn, Michael Larsen, and James Propp. The shape of a typical boxed plane partition. *New York J. Math.*, 4:137–165 (electronic), 1998. arXiv:math.CO/9801059.

[9] N. Destainville. Entropy and boundary conditions in random rhombus tilings. *J. Phys. A*, 31(29):6123–6139, 1998. arXiv:cond-mat/9804062.

[10] Noam Elkies, Greg Kuperberg, Michael Larsen, and James Propp. Alternating-sign matrices and domino tilings. II. *J. Algebraic Combin.*, 1(3):219–234, 1992.

[11] Sen-Peng Eu and Tung-Shan Fu. A Simple Proof of the Aztec Diamond Theorem. 2004. preprint, arXiv:math.CO/0412041.

[12] I. Fischer. Moments of Inertia Associated with the Lozenge Tilings of a Hexagon. *Seminaire Lotharingien de Combinatoire*, 45:B45f, 2001. arXiv:math.CO/0012126.

[13] Ira Gessel and Xavier G. Viennot. Binomial determinants, paths, and hook length formulae. *Adv. in Math.*, 58:300–321, 1985.

[14] Ira Gessel and Xavier G. Viennot. Determinants, paths, and plane partitions. 1989. preprint, available at http://www.cs.brandeis.edu/∼ira/papers/pp.pdf.

[15] Ronald L. Graham, Donald E. Knuth, and Oren Patashnik. *Concrete Mathematics: A Foundation for Computer Science*. Addison-Wesley Longman Publishing Co., Inc., 1994.

[16] D. Grensing, I. Carlsen, and H.-C. Zapp. Some Exact Results for the Dimer Problem on Plane Lattices with Non-Standard Boundaries. *Phil. Mag. A*, 41:777–781, 1980.

[17] H. Helfgott. Edge Effects on Local Statistics in Lattice Dimers: A Study of the Aztec Diamond (Finite Case), Senior Thesis, Brandeis University, May 1998. arXiv:math.CO/0007136.

[18] William Jockusch. Perfect Matchings and Perfect Squares. *J. Comb. Theory Ser. A*, 67(1):100–115, 1994.

[19] William Jockusch, James Propp, and Peter Shor. Random Domino Tilings and the Arctic Circle Theorem. arXiv:math.CO/9801068.

[20] Samuel Karlin and James McGregor. Coincidence probabilities. *Pacific J. Math.*, 9:1141–1164, 1959.

[21] P. W. Kasteleyn. The Statistics of Dimers on a Lattice I. The Number of Dimer Arrangements on a Quadratic Lattice. *Physica*, 27:1209–1225, 1961.

[22] Richard Kenyon. Local statistics of lattice dimers. *Ann. Inst. H. Poincaré Probab. Statist.*, 33(5):591–618, 1997. arXiv:math.CO/0105054.

[23] Ilia Krasikov and Simon Litsyn. On integral zeros of Krawtchouk polynomials. *J. Combin. Theory Ser. A*, 74(1):71–99, 1996.

[24] Eric H. Kuo. Applications of Graphical Condensation for Enumerating Matchings and Tilings, 2003. arXiv:math.CO/0304090.

[25] Greg Kuperberg. An exploration of the permanent-determinant method. *Electron. J. Combin.*, 5(1):Research Paper 46, 34 pp. (electronic), 1998. arXiv:math.CO/9810091.

[26] Greg Kuperberg. Kasteleyn cokernels. *Electron. J. Combin.*, 9(1):Research Paper 29, 30 pp. (electronic), 2002. arXiv:math.CO/0108150.

[27] B. Lindström. On the vector representations of induced matroids. *Bull. London Math. Soc.*, 5:85–90, 1973.

[28] L. Lovász and M. D. Plummer. *Matching theory*, volume 121 of *North-Holland Mathematics Studies*. North-Holland Publishing Co., Amsterdam, 1986. Annals of Discrete Mathematics, 29.

[29] F. J. MacWilliams and N. J. A. Sloane. *The Theory of Error-Correcting Codes*. North Holland Publishing Company, Amsterdam, 1977.

[30] M. E. Mays and Jerzy Wojciechowski. A determinant property of Catalan numbers. *Discrete Math.*, 211(1-3):125–133, 2000.

[31] T. Muir. *The Theory of Determinants in the Historical Order of Development*, volume 3. Macmillan, London, 1960.

[32] Lior Pachter. Combinatorial approaches and conjectures for 2-divisibility problems concerning domino tilings of polyominoes. *Electron. J. Combin.*, 4(1):Research Paper 29, 10 pp. (electronic), 1997.

[33] J. Percus. One More Technique for the Dimer Problem. *Journal of Mathematical Physics*, 10:1881–1884, 1969.

[34] James Propp. Dimers and Dominoes, 1997. http://www.math.wisc.edu/˜propp/articles.html.

[35] James Propp. Enumeration of matchings: problems and progress. In *New perspectives in algebraic combinatorics (Berkeley, CA, 1996–97)*, volume 38 of *Math. Sci. Res. Inst. Publ.*, pages 255–291. Cambridge Univ. Press, Cambridge, 1999. arXiv:math.CO/9904150.

[36] James Propp. Generalized domino-shuffling. *Theoret. Comput. Sci.*, 303(2-3):267–301, 2003. Tilings of the plane arXiv:math.CO/0111034.

[37] Scott Sheffield. Ribbon tilings and multidimensional height functions. *Trans. Amer. Math. Soc.*, 354(12):4789–4813 (electronic), 2002. arXiv:math.CO/0107095.

[38] N. J. A. Sloane. The On-Line Encyclopedia of Integer Sequences, published electronically at http://www.research.att.com/˜njas/sequences/, 2004.

[39] Richard P. Stanley. *Enumerative Combinatorics. Vol. 1.* Cambridge University Press, Cambridge, 1997.

[40] David Tao and Mark Yasuda. A spectral characterization of generalized real symmetric centrosymmetric and generalized real symmetric skew-centrosymmetric matrices. *SIAM J. Matrix Anal. Appl.*, 23(3):885–895 (electronic), 2001/02. http://epubs.siam.org/sam–bin/dbq/article/38673.

[41] William P. Thurston. Conway's tiling groups. *Amer. Math. Monthly*, 97(8):757–773, 1990.

[42] J. R. Weaver. Centrosymmetric (cross-symmetric) matrices, their basic properties, eigenvalues, eigenvectors. *Amer. Math. Monthly*, 92:711–717, 1985.

Appendix A

3-PILLOW DATA

A.1 Table of Values

Propp calculated the number of tilings of ordinary Aztec pillows (3-pillows). A table is shown below for completeness. The non-square part was calculated using a product of the bold faced terms. When the power of a bolded factor is not bold, then the power of the factor as a factor of the non-square part is less than the total power shown. For example, $\#AP_5 = 2^{10}$ and $s_5 = 2^4$, so the 10 in the power of 2 is not bolded. However, $\#AP_7 = 2^4 \cdot 3^2 \cdot 5 \cdot 19^2$ and $s_7 = 3^2 \cdot 5$, so the 2 in the power of 3 is bolded.

n	$\#AP_n^3$	Non-Square Part
1	$\mathbf{2}$	2
2	$\mathbf{5}$	5
3	$2^2 \cdot \mathbf{5}$	5
4	$3^2 \cdot \mathbf{13}$	13
5	$\mathbf{2}^{10}$	16
6	$19^2 \cdot \mathbf{37}$	37
7	$2^4 \cdot \mathbf{3^2} \cdot \mathbf{5} \cdot 19^2$	45
8	$\mathbf{109} \cdot 263^2$	109
9	$\mathbf{2}^9 \cdot 3^4 \cdot \mathbf{5} \cdot 11^2 \cdot \mathbf{13}$	130
10	$3^4 \cdot \mathbf{313} \cdot 911^2$	313
11	$2^6 \cdot 3^2 \cdot \mathbf{13} \cdot \mathbf{29} \cdot 43^2 \cdot 71^2$	377
12	$\mathbf{5} \cdot 11^4 \cdot 31^2 \cdot 151^2 \cdot \mathbf{181}$	905
13	$\mathbf{2}^{28} \cdot 7^2 \cdot \mathbf{17}^3 \cdot 31^2$	1088
14	$101^2 \cdot 103^2 \cdot \mathbf{2617} \cdot 8363^2$	2617
15	$2^8 \cdot \mathbf{5} \cdot \mathbf{17}^3 \cdot 19^2 \cdot \mathbf{37} \cdot 53^2 \cdot 71^2 \cdot 89^2$	3145
16	$31^2 \cdot \mathbf{7561} \cdot 27283^2 \cdot 35149^2$	7561
17	$\mathbf{2}^{17} \cdot \mathbf{3^2} \cdot \mathbf{5} \cdot 11^2 \cdot 19^4 \cdot 59^2 \cdot 61^2 \cdot \mathbf{101} \cdot 241^2$	9090
18	$3^{10} \cdot 5^2 \cdot \mathbf{13} \cdot 29^2 \cdot \mathbf{41}^4 \cdot 43^2 \cdot 211^2 \cdot 1723^2$	21853
19	$2^{10} \cdot 23^2 \cdot 43^2 \cdot \mathbf{109} \cdot \mathbf{241} \cdot 263^2 \cdot 439^2 \cdot 461^2 \cdot 593^2$	26269
20	$47^2 \cdot \mathbf{137} \cdot \mathbf{461} \cdot 313949^2 \cdot 8647^2 \cdot 298999^2$	63157
21	$\mathbf{2}^{34} \cdot 3^4 \cdot \mathbf{5}^3 \cdot 7^4 \cdot 11^2 \cdot \mathbf{13}^3 \cdot 19^2 \cdot 23^2 \cdot 47^2 \cdot 71^2 \cdot \mathbf{73} \cdot 167^2$	75920
22	$\mathbf{5}^{10} \cdot \mathbf{7^2} \cdot \mathbf{149} \cdot 10399^2 \cdot 39551^2 \cdot 55201^2 \cdot 10099^2$	182525
23	$2^{12} \cdot 3^4 \cdot 5^4 \cdot 79^2 \cdot \mathbf{313} \cdot \mathbf{701} \cdot 911^2 \cdot 1429^2 \cdot 1481^2 \cdot 1741^2 \cdot 3691^2$	219413
24	$19^2 \cdot \mathbf{37} \cdot \mathbf{53}^3 \cdot 107^2 \cdot \mathbf{269} \cdot 431^2 \cdot 809^2 \cdot 89317^2 \cdot 61723^2 \cdot 5779^2$	527509

Table A.1: Number of tilings of 3-pillows AP_n^3 up to $n = 24$

A.2 Supplementary Data for 3-pillows

For comparison with the q-pillows for q equal to 5, 7, or 9 presented in Appendices C and D, we include the following data. We let $\#AP_n = \ell_n^2 s_n$ as in the previous section. Tables A.2 and A.3 give the ratio of consecutive terms of s_n split into the two cases when n is even or n is odd. It appears that each table has a limiting value, and that the limiting value for Table A.2 is twice that of the limiting value of Table A.3. A more illuminating picture comes from the ratio of s_n/s_{n-2}. This data is presented numerically in Table A.4 and is plotted in Figure A.1. The intriguing property of this plot is the appearance of a damped sine curve. As we might expect, the limit of this apparent damped sine curve is the largest real root of $x^4 - 2x^3 - 2x^2 - 2x + 1$.

n	s_n/s_{n-1}
2	2.500000000000000000000000000000000000000
4	2.600000000000000000000000000000000000000
6	2.312500000000000000000000000000000000000
8	2.422222222222222222222222222222222222222
10	2.407692307692307692307692307692307692308
12	2.400530503978779840848806366047745358090
14	2.405330882352941176470588235294117647059
16	2.404133545310015898251192368839427662957
18	2.404070407040704070407040704070407040704
20	2.404240740035783623282195744032890479272
22	2.404175447839831401475237091675447839831
24	2.404182979130680497509263352672813370220
26	2.404187575104791882847563687286513150632
28	2.404184707727985812700361503308096309938
30	2.404185383839238242544347237662525979989
32	2.404185437967475048561645638911720014192
34	2.404185333868926344733673210350387690825
36	2.404185371911035420400679242189155579214
38	2.404185368103824749725513783419278751335
40	2.404185365177531615032303625900585022565

Table A.2: Ratios of s_n to s_{n-1} for n even

n	s_n/s_{n-1}
3	1.000000000000000000000000000000000000000
5	1.230769230769230769230769230769230769231
7	1.216216216216216216216216216216216216216
9	1.192660550458715596330275229357798165138
11	1.204472843450479233226837060702875399361
13	1.202209944751381215469613259668508287293
15	1.201757737867787542988154375238823079862
17	1.202221928316360269805581272318476392012
19	1.202077517960920697387086441220885004347
21	1.202083696185695964026157037224694016499
23	1.202098342692781810710861525818381043693
25	1.202091338725974343565702196550201039224
27	1.202092580724932093781095669547775083321
29	1.202092888079784492355711081943608772554
31	1.202092607925447612983370072412989087280
33	1.202092690948334484360455771414844893944
35	1.202092688981407483370107391998088821455
37	1.202092679882664742504530487175249692821
39	1.202092684009664090498879348781539957065

Table A.3: Ratios of s_n to s_{n-1} for n odd

n	s_n/s_{n-2}
3	2.500000000000000000000000000000000000000
4	2.600000000000000000000000000000000000000
5	3.200000000000000000000000000000000000000
6	2.846153846153846153846153846153846153846
7	2.812500000000000000000000000000000000000
8	2.945945945945945945945945945945945945946
9	2.888888888888888888888888888888888888889
10	2.871559633027522935779816513761467889908
11	2.900000000000000000000000000000000000000
12	2.891373801916932907348242811501597444089
13	2.885941644562334217506631299734748010610
14	2.891712707182320441988950276243093922652
15	2.890625000000000000000000000000000000000
16	2.889186090943828811616354604508979747803
17	2.890302066772655007949125596184419713831
18	2.890226160560772384605210950932416347044
19	2.889878987898789878987898789878987898790
20	2.890083741362741957625955246419255937400
21	2.890098595302447752103239559937568997678
22	2.890020108618205424576848172015770223411
23	2.890055321390937829293993677555321390938
24	2.890064374743185864950006848376934666484
25	2.890047535925400956187646128533860801320
26	2.890053060706073261309285718347933400188
27	2.890056046704535777478497557221572146333
28	2.890052599852151057802114620318800101540
29	2.890053338789987040447445603983357206193
30	2.890054151538515137078812855923407540997
31	2.890053477995553192517763062496979071004
32	2.890053543062706537069298131878858967876
33	2.890053742665122171255151212533644288142
34	2.890053617529017636054327030922027751552
35	2.890053612800160587482540293239434263681
36	2.890053658530301780775097497006191049198
37	2.890053636655237580404356706913562504139
38	2.890053632078617502414569695520621483687
39	2.890053642000688949036608049704793348849
40	2.890053638483013380554193573197159505526

Table A.4: Ratios of s_n to s_{n-2}

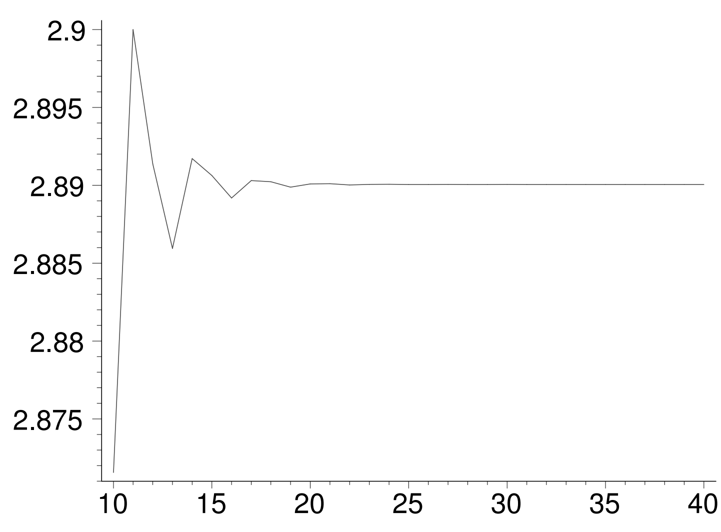

Figure A.1: Damped sinusoidal behavior observed in 3-pillows

Appendix B

AZTEC PILLOWS OF THE FORM $(1,\dots,1,3,1,\dots,1)$

n	$(3, 1\text{'s})_n$	$(1, 3, 1\text{'s})_n$	$(1, 1, 3, 1\text{'s})_n$	$(1, 1, 1, 3, 1\text{'s})_n$	$(\overbrace{1,\dots,1}^{4}, 3, 1\text{'s})_n$	$(\overbrace{1,\dots,1}^{5}, 3, 1\text{'s})_n$	$(\overbrace{1,\dots,1}^{6}, 3, 1\text{'s})_n$	$(\overbrace{1,\dots,1}^{7}, 3, 1\text{'s})_n$	$(\overbrace{1,\dots,1}^{8}, 3, 1\text{'s})_n$
1	5								
2	10	25							
3	17	65	113						
4	26	146	346	481					
5	37	292	932	1637	1985				
6	50	533	2248	5013	7218	8065			
7	65	905	4937	13897	24201	30529	32513		
8	82	1450	10018	35218	74530	108970	126034	130561	
9	101	2216	19016	82436	211460	363080	469160	513125	523265
10	122	3257	34112	179972	556040	1126148	1656128	1963193	2072698

Appendix C

5-PILLOW DATA

C.1 Table of Values

As the first previously unknown case of nicely behaving generalized Aztec pillows, we present as much data as collected about AP_n^5, also called 5-pillows. Table C.1 contains the number of tilings of AP_n^5 for n up to 40, while Table C.2 continues this data for n up to 70. The non-square part was calculated using a product of the bold faced terms. The same bolding convention is used as in Appendix A. The factorization of and the non-square part of AP_n^5 was calculated using PARI, as outlined in Section C.3.

n	$\#AP_n^5$	Non-Square Part
1	$\mathbf{2}$	2
2	$\mathbf{5}$	5
3	$\mathbf{13}$	13
4	$2^2 \cdot \mathbf{13}$	13
5	$3^2 \cdot \mathbf{29}$	29
6	$\mathbf{2} \cdot 7^2 \cdot \mathbf{17}$	34
7	$\mathbf{2^6} \cdot 3^2 \cdot \mathbf{5^2}$	100
8	$\mathbf{2} \cdot \mathbf{5^3} \cdot 7^2 \cdot \mathbf{13}$	130
9	$3^2 \cdot \mathbf{5} \cdot 29^2 \cdot \mathbf{61}$	305
10	$2^4 \cdot 3^2 \cdot \mathbf{19^2} \cdot 29^2$	361
11	$3^6 \cdot 41^2 \cdot \mathbf{881}$	881
12	$2^2 \cdot \mathbf{5} \cdot 31^2 \cdot 89^2 \cdot \mathbf{229}$	1145
13	$\mathbf{2^{13}} \cdot 3^6 \cdot 13^2 \cdot \mathbf{1453}$	2906
14	$2^2 \cdot 79^2 \cdot 953^2 \cdot \mathbf{3557}$	3557
15	$19^2 \cdot \mathbf{8669} \cdot 43003^2$	8669
16	$2^6 \cdot 3^4 \cdot \mathbf{17^2} \cdot \mathbf{37} \cdot 98873^2$	10693
17	$\mathbf{26893} \cdot 49644383^2$	26893
18	$\mathbf{2^{10}} \cdot \mathbf{5^3} \cdot \mathbf{421} \cdot 14010851^2$	33680
19	$\mathbf{2^{35}} \cdot \mathbf{5^5} \cdot \mathbf{521} \cdot 6277^2$	83360
20	$\mathbf{2^{10}} \cdot \mathbf{5^2} \cdot 37^2 \cdot 257 \cdot 258007163^2$	102800
21	$\mathbf{3^2} \cdot \mathbf{5^3} \cdot 1677^2 \cdot \mathbf{5657} \cdot 107775611^2$	254565
22	$2^8 \cdot 3^2 \cdot \mathbf{5} \cdot \mathbf{229} \cdot \mathbf{277} \cdot 5273^2 \cdot 69689357^2$	317165
23	$3^6 \cdot \mathbf{829} \cdot \mathbf{953} \cdot 1321^2 \cdot 68947^2 \cdot 111791^2$	790037
24	$2^4 \cdot 3^2 \cdot \mathbf{17} \cdot \mathbf{23^2} \cdot 29^2 \cdot 31^2 \cdot \mathbf{109} \cdot 3593^2 \cdot 178947631^2$	980237
25	$\mathbf{2^{21}} \cdot 11^2 \cdot 31^6 \cdot \mathbf{97} \cdot 1789^2 \cdot \mathbf{12517} \cdot 235723^2$	2428298
26	$2^4 \cdot \mathbf{3^2} \cdot \mathbf{5} \cdot 17^2 \cdot 31^2 \cdot \mathbf{61} \cdot \mathbf{1097} \cdot 2211657330256441^2$	3011265
27	$\mathbf{13} \cdot 17^2 \cdot \mathbf{575677} \cdot 18231881^2 \cdot 399960749339^2$	7483801
28	$2^{10} \cdot 13^2 \cdot 127^2 \cdot \mathbf{9301217} \cdot 1007998365484088 41^2$	9301217
29	$\mathbf{3^4} \cdot 29^2 \cdot \mathbf{137} \cdot \mathbf{2081} \cdot 12149633^2 \cdot 524888608699277^2$	23092857
30	$\mathbf{2^9} \cdot \mathbf{13} \cdot \mathbf{29} \cdot 113^2 \cdot \mathbf{37993} \cdot 1471746643^2 \cdot 3901319205691^2$	28646722
31	$\mathbf{2^{44}} \cdot \mathbf{5} \cdot 11^2 \cdot \mathbf{149} \cdot \mathbf{23857} \cdot 1185523^2 \cdot 1573399^2 \cdot 10939021^2$	71093860
32	$\mathbf{2^9} \cdot 11^2 \cdot 59^2 \cdot \mathbf{149^3} \cdot \mathbf{296237} \cdot 7549169^2 \cdot 2951523929123521^2$	88278626
33	$3^2 \cdot \mathbf{5} \cdot \mathbf{149} \cdot 49831^2 \cdot \mathbf{294317} \cdot 7516933^2 \cdot 1815129504984124853^2$	219266165
34	$2^{12} \cdot \mathbf{5^3} \cdot \mathbf{54442097} \cdot 80619627749^2 \cdot 7559882680695003557^2$	272210485
35	$\mathbf{3^4} \cdot \mathbf{5} \cdot 19^2 \cdot 109^2 \cdot \mathbf{593} \cdot 3581^2 \mathbf{25321} \cdot 201800713^2 \cdot 3356075623404281417^2$	675690885
36	$2^6 \cdot 3^4 \cdot \mathbf{5} \cdot \mathbf{167733113} \cdot 1203004071587^2 \cdot 2171643672977970721 43^2$	838665565
37	$\mathbf{2}^{31} \cdot 3^{12} \cdot 43^2 \cdot 109^2 \cdot 167^2 \cdot \mathbf{18973} \cdot \mathbf{54877} \cdot 1014463606545094808223 0019^2$	2082362642
38	$2^6 \cdot 241^2 \cdot 57901^2 \cdot \mathbf{2585391353} \cdot 27684765164678326816667455250155 3^2$	2585391353
39	$\mathbf{11^2} \cdot \mathbf{37} \cdot 1451^2 \cdot 45817^2 \cdot \mathbf{1433821} \cdot 6119671347028272438671820421061199 7^2$	6419216617
40	$2^{14} \cdot 163^2 \cdot \mathbf{229} \cdot \mathbf{277} \cdot 2707^2 \cdot \mathbf{125617} \cdot 349663^2 \cdot 1278701^2 \cdot 2825489^2 \cdot 12128912470613677381^2$	7968263161

Table C.1: Number of tilings of 5-pillows AP_n^5 up to $n = 40$

n	$\#(5,\ldots,5,5)_n$	Non-Square Part
41	$\mathbf{3}^{4} \cdot \mathbf{61}^{4} \cdot 71^{2} \cdot 11981^{2} \cdot \mathbf{590713} \cdot 9553690728782586143221708883903769827 17^{2}$	19782387657
42	$\mathbf{2}^{28} \cdot \mathbf{5} \cdot \mathbf{17} \cdot 3338639^{2} \cdot \mathbf{4514357} \cdot 1448355027841^{2} \cdot 416989344863505711582865926 1^{2}$	24558102080
43	$\mathbf{2}^{97} \cdot \mathbf{5}^{5} \cdot 97^{2} \cdot 101^{2} \cdot \mathbf{95274169} \cdot 4107494623^{2} \cdot 2617071745547895612423 77^{2}$	60975468160
44	$\mathbf{2}^{28} \cdot \mathbf{3}^{8} \cdot \mathbf{5}^{3} \cdot \mathbf{37} \cdot \mathbf{78929} \cdot 5981377^{2} \cdot 495479432683637^{2} \cdot 1229351478285509654304061461 1^{2}$	75696068160
45	$\mathbf{29} \cdot \mathbf{41} \cdot 71^{2} \cdot 73^{2} \cdot 613^{2} \cdot 829^{2} \cdot 12049^{2} \cdot 35671^{2} \cdot \mathbf{158060741} \cdot 565335654991^{2} \cdot 153642591368618123663338500 7^{2}$	187934221049
46	$2^{16} \cdot \mathbf{5} \cdot \mathbf{101}^{3} \cdot 113^{2} \cdot 173^{2} \cdot 10753^{2} \cdot \mathbf{461972561} \cdot 5623943161^{2} \cdot 1415133984581972329^{2} \cdot 1075597124957601983 3^{2}$	233296143305
47	$\mathbf{5}^{3} \cdot 53^{2} \cdot \mathbf{6317} \cdot 52253^{2} \cdot \mathbf{18338681} \cdot 15811368983048738425802036 81^{2} \cdot 812368187637948569467158286 9^{2}$	579227239385
48	$2^{8} \cdot 3^{4} \cdot \mathbf{5} \cdot 7^{2} \cdot \mathbf{53} \cdot 103^{2} \cdot \mathbf{241} \cdot \mathbf{349} \cdot \mathbf{32261} \cdot 201942991^{2} \cdot 5239784811304896865840289270728435738420421469035807^{2}$	719061718985
49	$\mathbf{2}^{43} \cdot \mathbf{3}^{2} \cdot \mathbf{53}^{3} \cdot 109^{2} \cdot \mathbf{269} \cdot \mathbf{673} \cdot 6131^{2} \cdot 8779^{2} \cdot \mathbf{10337} \cdot 97111639^{2} \cdot 19713846562349^{2} \cdot 439145383101671558134468286 17^{2}$	1785296013426
50	$2^{8} \cdot 3^{2} \cdot \mathbf{5} \cdot \mathbf{13} \cdot \mathbf{53} \cdot \mathbf{281} \cdot \mathbf{2289409} \cdot 29815464978238573^{2} \cdot 308877776424379545184158050936726391550257733523395 19^{2}$	2216250935405
51	$3^{8} \cdot 29^{2} \cdot 61^{2} \cdot 281^{2} \cdot \mathbf{401} \cdot \mathbf{13721838469} \cdot 168629791072742475148405672063^{2} \cdot 424115273654697478809506650595692247 9^{2}$	5502457226069
52	$2^{18} \cdot 3^{4} \cdot \mathbf{17} \cdot \mathbf{173} \cdot \mathbf{10733} \cdot \mathbf{216397} \cdot 657777308421172174357844412419988667435239493898163339571096555494760149 7^{2}$	6830734251941
53	$17^{4} \cdot \mathbf{173}^{3} \cdot 401^{2} \cdot 499^{2} \cdot \mathbf{339208217} \cdot 15060848919125717377^{2} \cdot 290812043127282613090888754805015807353528866792786 1^{2}$	16959393225349
54	$\mathbf{2}^{17} \cdot \mathbf{13}^{2} \cdot \mathbf{17}^{3} \cdot 31^{2} \cdot \mathbf{61} \cdot \mathbf{173} \cdot 677^{2} \cdot \mathbf{347201} \cdot 38775808828504711500067747729013422147417012752705790757729167146256732672 9^{2}$	21053413831138
55	$\mathbf{2}^{70} \cdot 3^{2} \cdot \mathbf{5}^{8} \cdot 11^{4} \cdot 19^{2} \cdot 31^{6} \cdot 59^{2} \cdot \mathbf{61}^{5} \cdot 359^{2} \cdot 367^{2} \cdot \mathbf{653}^{3} \cdot \mathbf{13122601} \cdot 682671253276850974 27^{2} \cdot 6910106506573455016318408129334 3^{2}$	52271256563300
56	$\mathbf{2}^{17} \cdot 3^{10} \cdot 31^{2} \cdot \mathbf{41} \cdot \mathbf{61}^{2} \cdot 501659^{2} \cdot \mathbf{212666609} \cdot 3283503871243951^{2} \cdot 375453695847331549079^{2} \cdot 591277098226018330038239072326954917500 57^{2}$	64889261071298
57	$3^{2} \cdot \mathbf{61}^{3} \cdot \mathbf{12473} \cdot \mathbf{211744837} \cdot 7689460136837^{2} \cdot 120317615730711656113^{2} \cdot 6035692272284231703219414782906771341769730565780822939 01^{2}$	161106694465961
58	$2^{20} \cdot \mathbf{61} \cdot 127^{2} \cdot \mathbf{977} \cdot \mathbf{3355836277} \cdot 2104902616309^{2} \cdot 874090577800454614414396273583286701969460419238366722014621226920425311268037^{2}$	199997774600369
59		496554148265225
60		616421080464625
61		1530446326625450
62		1899892268297341
63		4717046233150309
64		5855733366505309
65		14538589112770421
66		18048168441997840
67		44809909783257760
68		55626932047995920
69		138110327480493437
70		171449865342371029

Table C.2: Number of tilings of 5-pillows AP_n^5 up to $n = 70$

C.2 Supplementary Data for 5-pillows

We can write $\#AP_n^5 = (\ell_{n,5})^2(s_{n,5})$. The ratio of consecutive terms of $s_{n,5}$ split into two cases when n is even or n is odd; these two cases are presented in Tables C.3 and C.4. It appears that each table has a limiting value, and that the limiting value for Table C.4 is twice that of the limiting value of Table C.3. A more illuminating picture comes from the ratio of $s_{n,5}/s_{n-2,5}$. This data is presented numerically in Table C.5 and is plotted in Figures C.1 and C.2 for different ranges of n. The intriguing property of this plot is the appearance of a damped sine curve. We would hope to estimate the limiting value of the damped sine curve since if the $s_{n,5}$ satisfy some linear recurrence then the limit the largest real root of the recursion polynomial, as it was in the 3-pillow case discussed in Section A.2.

n	$s_{n,5}/s_{n-1,5}$
2	2.5000000000000000000000000000000000000
4	1.0000000000000000000000000000000000000
6	1.1724137931034482758620689655172413793 10
8	1.3000000000000000000000000000000000000
10	1.1836065573770491803278688524590163934 43
12	1.2996594778660612939841089670828603859 25
14	1.2240192704748795595320027529249827942 19
16	1.2334756027223439843119160226092974968 28
18	1.2523705053359610307514966719964302978 47
20	1.2332053742802303262955854126679462571 98
22	1.2459096890774458389802211615893779584 78
24	1.2407482181214297558215627875656456596 34
26	1.2400722646067327815614063842246709423 64
28	1.2428466497171691230164992361501862489 40
30	1.2405014243148866335594595333093692131 73
32	1.2417194114934819968981850190719704908 41
34	1.2414614220119187107595921149074687378 24
36	1.2411970971015836627720677333097367444 88
38	1.2415663347268213237567292085525226206 01
40	1.2413139540886753658526678754701385394 92
42	1.2414124374572203339569810554339800641 79
44	1.2414184006160158688972663723784355442 66
46	1.2413712734317440121873522087433972005 11
48	1.2414155793993227620485933960217149638 08
50	1.2413912979909664465574809379056811462 52
52	1.2413970652200656657135121669850428493 78
54	1.2414013609678981262622503732844766691 07
56	1.2413947040419377566358164741066214313 99
58	1.2413995288235834207474597280550795589 89
60	1.2413975044175350376709757535520888565 09
62	1.2413975160347498025200693879243058154 28
64	1.2413983406294749489724418925140734849 31
66	1.2413975181501395527346994560033467510 52
68	1.2413979924766486168102540018570915971 82
70	1.2413978626369301355511782695304056725 14

Table C.3: Ratios of $s_{n,5}$ to $s_{n-1,5}$ for n even

C.3 PARI Code to Calculate Factorizations

To factor some large number n with relatively small factors, we use an elliptic curve factorization. The code that follows is taken from William A Stein's notes on elliptic curve factorization, available online at
http://modular.fas.harvard.edu/edu/Fall2001/124/lectures/lecture31/lecture31/.
Factor the small factors out of n, and define the remainder to be N. Input this value as `N` in PARI, and use the following code.

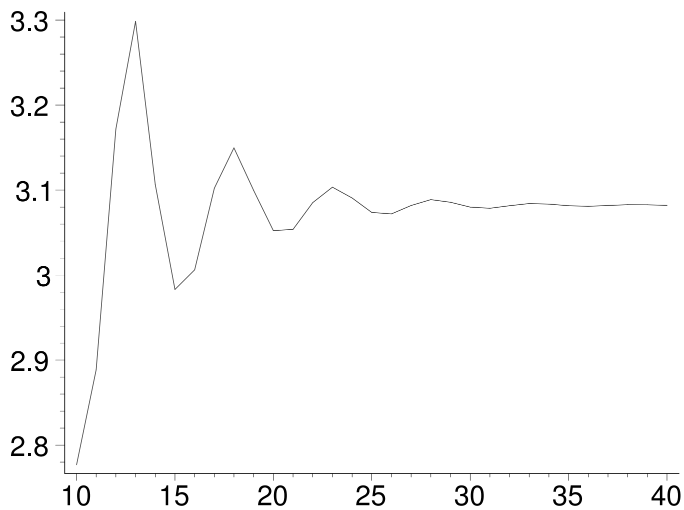

Figure C.1: Damped sinusoidal behavior observed in 5-pillows ($10 \leq n \leq 40$)

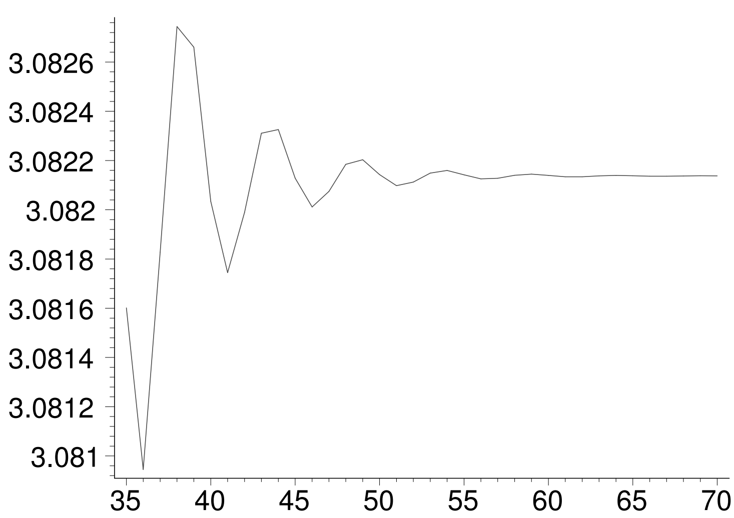

Figure C.2: Damped sinusoidal behavior observed in 5-pillows ($35 \leq n \leq 70$)

n	$s_{n,5}/s_{n-1,5}$
3	2.6000000000000000000000000000000000000000
5	2.2307692307692307692307692307692307692231
7	2.9411764705882352941176470588235294117651
9	2.3461538461538461538461538461538461538461
11	2.4404432132963988919667590027700831024931
13	2.5379912663755458515283842794759825327511
15	2.4371661512510542592071970761877987067751
17	2.5150098195080894042831759094734873281591
19	2.4750593824228028503562945368171021377671
21	2.4763132295719844357976653696498054474711
23	2.4909337411126700613245471599955858937781
25	2.4772560105362274633583510926439218270681
27	2.4852681514247334591940596393874335204641
29	2.4827780063619631710560026714783667556621
31	2.4817450317701271370595211556840604659761
33	2.4837967573260598777330313228934940604991
35	2.4822368065653312362306690721336468725661
37	2.4829475882916451923240702031208351805881
39	2.4828800520088998688625226480364112210291
41	2.4826473796477063918095161917557054940751
43	2.4829063728690226211487431035224363722491
45	2.4827474612256003337439396006800467349401
47	2.4827981773695528086903965375433963177411
49	2.4828133194825828292942941973516662941141
51	2.4827771702952379108778260463968988472011
53	2.4828067671538930188880197835742700135181
55	2.4827924336902934572896506849124324423431
57	2.4827944070582453445657398290165745865221
59	2.4827983674189785079859703445447896345891
61	2.4827936213211300523558830100751062186971
63	2.4827966889815626902175135164706266984501
65	2.4827956129168880657727304396483081525391
67	2.4827954109174710260102514693394383682121
69	2.4827960557186464307147534831352760746131

Table C.4: Ratios of $s_{n,5}$ to $s_{n-1,5}$ for n odd

```
{ ECM(N, m)= local(E);
  E = ellinit([0,0,0,random(N),1]*Mod(1,N));
  print("E: y^2 = x^3 + ",lift(E[4]),"x+1, P=[0,1]");
  ellpow(E,[0,1]*Mod(1,N),m); }

{ lcmfirst(B) =
  local(L,i); L=1; for(i=2,B,L=lcm(L,i));
  return(L); }

m=lcmfirst(10^5)
ECM(N,m)
```

The hope is that you get an error message of the form:

```
***   impossible inverse modulo:  Mod(x,y)
```

If this is the case, the value x divides N and therefore n, so we are one step closer to knowing the factorization of n. Once we have calculated all the squarefree factors, we can infer s_n by appealing to the sinusoidal behavior of the ratios of successive terms.

n	$s_{n,5}/s_{n-2,5}$	n	$s_{n,5}/s_{n-2,5}$
3	6.5000000000000000000000000000000000000	41	3.081744835438383212921571361267555118556
4	2.6000000000000000000000000000000000000	42	3.081989334915240257336676584193452192134
5	2.230769230769230769230769230769230769231	43	3.082310852321399334915479965108844697229
6	2.615384615384615384615384615384615384615	44	3.082325658286375198583749840003922648407
7	3.448275862068965517241379310344827586207	45	3.082128382448158639935237850250890144211
8	3.823529411764705882352941176470588235294	46	3.082011377551052976646442503943126865838
9	3.0500000000000000000000000000000000000	47	3.082074335115254808113699071349165011857
10	2.776923076923076923076923076923076923077	48	3.082184337890805922767888166740048116202
11	2.888524590163934426229508196721311475410	49	3.082203135545826415830656109570837012752
12	3.171745152354570637119113573407202216066	50	3.082142849341743560040812231586218238763
13	3.298524404086265607264472190692395005675	51	3.082097974055144133149704513051094724783
14	3.106550218340611353711790393013100436681	52	3.082112292799887536839796323686551536145
15	2.983138334480385409497591190640055058500	53	3.082149034253361721023311784168586554114
16	3.006184987348889513635085746415518695530	54	3.082159699765150140741581855101534599922
17	3.102203252970354135425077863652093667090	55	3.082141906183930261145401818399092799228
18	3.149724118582250070139343495744879827925	56	3.082125378418524218946572591968036206617
19	3.099691369501357230506079648979288290633	57	3.082127828147048817896539560458988503996
20	3.052256532066508313539192399049881235154	58	3.082139807087933950029797461104935385505
21	3.053802783109404990403071017274472168906	59	3.082144723477882070521058501380067172370
22	3.085262645914396887159533073929961089494	60	3.082139697285850151913147944066893874371
23	3.103478482902205723489089230648360929429	61	3.082133805491825357661558834695734045238
24	3.090621600744092191761386029353806378383	62	3.082133834334972073346540323412307220633
25	3.073650980903426042071447286646068475274	63	3.082137642521013188073890218557841382804
26	3.071976470996299874418125412527786647515	64	3.082139689822066533347572376618514393556
27	3.081912104692257704779232202966851679654	65	3.082138353997165044565939093121527660221
28	3.088807195647012136095627585084673716860	66	3.082136311949079407989103893469256349452
29	3.085712327198438333675628200161923065565	67	3.082136061187504427052953063180663114686
30	3.079889653149689981429311884670575904207	68	3.082137238843184407843964717709217785224
31	3.078608246697236292590388447821765838675	69	3.082138039298069101827509245273700559571
32	3.081630980326475050094736842840168588923	70	3.082137716932528180938034332541521060663
33	3.084178647776333990023892358636878065138		
34	3.083537854338602868603777317512848466853		
35	3.081601235648920114966210130961153992911		
36	3.080945118627594377931474608702159286774		
37	3.081827338842968112556379978397962257549		
38	3.082744136514058497203232613944272291661		
39	3.082660285739029311687008261263265594063		
40	3.082033654887063436387999708762080013037		

Table C.5: Ratios of $s_{n,5}$ to $s_{n-2,5}$

Appendix D

7-PILLOW AND 9-PILLOW DATA

D.1 Table of Values

In search of a more general form of Propp's Conjecture, we present the number of tilings of 7-pillows (AP_n^7) and 9-pillows (AP_n^9). As stated in Conjecture 11, the number of tilings of AP_n^q for q odd is thought to be of the form $(\ell_{n,q})^2 s_{n,q}$ for some values $\ell_{n,q}$ and $s_{n,q}$. As the first previously unknown case of nicely behaving generalized Aztec pillows, we present as much data as collected about AP_n^5, also called 5-pillows. Table D.1 contains the number of tilings of AP_n^7 and $s_{n,7}$ for n up to 40 and Table D.2 contains the number of tilings of AP_n^9 and $s_{n,9}$ for the same range. The non-square part was calculated using a product of the bold faced terms. The same bolding convention is used as in Appendix A. The factorization of and the non-square part of AP_n^7 and AP_n^9 was calculated using PARI, as outlined in Section C.3.

n	$\#AP_n^7$	Non-Square Part
1	$\mathbf{2}$	2
2	$\mathbf{5}$	5
3	$\mathbf{13}$	13
4	$\mathbf{2} \cdot \mathbf{17}$	34
5	$\mathbf{2}^3 \cdot \mathbf{17}$	34
6	$\mathbf{2} \cdot 3^2 \cdot \mathbf{37}$	74
7	$7^2 \cdot \mathbf{73}$	73
8	$11^2 \cdot \mathbf{193}$	193
9	$\mathbf{2}^{12} \cdot 7^2$	256
10	$3^2 \cdot \mathbf{13} \cdot 17^2 \cdot \mathbf{61}$	793
11	$2^2 \cdot 7^2 \cdot 11^2 \cdot \mathbf{1049}$	1049
12	$\mathbf{5} \cdot \mathbf{17} \cdot \mathbf{29} \cdot 389^2$	2465
13	$2^4 \cdot 389^2 \cdot \mathbf{2857}$	2857
14	$3^6 \cdot 179^2 \cdot \mathbf{6577}$	6577
15	$\mathbf{2} \cdot \mathbf{3^2} \cdot 7^2 \cdot 13^4 \cdot 19^2 \cdot \mathbf{457}$	8226
16	$\mathbf{2}^6 \cdot \mathbf{3}^6 \cdot \mathbf{593} \cdot 2237^2$	21348
17	$\mathbf{2}^{15} \cdot \mathbf{3^2} \cdot \mathbf{401} \cdot 6883^2$	28872
18	$\mathbf{2}^6 \cdot 3^2 \cdot \mathbf{5}^3 \cdot 17^2 \cdot \mathbf{37} \cdot \mathbf{101} \cdot 1879^2$	74740
19	$\mathbf{2} \cdot \mathbf{5} \cdot \mathbf{17} \cdot 131^2 \cdot \mathbf{541} \cdot 102203^2$	91970
20	$13^2 \cdot \mathbf{317} \cdot \mathbf{701} \cdot 733^2 \cdot 7741^2$	222217
21	$2^6 \cdot \mathbf{397} \cdot \mathbf{677} \cdot 79094333^2$	268769
22	$3^4 \cdot \mathbf{5} \cdot \mathbf{133853} \cdot 463962211^2$	669265
23	$2^4 \cdot \mathbf{5} \cdot 11^2 \cdot 59^2 \cdot \mathbf{373} \cdot \mathbf{457} \cdot 16412281^2$	852305
24	$\mathbf{5}^3 \cdot 44491^2 \cdot \mathbf{440389} \cdot 1514101^2$	2201945
25	$\mathbf{2}^{34} \cdot 3^8 \cdot \mathbf{5} \cdot 7^4 \cdot 11^2 \cdot \mathbf{137} \cdot 46769^2$	2805760
26	$5^2 \cdot \mathbf{7^2} \cdot 191^2 \cdot \mathbf{142873} \cdot 42912379721^2$	7000777
27	$2^2 \cdot 7^4 \cdot \mathbf{8636081} \cdot 6437320730171^2$	8636081
28	$\mathbf{2}^{11} \cdot 3^{14} \cdot 7^2 \cdot \mathbf{17} \cdot 797^2 \cdot \mathbf{626797} \cdot 19405319^2$	21311098
29	$\mathbf{2}^{15} \cdot \mathbf{5} \cdot 11^2 \cdot \mathbf{13^2} \cdot 13217^2 \cdot \mathbf{15733} \cdot 46451^2 \cdot 163411^2$	26588770
30	$\mathbf{2}^{15} \cdot \mathbf{5} \cdot 7^4 \cdot \mathbf{41} \cdot 143791^2 \cdot \mathbf{163637} \cdot 2267651423^2$	67091170
31	$2^2 \cdot \mathbf{85150213} \cdot 230446162371608143932^2$	85150213
32	$3^4 \cdot 7^4 \cdot 61^2 \cdot 191^2 \cdot \mathbf{3169} \cdot \mathbf{67901} \cdot 311341^2 \cdot 507890951^2$	215178269
33	$\mathbf{2}^{17} \cdot 3^8 \cdot 11^2 \cdot 37^2 \cdot \mathbf{157} \cdot \mathbf{858301} \cdot 43817759^2 \cdot 60737527^2$	269506514
34	$\mathbf{3^2} \cdot \mathbf{17} \cdot 19^2 \cdot 29^2 \cdot 521^2 \cdot 653^2 \cdot 2341^2 \cdot 7459^2 \cdot \mathbf{4386857} \cdot 148529957^2$	671189121
35	$2^6 \cdot \mathbf{53} \cdot 33037^2 \cdot \mathbf{15762997} \cdot 5650088053^2 \cdot 11004114937^2$	835438841
36	$\mathbf{5^3} \cdot \mathbf{593} \cdot \mathbf{28181} \cdot 4325893666414356709802393592^2$	2088916625
37	$2^{10} \cdot \mathbf{17} \cdot \mathbf{154411273} \cdot 195045899^2 \cdot 2841516944954857861^2$	2624991641
38	$\mathbf{317} \cdot 3847^2 \cdot 115163^2 \cdot \mathbf{20868733} \cdot 1279427472756836707441^2$	6615388361
39	$\mathbf{2}^{10} \cdot \mathbf{3^2} \cdot \mathbf{5} \cdot \mathbf{61} \cdot 127^2 \cdot \mathbf{47381} \cdot 557148176550104794583052901332^2$	8323894080
40	$\mathbf{2}^{33} \cdot \mathbf{5}^3 \cdot 1006949^2 \cdot \mathbf{130445921} \cdot 1339855209164335703380 3^2$	20871347360

Table D.1: Number of tilings of 7-pillows AP_n^7 up to $n = 40$

D.2 Supplementary Data for 7-pillows

As in Appendices A and C, patterns emerge in $s_{n,7}$ when we write $\#AP_n^7 = (\ell_{n,7})^2(s_{n,7})$. Tables D.3 and D.4 give the ratio of consecutive terms of $s_{n,7}$ split into the two cases when n is even or n is odd. It appears that each table has a limiting value, and that the limiting value for Table D.3 is twice that of the limiting value of Table D.4. Considering the ratio $s_{n,7}/s_{n-2,7}$ yields the data presented numerically in Table D.5. Again, a damped sine curve form appears when the data is plotted in Figure D.1. This damped sine curve converges more slowly to a limit, making it unlikely that we might estimate its limiting value precisely without many more calculations.

D.3 Supplementary Data for 9-pillows

As with the 7-pillows in Section D.2, we notice patterns in $s_{n,9}$ when we write $\#AP_n^9 = (\ell_{n,9})^2(s_{n,9})$. Tables D.6 and D.7 give the ratio of consecutive terms of $s_{n,9}$ split into the two

n	$\#AP_n^9$	Non-Square Part
1	$\mathbf{2}$	2
2	$\mathbf{5}$	5
3	$\mathbf{13}$	13
4	$\mathbf{2} \cdot \mathbf{17}$	34
5	$\mathbf{89}$	89
6	$2^2 \cdot \mathbf{89}$	89
7	$3^2 \cdot \mathbf{193}$	193
8	$\mathbf{5} \cdot 7^2 \cdot \mathbf{37}$	185
9	$\mathbf{2} \cdot \mathbf{5} \cdot 11^2 \cdot \mathbf{41}$	410
10	$\mathbf{2}^3 \cdot 13^2 \cdot \mathbf{241}$	482
11	$\mathbf{2}^6 \cdot 11^2 \cdot \mathbf{19^2}$	1444
12	$\mathbf{2}^3 \cdot 59^2 \cdot \mathbf{1009}$	2018
13	$\mathbf{2} \cdot 13^2 \cdot 17^2 \cdot \mathbf{3181}$	6362
14	$677^2 \cdot \mathbf{8461}$	8461
15	$\mathbf{5} \cdot \mathbf{41} \cdot \mathbf{97} \cdot 1721^2$	18655
16	$2^4 \cdot 1721^2 \cdot \mathbf{22861}$	22861
17	$3^2 \cdot \mathbf{5}^5 \cdot 17^2 \cdot 83^2 \cdot \mathbf{409}$	51125
18	$\mathbf{2}^{10} \cdot 5^4 \cdot \mathbf{37} \cdot \mathbf{101} \cdot 479^2$	59792
19	$3^4 \cdot 43^2 \cdot 839^2 \cdot \mathbf{146749}$	146749
20	$2^2 \cdot 17^2 \cdot \mathbf{61} \cdot 107^2 \cdot 449^2 \cdot \mathbf{3209}$	195749
21	$\mathbf{2}^{11} \cdot 7^2 \cdot \mathbf{61} \cdot \mathbf{4337} \cdot 27917^2$	529114
22	$2^2 \cdot \mathbf{5} \cdot 13^2 \cdot 71^2 \cdot 19457^2 \cdot \mathbf{146093}$	730465
23	$\mathbf{5}^3 \cdot 7^6 \cdot 94201^2 \cdot \mathbf{381509}$	1907545
24	$2^4 \cdot 3^4 \cdot 11^2 \cdot 73^2 \cdot \mathbf{149} \cdot \mathbf{15773} \cdot 39829^2$	2350177
25	$17^2 \cdot \mathbf{5638489} \cdot 375744331^2$	5638489
26	$2^6 \cdot \mathbf{3^2} \cdot \mathbf{461} \cdot \mathbf{1613} \cdot 6790628003^2$	6692337
27	$3^4 \cdot \mathbf{5} \cdot 83^2 \cdot \mathbf{3233509} \cdot 466643687^2$	16167545
28	$\mathbf{2} \cdot \mathbf{5}^3 \cdot \mathbf{29^2} \cdot 61^2 \cdot \mathbf{2389} \cdot 3583^2 \cdot 3089447^2$	20091490
29	$\mathbf{2}^6 \cdot \mathbf{5}^{10} \cdot 11^2 \cdot \mathbf{13} \cdot \mathbf{29} \cdot 89^2 \cdot 457^2 \cdot \mathbf{1373} \cdot 22051^2$	51762100
30	$\mathbf{2}^{15} \cdot \mathbf{5}^3 \cdot \mathbf{17^2} \cdot 31^2 \cdot \mathbf{5861} \cdot 27572404169^2$	67753160
31	$\mathbf{2}^{28} \cdot \mathbf{5} \cdot 12109^2 \cdot \mathbf{2226893} \cdot 46528903^2$	178151440
32	$\mathbf{2}^{15} \cdot \mathbf{53} \cdot 3001^2 \cdot \mathbf{540373} \cdot 156547018619^2$	229118152
33	$\mathbf{2}^6 \cdot 3^2 \cdot 7^4 \cdot 89^2 \cdot 14303^2 \cdot \mathbf{143289121} \cdot 406603069^2$	573156484
34	$\mathbf{2} \cdot 3^{10} \cdot 7^2 \cdot 2113^2 \cdot \mathbf{352173793} \cdot 1324886982313^2$	704347586
35	$3^{12} \cdot \mathbf{5}^3 \cdot \mathbf{13} \cdot \mathbf{281} \cdot \mathbf{94201} \cdot 8951389^2 \cdot 1750246153^2$	1720581265
36	$2^8 \cdot 3^4 \cdot \mathbf{5} \cdot 17^2 \cdot \mathbf{41} \cdot \mathbf{61} \cdot \mathbf{169313} \cdot 38282789^2 \cdot 11117517629^2$	2117259065
37	$\mathbf{5}^3 \cdot \mathbf{17} \cdot \mathbf{62238541} \cdot 1289343199^2 \cdot 2238169218731^2$	5290275985
38	$2^6 \cdot \mathbf{5} \cdot 83^2 \cdot 1579^2 \cdot 108084269^2 \cdot \mathbf{1345114501} \cdot 2676950597^2$	6725572505
39	$3^4 \cdot 7^2 \cdot \mathbf{17} \cdot 19^2 \cdot \mathbf{73} \cdot \mathbf{109} \cdot 127^2 \cdot \mathbf{127717} \cdot 319327108465072741 21^2$	17276150873
40	$2^4 \cdot 3^2 \cdot 13^2 \cdot \mathbf{29} \cdot \mathbf{41} \cdot \mathbf{101} \cdot \mathbf{185057} \cdot 7604008179971773319847 31^2$	22223310073

Table D.2: Number of tilings of 9-pillows AP_n^9 up to $n = 40$

cases when n is even or n is odd. It appears that each table has a limiting value, and that the limiting value for Table D.7 is twice that of the limiting value of Table D.6. Considering the ratio $s_{n,9}/s_{n-2,9}$ yields the data presented numerically in Table D.8. Once more, a damped sine curve form appears when the data is plotted in Figure D.2. This damped sine curve converges even more slowly to a limit, making it unlikely that we might estimate its limiting value precisely without many more calculations.

n	$s_{n,7}/s_{n-1,7}$
2	2.5000000000000000000000000000000000000
4	2.6153846153846153846153846153846153846 15
6	2.1764705882352941176470588235294117647 06
8	2.6438356164383561643835616438356164383 56
10	2.8867187500000000000000000000000000000 00
12	2.3498570066730219256434699714013346043 85
14	2.3020651032551627581379068953447672383 62
16	2.5951859956236323851203501094091903719 91
18	2.5886672208367968966472707121086173455 25
20	2.4161900619767315428944220941611395020 12
22	2.4901123269424673232404034691500879937 79
24	2.5835176374654613078651421732830383489 48
26	2.4951446310447080291970802919708029197 08
28	2.4676815791792596665084544714205436470 55
30	2.5232897196824072719422523117842607988 26
32	2.5270432265389635607840464239355455282 30
34	2.4904374704649995955199806413584496885 30
36	2.5003824606713491311089281758687108970 55
38	2.5201559721842939003857955523295321609 75
40	2.5074018433449359797716215053039214069 38

Table D.3: Ratios of $s_{n,7}$ to $s_{n-1,7}$ for n even

n	$s_{n,7}/s_{n-1,7}$
3	2.6000000000000000000000000000000000000000
5	1.0000000000000000000000000000000000000000
7	0.9864864864864864864864864864864864864486
9	1.3264248704663212435233160621761658031 09
11	1.4194857916102841677943166441136671177 27
13	1.1590263691683569979716024340770791075 05
15	1.2507222137752774821347118747149156150 22
17	1.3524451939291736930860033726812816188 87
19	1.2305325127107305325127107305325127107 31
21	1.2094889229896902577210564448264534216 55
23	1.2734940569131808775298274973291596004 57
25	1.2742189291739802765282511597701123325 06
27	1.2335889287717634771111835157726063835 49
29	1.2476489949039697532243528700398261975 99
31	1.2691716808635175090850256449544701635 10
33	1.2524801656434925591858906532982659136 46
35	1.2447145146740243425369822107113681897 71
37	1.2566282491049636794383787337610949407 81
39	1.2582623461794369474962408786691034298 30

Table D.4: Ratios of $s_{n,7}$ to $s_{n-1,7}$ for n odd

n	$s_{n,7}/s_{n-2,7}$
3	6.5000000000000000000000000000000000000
4	6.8000000000000000000000000000000000000
5	2.6153846153846153846153846153846153846
6	2.1764705882352941176470588235294117647
7	2.1470588235294117647058823529411764706
8	2.6081081081081081081081081081081081081
9	3.5068493150684931506849315068493150685
10	3.8290155440414507772020725388601036269
11	4.0976562500000000000000000000000000000
12	3.3355886332882273342354533152909336942
13	2.7235462345090562440419447092469018112
14	2.6681541582150101419878296146044624746
15	2.8792439621981099054952747637381869093
16	3.2458567736049870761745476661091683138
17	3.5098468271334792122538293216630196937
18	3.5010305415027168821435263256511148585
19	3.1854391798282072596287060127459129953
20	2.9732004281509232004281509232004281509
21	2.9223551157986299880395781233010764380
22	3.0117632764369962694123311897829598996
23	3.1711432494074837499860474980373480573
24	3.2900943572426467841587413057607972926
25	3.2919670775133314951807158235608144972
26	3.1793605199039939689683438959647039322
27	3.0779827925410583941605839416058394161
28	3.0441046758095565677924036146273477930
29	3.0788004420060441767510054618524305180
30	3.1481798826132750175518877535075855782
31	3.2024878548349547572151701639451542888
32	3.2072516994412230402301823026785790142
33	3.1650715189637869725587180856494158153
34	3.1192235355327633014837571725237737645
35	3.0998836673758468042074856862272353091
36	3.1122623410339810915975796931905277410
37	3.1420512336461981661683359536308654819
38	3.1668991867973667929422506271642124539
39	3.1710173662987294823160924496063947657
40	3.1549693262218441660435118935264577734

Table D.5: Ratios of $s_{n,7}$ to $s_{n-2,7}$

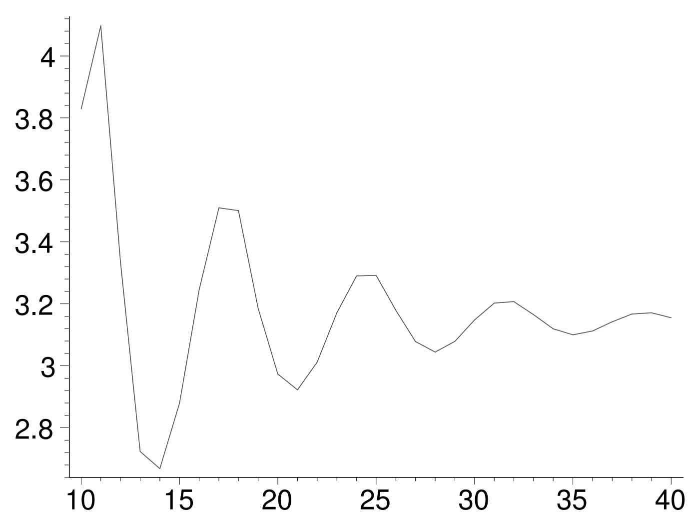

Figure D.1: Damped sinusoidal behavior observed in 7-pillows

n	$s_{n,9}/s_{n-1,9}$
2	2.50000000000000000000000000000000000000
4	2.61538461538461538461538461538461538461 5
6	1.00000000000000000000000000000000000000
8	0.95854922279792746113989637305699481865 3
10	1.17560975609756097560975609756097560975 6
12	1.39750692520775623268698060941828254847 6
14	1.32992769569317824583464319396416221314 1
16	1.22546234253551326722058429375502546234 3
18	1.16952567237163814180929095354523227383 9
20	1.33390346782601585019318700638505202761 2
22	1.38054370135736344152677872821357968226 1
24	1.23204275652736894804578660005399610494 1
26	1.18690255492207220764286318550945120226 4
28	1.24270506128172211674685303179920018778 4
30	1.30893375655160822300486263115290917486 0
32	1.28608644420724300628723517474795600866 3
34	1.22889229322580602612531903241977456195 0
36	1.23054871517504289458830065780124602251 8
38	1.27130843911917385535038395544122070977 4
40	1.28635772148364705937237851997774689727 9

Table D.6: Ratios of $s_{n,9}$ to $s_{n-1,9}$ for n even

n	$s_{n,9}/s_{n-1,9}$
3	2.60000000000000000000000000000000000000
5	2.61764705882352941176470588235294117647 1
7	2.16853932584269662921348314606741573033 7
9	2.21621621621621621621621621621621621621 6
11	2.99585062240663900414937759336099585062 2
13	3.15262636273538156590683845391476709613 5
15	2.20482212504432100224559744711027065358 7
17	2.23634136739425221993788548182494204103 1
19	2.45432499331014182499331014182499331014 2
21	2.70302274851978809598005609224057338734 8
23	2.61141190885258020575934507471268301698 2
25	2.39917631735822450819661668036067070693 0
27	2.41582947780424088027844383807928381371 1
29	2.57631962587145104718465380118647248163 3
31	2.62941890828413021621426956322037230440 6
33	2.50157606019797156883493019793560485770 7
35	2.44280139408329000789675454357275244498 4
37	2.49864368156572280397817071100838574045 7
39	2.56872568991805107303649535185555181223 9

Table D.7: Ratios of $s_{n,9}$ to $s_{n-1,9}$ for n odd

n	$s_{n,9}/s_{n-2,9}$
3	6.500000000000000000000000000000000000000
4	6.800000000000000000000000000000000000000
5	6.846153846153846153846153846153846153846
6	2.617647058823529411764705882352941176471
7	2.168539325842696629213483146067415730337
8	2.078651685393258426966292134831460674157
9	2.124352331606217616580310880829015544041
10	2.605405405405405405405405405405405405405
11	3.521951219512195121951219512195121951220
12	4.186721991701244813278008298755186721992
13	4.405817174515235457063711911357340720222
14	4.192765113974231912784935579781962338949
15	3.125589437283872995913234831813895001572
16	2.701926486230941969034393097742583618958
17	2.571033442293185818456122705556952476741
18	2.6154586413542714666689996063164341017453
19	2.870396088019559902200488997555012224939
20	3.273832619748461332619748461332619748461
21	3.605571417863154093043223463192253439546
22	3.731641030094662041696253876137298274832
23	3.605168262416038887649920433025775163764
24	3.217371126611131265700615361447844865942
25	2.955887803433208653006875329284499186127
26	2.847588500781005005154930883929167888206
27	2.867354179461909032721354958748700228022
28	3.002163519260909903371572591159112280209
29	3.201605438549884970167084736736468029005
30	3.372231725969552283081045756188316545961
31	3.441735169168175170636430902146551241159
32	3.381660014086427850745264132329768825543
33	3.217243060173973334147621821075372727832
34	3.074167541295462264377900534044111878137
35	3.001939807070210166199567935098157242517
36	3.005986116916996149114366383304393123880
37	3.074702772030939207047567148768180967029
38	3.176546798726305134511255475484290818233
39	3.265642647375040491389410943935848367654
40	3.304300125599493481335980333766396590204

Table D.8: Ratios of $s_{n,9}$ to $s_{n-2,9}$

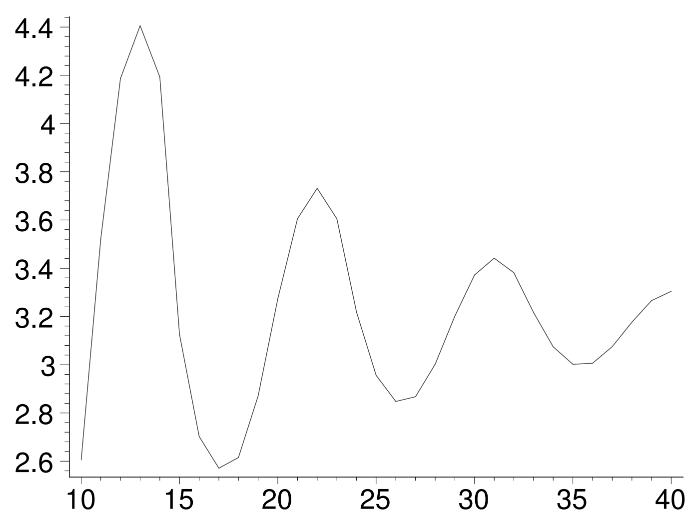

Figure D.2: Damped sinusoidal behavior observed in 9-pillows